DETERMINATION OF CONNECTIVITY IN RESERVOIRS USING DOWNHOLE FLUID ANALYSIS

Mr. John Thomas Ludwig

A Thesis Submitted in Partial Fulfillment of the Requirements

for the Degree of Master of Engineering Program in Petroleum Engineering

Department of Mining and Petroleum Engineering

Faculty of Engineering

Chulalongkorn University

Academic Year 2012

การหาการเชื่อมต่อในแหล่งกักเก็บโดยใช้การวิเคราะห์ของไหลภายในหลุม

นายจอห์น โธมัส ลูดวิก

วิทยานิพนธ์นี้เป็นส่วนหนึ่งของการศึกษาตามหลักสูตรปริญญาวิศวกรรมศาสตรมหาบัณฑิต
สาขาวิชาวิศวกรรมปิโตรเลียม ภาควิชาวิศวกรรมเหมืองแร่และปิโตรเลียม
คณะวิศวกรรมศาสตร์ จุฬาลงกรณ์มหาวิทยาลัย
ปีการศึกษา 2555

Thesis Title	DETERMINATION OF CONNECTIVITY IN RESERVOIRS USING DOWNHOLE FLUID ANALYSIS
By	Mr. John Thomas Ludwig
Field of Study	Petroleum Engineering
Thesis Advisor	Assistant Professor Suwat Athichanagorn, Ph.D.
Thesis Co-advisor	Saifon Daungkaew, Ph.D.

Accepted by the Faculty of Engineering, Chulalongkorn University in Partial Fulfillment of the Requirements for the Master's Degree

...…….…… Dean of the Faculty of Engineering
(Associate Professor Boonsom Lerdhirunwong, Dr.Ing.)

THESIS COMMITTEE

…..…… Chairman
(Associate Professor Sarithdej Pathanasethpong)

……. Thesis Advisor
(Assistant Professor Suwat Athichanagorn, Ph.D.)

……. Thesis Co-advisor
(Saifon Daungkaew, Ph.D.)

…..…… Examiner
(Falan Srisuriyachai, Ph.D.)

…..…… External Examiner
(Thotsaphon Chaianansutcharit, Ph.D.)

จอห์น โธมัส ลูดวิก: การหาการเชื่อมต่อในแหล่งกักเก็บโดยใช้การวิเคราะห์ของไหลภายในหลุม. (DETERMINATION OF CONNECTIVITY IN RESERVOIRS USING DOWNHOLE FLUID ANALYSIS) อ. ที่ปรึกษาวิทยานิพนธ์หลัก: ผศ. ดร. สุวัฒน์ อธิชนากร, อ.ที่ปรึกษาวิทยานิพนธ์ร่วม: ดร.สายฝน ดวงแก้ว, 127 หน้า.

การวิเคราะห์ของไหลภายในหลุม ใช้หลักการวิเคราะห์สเปกตรัมของแสง เพื่อวัดค่าต่างๆ ที่มีคุณภาพเช่นเดียวกับค่าที่วัดได้ในห้องทดลอง ซึ่งการวิเคราะห์นี้เป็นส่วนหนึ่งของการทดสอบชั้นหินขั้นสูง การวิเคราะห์ของไหลภายในหลุมสามารถระบุคุณสมบัติของของไหล เช่น อัตราส่วนระหว่างแก๊สและน้ำมัน องค์ประกอบของสารไฮโดรคาร์บอน การประมาณค่าความเจือปนและสีของของไหล ความก้าวหน้าเกี่ยวกับวิทยาศาสตร์ของสารประกอบแอสฟัลต์ ทำให้เราเห็นความสัมพันธ์ระหว่างสีของของไหลกับสารประกอบแอสฟัลต์ในของไหล โดยที่สารประกอบแอสฟัลต์มีการแสดงระดับสีเปลี่ยนไปอย่างต่อเนื่องตามระดับความสูงของน้ำมัน ดังนั้น ความต่อเนื่องของอัตราการเปลี่ยนแปลงของสารประกอบแอสฟัลต์ สามารถระบุว่าแหล่งกักเก็บน้ำมันมีความต่อเนื่องด้วยความน่าจะเป็นที่สูง ในขณะที่การเบี่ยงเบนจากอัตราการเปลี่ยนแปลงของสารประกอบแอสฟัลต์บ่งบอกว่า แหล่งกักเก็บน้ำมันน่าจะไม่มีความต่อเนื่องของของไหลและน่าจะไม่เชื่อมกัน การทดสอบชั้นหินโดยวิเคราะห์ของไหลภายในหลุมด้วยนั้น สามารถใช้หาอัตราการเปลี่ยนแปลงของสารประกอบแอสฟัลต์ในน้ำมันและแก๊ส สมการระบุสถานะของ Flory-Huggins-Zuo (FHZ) ได้รับการพัฒนาขึ้นเพื่อพยากรณ์อัตราการเปลี่ยนแปลงของสารประกอบแอสฟัลต์ การศึกษานี้ได้เปรียบเทียบอัตราการเปลี่ยนแปลงของสารประกอบแอสฟัลต์ที่คำนวณจากสมการ FHZ สำหรับน้ำมันดิบที่มีอัตราส่วนระหว่างแก๊สและน้ำมันต่ำ กับข้อมูลจากห้องปฏิบัติการ เพื่อใช้หาความเชื่อมกันในแหล่งกักเก็บ

ภาควิชา วิศวกรรมเหมืองแร่และปิโตรเลียม ลายมือชื่อนิสิต.....

สาขาวิชา วิศวกรรมปิโตรเลียม ลายมือชื่อ อ. ที่ปรึกษาวิทยานิพนธ์หลัก.....

ปีการศึกษา 2555 ลายมือชื่อ อ. ที่ปรึกษาวิทยานิพนธ์ร่วม.....

5371631321: MAJOR PETROLEUM ENGINEERING
KEYWORDS: RESERVOIR CONNECTIVITY / DOWNHOLE FLUID ANALYSIS / DFA / LOW GOR WAXY CRUDE / FHZ EOS / DECONTAMINATION

JOHN THOMAS LUDWIG: DETERMINATION OF CONNECTIVITY IN RESERVOIRS USING DOWNHOLE FLUID ANALYSIS. ADVISOR: ASST. PROF. SUWAT ATHICHANAGORN, Ph.D., CO-ADVISOR: SAIFON DAUNGKAEW, Ph.D.,127 pp.

Downhole Fluid Analysis (DFA) is a concept that utilizes downhole optical spectroscopy to provide laboratory quality measurements as part of advanced formation tester (FT) operations. With DFA, several fluid properties including GOR, hydrocarbon composition, contamination estimation, and color can be determined. Recent advances in asphaltene science have related the fluid color to the asphaltene content of the fluid. Asphaltenes have been shown to grade continuously in an oil column; therefore a continuous asphaltene gradient would indicate a reservoir with a higher probability of fluid communication while a deviation from this gradient would indicate a reservoir which would likely not have fluid communication and is likely not connected. DFA-enabled FT operations can be used to determine the asphaltene gradient in an oil and gas column. The Flory-Huggins-Zuo (FHZ) equation of state (EOS) has been developed to predict the asphaltene gradient. In this study, the predicted asphaltene gradient determined from the FHZ EOS for low GOR crudes is compared to the DFA and laboratory data in order to determine connectivity in a reservoir.

Department: Mining and Petroleum Engineering Student's Signature……..…..
Field of Study: Petroleum Engineering Advisor's Signature…….....……...
Academic Year: 2012 Co-Advisor's Signature……...

Acknowledgements

I would like to thank my research advisors, Assistant Professor Dr. Suwat Athichanagorn (Chulalongkorn University) and Dr. Saifon Daungkaew (Schlumberger), for sharing their time and expertise while guiding me through my research.

I would like to thank the other members of the thesis committee who were involved in my thesis proposal and final defense; Associate Professor Sarithdej Pathanasethpong (Chulalongkorn University), Dr. Falan Srisuriyachai (Chulalongkorn University), Dr. Thotsaphon Chaianansutcharit (Chevron), and Dr. Kreangkrai Maneeintr (Chulalongkorn University). Their comments and recommendations were instrumental in forming this final document. I would also like to thank my classmates and the faculty members in the Department of Mining and Petroleum Engineering who collectively contributed to a successful and memorable graduate study.

I would like to thank Pearl Energy for allowing the use of their reservoir data for my project and Chevron for providing a research fellowship in support of my project. I would also like to thank Schlumberger for providing the PVT Pro software necessary to complete the modeling portion of my research. I would like to thank the Schlumberger Data Consulting Services group in Bangkok for sharing their resources and knowledge with me over the last year. I would like to thank the Schlumberger community of DFA experts from around the world, several of whom have authored papers that are referenced in this work. My interest in this subject is a result of their previously published work and they provided the foundation for which I based my research. In particular, Julian Zuo was a great help in providing guidance related to the FHZ EOS and the workings of PVT Pro.

This work is dedicated to my father, mother, and brother, Michael. They have been a constant source of support and encouragement throughout my life and for that I will be forever grateful.

Contents

Page

List of Tables

Page

List of Figures

Page

Page

List of Abbreviations

cp	Centipoise
d_a	Asphaltene diameter
degF	Degrees Fahrenheit
DFA	Downhole Fluid Analysis
EOS	Equation of state
FHZ	Flory-Huggins-Zuo
FVF	Formation volume factor
ft	Feet
FT	Formation tester
GOR	Gas to oil ratio
IFA	Insitu Fluid Analyzer
IPTT	Interval Pressure Transient Test
KF	Katz and Firoozabadi 1978 convention
kg	Kilogram
LFA	Live Fluid Analyzer
m^3	Cubic meter
MDT	Modular Dynamic Formation Tester
mD	Millidarcies
nm	Nanometers
OBM	Oil-based mud
OD	Optical density
OFA	Optical Fluid Analyzer
psi	Pounds per square inch
psia	Pounds per square inch atmosphere
PTA	Pressure transient analysis
PVT	Pressure-volume-temperature
s	Seconds
TVDss	Subsea true vertical depth
Vis-NIR	Visible and near infrared spectrum

Nomenclature

α_λ	Absorption coefficient at a particular wavelength
D	Constant for fitting the OCM curve
h_1	A location in the oil column
Iλ	Intensity of light exiting the fluid
Iλo	Intensity of light entering the fluid
k	Boltzmann's constant
L	Optical path length
MW	Molecular weight
OD_{m_inf}	OD for a pure reservoir fluid
OD_m	OD difference of methane and reference channels
p	Pressure
P_c	Critical pressure
t	Time
T	Temperature
T_c	Critical temperature
T_λ	Transmittance at a particular wavelength
ω	Acentric factor

CHAPTER I

INTRODUCTION

The oil and gas that is easy to find and produce is gone and the oil industry has increasingly shifted their search offshore. Offshore exploration and production present an entirely different set of challenges and decisions, and are subject to a different decision making schedule than land based projects.[1] The ability to accurately characterize a reservoir has gained more importance as initially promising discoveries have had lower than expected production due to reservoir complexities involving the reservoir architecture and complexities in the reservoir fluid itself. The negative economic implications from failing to identify these issues early can be significant as improperly sized production facilities may be constructed for offshore locations that do not meet the projected production.

Mullins wrote that the reservoir is analogous to either a kitchen sponge with interconnected pores or as bubble wrap which has pores containing fluid but in some cases the fluid is unable to flow[2], even though it may be in the same system in terms of pressure. Although pressure communication between compartments is observed when there is fluid connectivity, pressure communication alone has been shown to be insufficient as a gauge to determine whether a reservoir will exhibit connectivity upon production. Evaluating the reservoir under dynamic conditions through extended well testing can be effective in identifying fluid connectivity issues although at that point costly decisions have already been made. Therefore, it is beneficial to identify these complexities under static conditions and a successful approach to determine fluid connectivity has been to focus on the reservoir fluid properties.

Upon establishing pressure communication, the reservoir fluid data acquired through Downhole Fluid Analysis (DFA) can be used to determine reservoir connectivity. DFA is a concept that utilizes downhole optical spectroscopy to provide laboratory quality measurements as part of advanced formation tester (FT) operations. Several fluid properties including GOR, CO2 content, hydrocarbon composition,

contamination estimation, and color can be determined. Recent advances in asphaltene science have related the fluid color, or optical density (OD), to the asphaltene content of the reservoir fluid which can then be used to determine the asphaltene gradient in an oil and gas column. Furthermore, the Flory-Huggins-Zuo (FHZ) equation of state (EOS) has been developed to predict the asphaltene gradient. At any particular location in the oil column, the predicted asphaltene gradient can then be compared to the actual OD measurement obtained from DFA operations. An OD measurement that deviates from this prediction indicates a reservoir that likely does not have fluid communication. Conversely, OD measurements that match the predicted asphaltene gradient would indicate that the reservoir has a higher probability of fluid connectivity and would be more likely to flow upon production. The challenge for this study is to determine reservoir connectivity for a thin bed reservoir containing low GOR, waxy crude.

Published works that resulted from this thesis are:

- Validating of Reservoir Connectivity and Compartmentalization Through the Use of the CO2 Compositional Gradient, and Mass Transportation Simulation Concepts. SPE paper 146110 presented at the Society of Petroleum Engineers Annual Technical Conference and Exhibition, Denver, USA. October 30-November 2, 2011.

- Validating of Reservoir Connectivity and Compartmentalization Through the Use of the CO2 Compositional Gradient, Mass Transportation Simulation, and Asphaltene Analysis. IPTC paper 14398 presented at the International Petroleum Technology Conference, Bangkok, Thailand. November, 11-15, 2011.

- Is There a Better Way to Determine the Viscosity of Waxy Crudes? SPE paper 159337 presented at the Asia Pacific Oil and Gas Conference and Exhibition, Perth, Australia. October, 22-24, 2012.

This thesis is broken down in the following way:

Chapter II Literature Review covers the previous work related to DFA and the recent advances in asphaltene science and EOS modeling.

Chapter III Theory and Concept covers the theory and concept of DFA and its associated subtopics that contribute to the assessment of reservoir connectivity.

Chapter IV Methodology describes the fluid data available for the project and the data preparation required before modeling.

Chapter V Results and Discussion provides the results of fluid modeling and discusses the interpretation derived from the results.

Chapter VI Conclusions and Recommendations draw conclusions from the modeling results and provide recommendations for further study associated with this project.

CHAPTER II

LITERATURE REVIEW

This chapter reviews previous work related to determining reservoir connectivity with Downhole Fluid Analysis (DFA).

2.1 Previous Works

Previous authors described the necessity and subsequent challenges involved in evaluating reservoirs under static conditions. Dake[1] wrote that there are different priorities offshore than on land with the main differences largely involving the timing of decision making. While land developments often have the luxury of extended well testing and flexible production facilities design, offshore developments usually are forced to base their facility design on static data.

Muggeridge et al.[3] described reservoir compartmentalization and the timing of decision making as the conundrum that engineers face offshore in their need to determine compartmentalization before production. However, the only way to really verify that a reservoir is compartmentalized is after production starts and the reservoir's dynamic response can be measured. Traditional reservoir engineering calculations and models have relied on simplifying assumptions usually based on a homogeneous reservoir rock containing a homogenous fluid. However, Vrolik et al.[4] noted that the standard assumptions about the frequency of compartmentalization are also likely wrong, as it is statistically much more likely that there are more, smaller compartments than fewer bigger compartments. Therefore, as the oil industry evaluates offshore or marginally commercial prospects, it is going to be increasingly necessary to make these decisions earlier under static conditions, without depending solely on extended well testing or broad simplifying assumptions about the rock and fluid.

As the study of complexity in the reservoir architecture progressed, so did the terminology. Mullins et al.[5] proposed that it was not adequate to just identify compartmentalization in a reservoir; instead, the discussion shifted to determining the connectivity of fluid between the compartments. Snedden et al.[6] proposed that characterizing a complex reservoir required that the connectivity between compartments be described by the 'inherent geology' of the reservoir and field. In other words, a complex reservoir should first be evaluated under static conditions based on the latest geological interpretation. This description of the reservoir architecture and fluid would be representative of the reservoir processes occurring on a geologic time scale. Pressure and fluid can slowly equalize across compartments over a geologic time frame but the viability of a project must be assessed over a production time scale. At the time of discovery, static measurements of the pressure and fluid may appear to indicate reservoir connectivity. Pfeiffer et al.[7] showed that the time required for fluid to migrate, mix, and reach compositional equilibrium is seven orders of magnitude greater than the time required for pressure equilibrium. Therefore, Mullins [2] wrote that the key to identifying reservoir complexities is found in the characteristics of the reservoir fluid as it exists in the reservoir.

Earlier, Mullins et al.[8] showed that petroleum fluids exhibited the exponential Urbach absorption tail, or electronic absorption edge, and that this phenomenon was related to the asphaltene content in the fluid. Furthermore, the electronic absorption edge could be utilized to determine an absorption coefficient which would be unique to a particular fluid composition. Smits et al.[9] wrote about the use of downhole spectroscopy to determine the contributing components of the optical density (OD) of a downhole fluid. The OD was a measure of the attenuation of light through a fluid and it could be related to the absorption of light over the visible and near-infrared range. Smits summarized Lambert's Law in the context of FT operations in which the transmittance of light at a particular wavelength could be utilized to determine an absorption coefficient and subsequently infer fluid composition. Felling et al.[10] wrote about utilizing optical spectroscopy concepts downhole with an optical fluid analyzer (OFA) module that could be added to a FT tool string to provide contamination monitoring during fluid sampling operations. After setting a sampling probe up against the formation, fluid could be drawn into the FT and past the light

source in the OFA. The OD could be measured over time and by knowing the typical optical signatures of downhole fluids (water, hydrocarbon, and drilling mud), the samples could be taken at the optimum time in order to obtain a sample that was representative of the reservoir fluid.

Improvements in sampling largely focused on achieving lower levels of OBM contamination and reducing sampling time. O'Keefe et al.[11] wrote about the improvements in sampling equipment and procedures and how the equipment could be configured in a number of ways depending on the sampling objectives, downhole conditions, and the formation rock and fluid properties anticipated. In the interest of reducing sampling time, Dong et al.[12] described a method for determining the contamination level of the fluid as it was pumped past the OFA. Through analyzing the ratio of the absorption peak of methane to the absorption peak of heavier components which were responsible for color, an algorithm for oil contamination monitoring (OCM) which predicted the time required to 'clean up' to certain contamination levels was developed. Planning and operations go to great lengths to avoid sample contamination; however, due to a number of different factors it is still possible that drilling mud will skew the real time OD measurement or contaminate the sample that is sent off for laboratory testing. Zuo[13] wrote about a procedure for adjusting the real time OD measurements for OBM contamination based on OCM and Gozalpour et al.[14] wrote about decontamination procedures for laboratory samples that have been developed based on the premise that the C8+ components of real reservoir fluids tends to decrease exponentially with increasing carbon number. The aim of these decontamination procedures was to determine a composition of the reservoir fluid with zero OBM contamination so that PVT tests could be performed on a clean sample.

Mullins developed the Yen-Mullins model which provided a breakthrough in describing the size and structure of asphaltenes[15] and the corresponding chemistry and physics which governed asphaltene behavior. Mullins explained that one useful aspect of asphaltene behavior was that they tend to grade continuously in an oil column exhibiting fluid equilibrium.[16] Therefore, a continuous asphaltene gradient would increase the likelihood that the reservoir would exhibit connectivity upon production. Based on the new information about asphaltene size and structure from

the Yen-Mullins model, Zuo et al.[17] developed the Flory-Huggins-Zuo EOS (FHZ EOS) that addressed the asphaltene portion of the reservoir fluid. Using inputs from real time DFA measurements, the FHZ EOS was used to predict the asphaltene gradient.[18] If the subsequent OD measurements taken at different depths in the oil column matched the FHZ EOS prediction then the reservoir was more likely to be connected. If the subsequent measurements did not match the prediction, then a fluid barrier was more likely to exist and the fluid was not as likely to flow upon production.

Over time the DFA technology has been expanded and DFA can now infer several fluid properties including GOR, hydrocarbon composition, color, density, viscosity, fluorescence, and other measurements as part of advanced FT operations. A common theme of the authors listed in this literature review, while their papers may have focused on specific approaches, was that the collective use of all the available data, taken within the context of the latest geological interpretation, provides the best interpretation of reservoir connectivity.

CHAPTER III

THEORY AND CONCEPT

This chapter presents the theory and concept for utilizing DFA to assess reservoir connectivity.

3.1 Downhole Fluid Analysis (DFA)

DFA is a concept which is a collection of downhole fluid measurements taken in real-time which includes pressure, composition, GOR, CO2 content, density, viscosity, pH, fluorescence, and color along with other measurements.

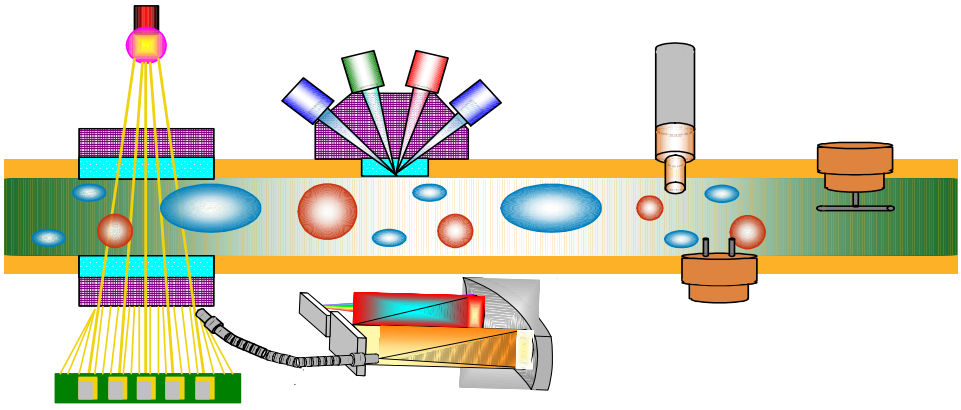

Figure 3.1: DFA module schematic. [19]

DFA is not a tool; instead it is incorporated as an additional module that is part of a new generation of formation testers (FT) that utilize downhole optical spectroscopy to infer fluid properties. Data acquired from the Live Fluid Analyzer (LFA) and the Insitu Fluid Analyzer (IFA) versions of the DFA technology are analyzed in this paper.

3.2 Formation Tester (FT)

For open hole logging operations, the first run in the hole is typically the 'triple combo' set of tools which include the gamma ray, neutron-density porosity, and resistivity measurements. Based on the interpretation of this first run, the initial pressure and fluid sampling locations can be determined. The FT is typically sent downhole as part of a second or third run to sample those locations of interest. Advanced FT equipped with a DFA module take pressure measurements to determine both formation pressure and to confirm the sampling probe has a good seal with the reservoir rock. Fluid is then drawn into the FT.

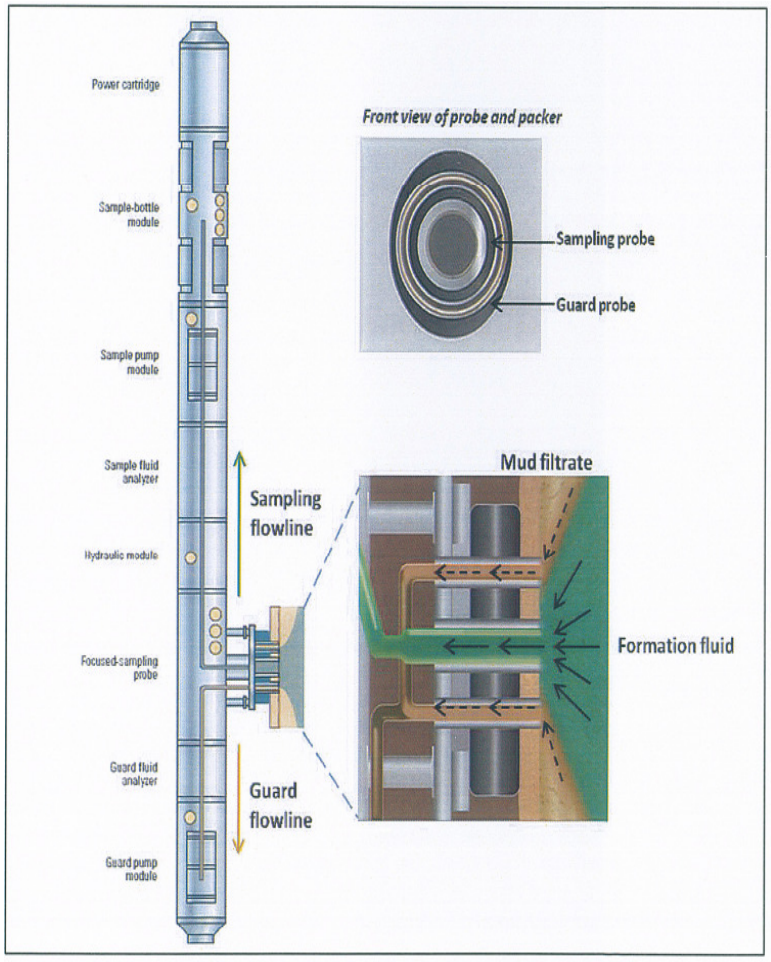

Figure 3.2: Advanced FT showing sampling tool.[20]

Plan and profile views of the FT tool, in this case Schlumberger's Modular Dynamic Tester (MDT) with a focused sampling probe, are shown in Figure 3.2.

A brief summary of the equipment utilized to measure pressure, fluid density and viscosity, and the optical density is provided here and the theory and concept for those measurements are provided later in Sections 3.3, 3.4, and 3.5, respectively. Pressure measurements are acquired with strain and quartz gauges which can obtain measurements with resolutions of 0.1 and 0.003 psi, respectively. The compensated quartz gauge (CQG) operates simultaneously in two modes which minimize thermal transient effects. One mode is more pressure sensitive and less temperature sensitive, and the other mode is more temperature sensitive and less pressure sensitive. Real-time fluid density and viscosity are determined by an oscillating mechanical sensor (D-V Rod) in the DFA module shown in Figure 3.3.

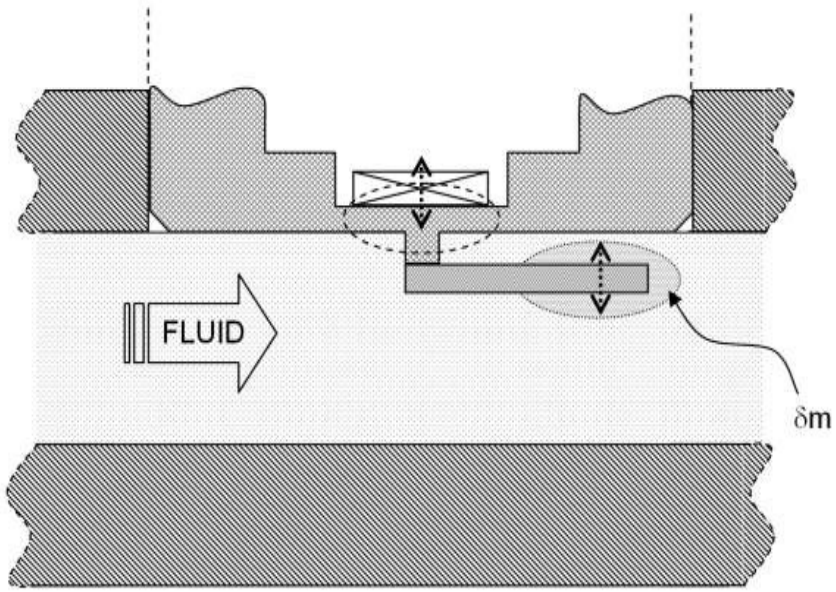

Figure 3.3: Schematic of the D-V Rod sensor in the DFA module. [21]

The D-V Rod operates in two different resonant frequencies to minimize effects of temperature and pressure[11]. Typical density measurement resolution is 0.01 g/cm3 and typical viscosity measurement resolution is 0.01 cp. For the OD measured with downhole spectroscopy, a focused sampling probe is shown in Figure 3.2. Fluid that

is drawn in by the guard probe is more likely to be contaminated with OBM and is pumped through the guard flowline, past the guard OFA and then pumped back out of the tool. As shown in Figure 3.4, the formation fluids are pumped past a tungsten light source in the OFA, and the light source is split into a source path and a measure path. The source light path bypasses the fluid and is used as a reference while the measure light path is routed through the fluid and is then recombined with the source path. The combined path is then split into discrete wavelength intervals, or channels, which are then measured at a photo detector. Depending on how the light attenuates for certain channels, several fluid properties can be inferred.

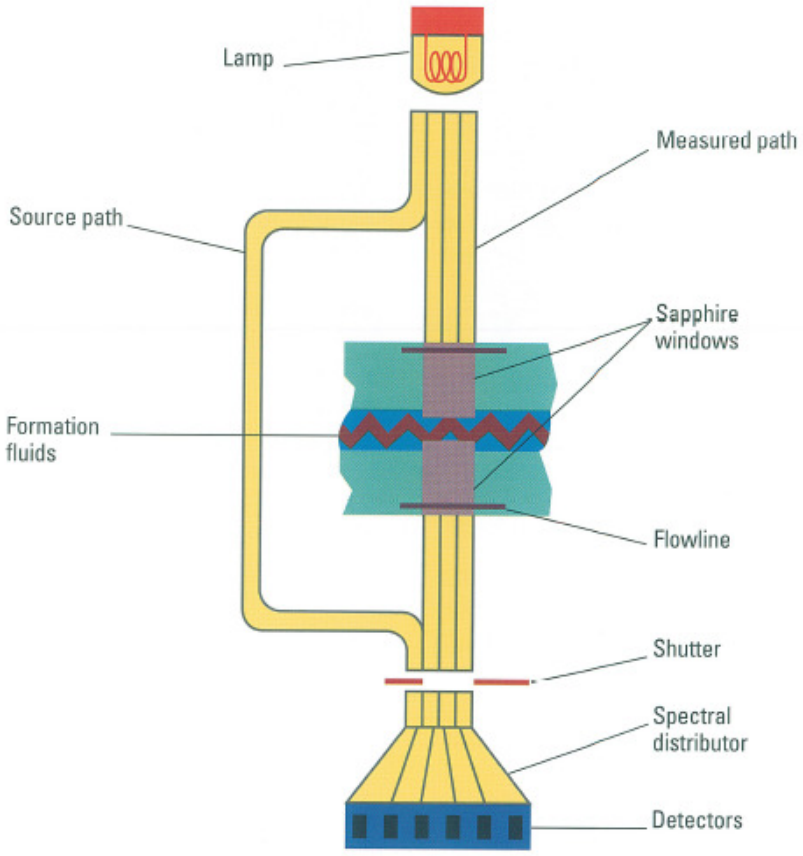

Figure 3.4: Optical fluid analyzer (OFA) used in an advanced FT. [19]

Although tools that are DFA-enabled rely on the same basic concept of measuring the attenuation of light through fluid, the technology has been constantly evolving over time and has expanded to include a suite of measurements. For this project, the Live Fluid Analyzer (LFA) and Insitu Fluid Analyzer (IFA) were utilized as part of FT operations. The LFA is an earlier generation tool which is capable of providing contamination monitoring by comparing the optical channels which are indicative of methane to the channels which are indicative of color. The LFA with a single probe was used to log M1. The IFA is a third generation DFA tool which in addition to contamination monitoring provides hydrocarbon composition, density, and viscosity measurements among several other measurements. The IFA with a dual packer was used to log M2 and M3. The MDT is fully modular so depending on the sampling location and the formation rock and fluid, the tool can be configured with or without the DFA module, in a number of ways as shown in Figure 3.5.

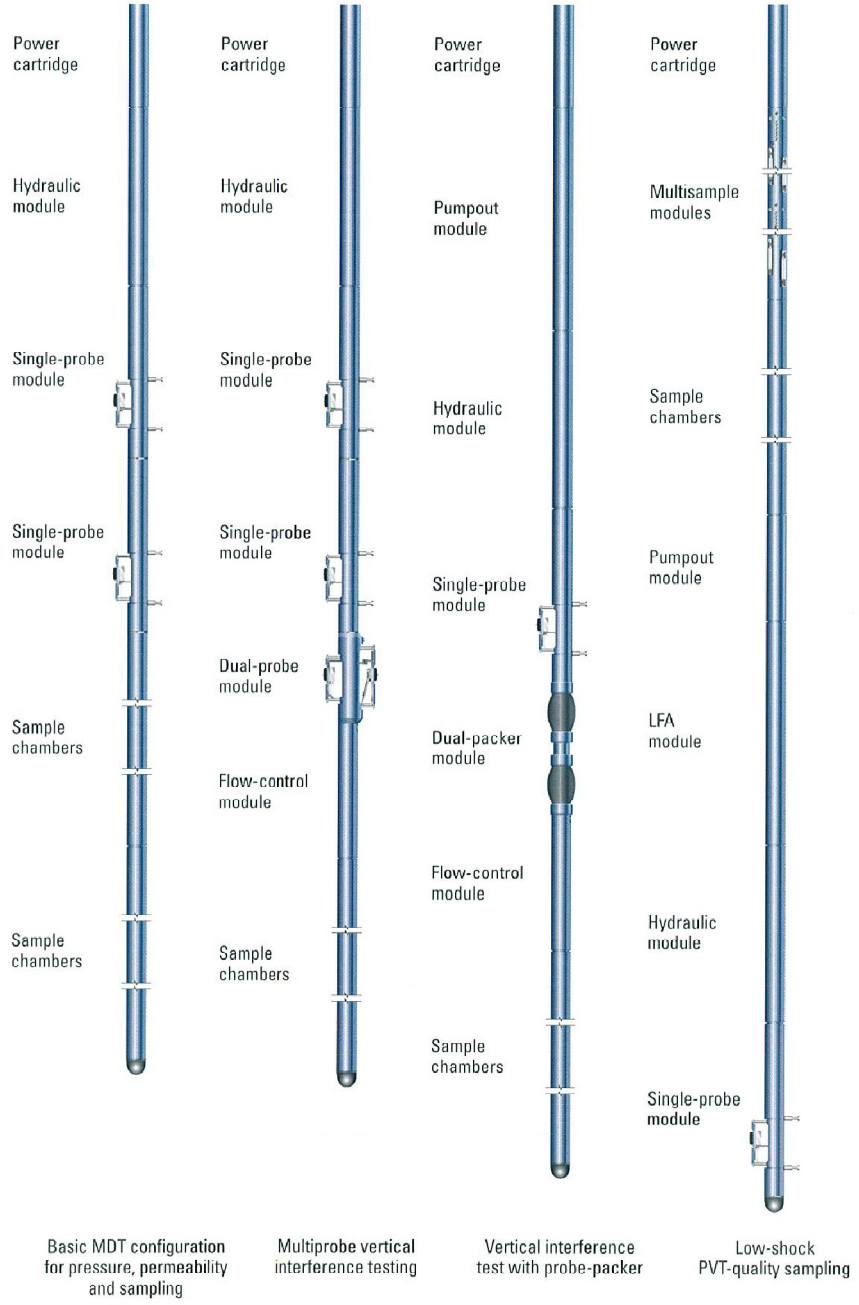

Figure 3.5: Different configurations of an advanced FT sampling tool.[19]

In addition to the real time contamination monitoring or real-time fluid property determination, depending on the objectives of the sampling program, a

sample can be captured and brought to the surface to be sent off for laboratory analysis which can then be compared to the DFA measurements for quality assurance purposes. The theory and concept for the pressure, fluid density and viscosity, and OD measurements determined from downhole spectroscopy are explained in the following sections of this chapter.

3.3 Pressure

For determination of reservoir connectivity, the analysis begins with pressure and then the focus turns to fluid properties analysis. Typically, a FT is sent downhole as the second or third run during open hole logging operations. The sampling tool is set against the formation and a pressure measurement is taken over time. This "pretest" is performed to determine formation pressure and to verify seal integrity for subsequent fluid sampling operations. If the sampling tool fails to make a good seal with the formation rock, it is unlikely that a valid formation pressure or a representative fluid sample will be acquired as the pressure measurement will be affected by the hydrostatic pressure and drilling mud may significantly contaminate the fluid sample. A typical pretest and the information it provides is shown in Figure 3.6.

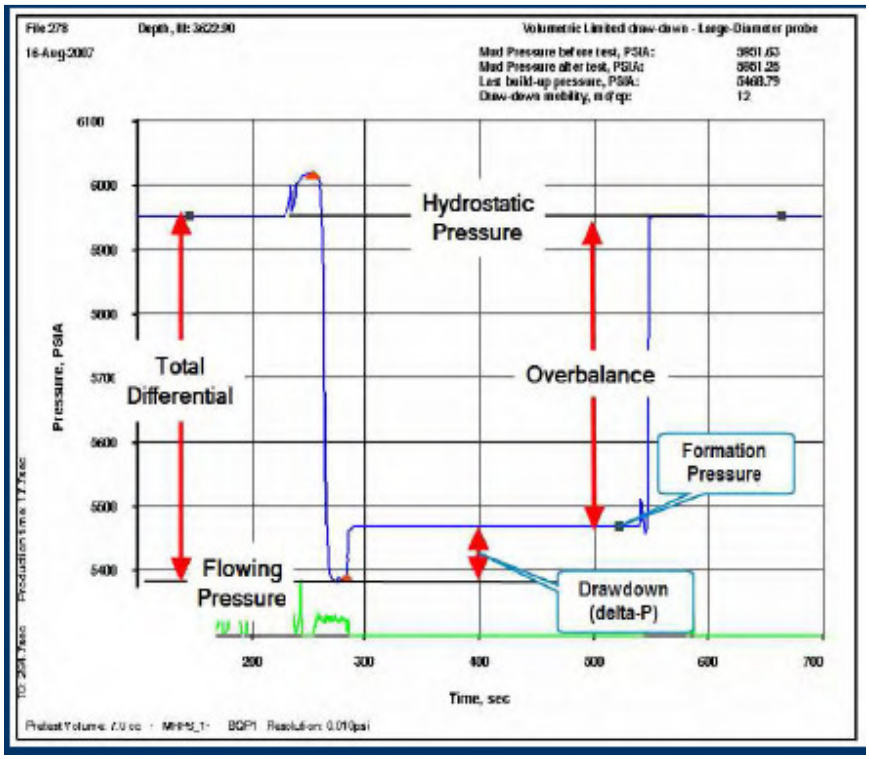

Figure 3.6: Characteristics of a typical pretest from FT operations.[22]

Starting at t=0s, the pressure observed is the hydrostatic pressure until the sampling tool is seated against the formation and a seal is created which is noted by the bump in pressure around t=250s. A pretest piston is withdrawn to a known volume, creating a pressure drop between the sampling tool and the formation which reduces the measured pressure to the flowing pressure observed at t=280s. The test continues with a buildup period which is shown from approximately t=280s to t=530s until the pressure stabilizes. Depending on the pressure response and the conditions encountered, the test procedure can be repeated to ensure the pressure reading comes from the actual formation response. The pressure test is then terminated by retracting the sampling tool, the seal between the sampling tool and the formation is broken, and the measured pressure returns to hydrostatic pressure.

For M1, a large diameter single probe was used due to the tight formation. For tight formations, a balance between the flow rate and the pressure drawdown must be achieved during sampling otherwise a constant flow rate or valid pressure response may not be acquired. The rate and volume of the fluid sampling can be adjusted in

the FT depending on what conditions are encountered downhole in order to obtain a valid pressure response and achieve the objectives for the sampling operations.

Darcy's Law which is shown in Figure 3.7 governs the relationship between pressure drawdown and fluid flow in a FT. From this relationship it is apparent that if all other variables are unchanged; if the sampling area is increased (as with the large diameter probe in M1), the required pressure drawdown can be reduced for a particular flow rate. Taking this approach a step further, an Interval Pressure Transient Test (IPTT) with dual packer, used for M2 and M3, serves to increase the sampling area even more than the large diameter probe used for sampling in M1.

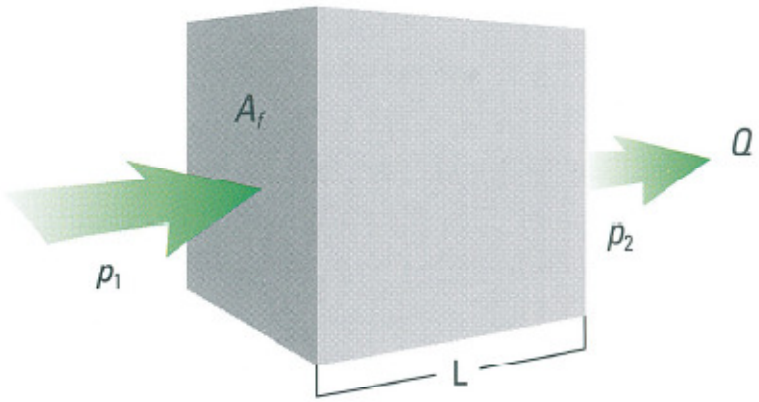

$$k = \frac{Q\mu * L}{A_f * p_2 - p_1}$$

k = 1 Darcy
Q = cm³/s
μ = cp
L = cm
A_f = cm²
$p_2 - p_1$ = atm

Figure 3.7: Darcy's Law.[19]

Under static conditions, pressure communication is required to infer connectivity, but is insufficient to establish whether the reservoir fluid will flow over a production time scale. The following sections will detail the theory and concepts for some of the measurements complementary to pressure which are utilized to determine connectivity.

3.4 Fluid Density and Viscosity

Fluid density and viscosity are important properties which impact a number of decisions including facility design and production strategies. While pressure gradients have traditionally been the method to determine fluid density, this approach can introduce some uncertainty as it requires some interpretation with picking pressure points to construct the gradient. This uncertainty is especially apparent in thin bed reservoirs which may not provide an adequate pressure survey across the formation. For this reason, a direct measurement of density provided by the D-V sensor in the IFA is useful. Density is inferred by measuring the resonance frequency of the vibrating rod which is in contact with the fluid in the FT flowline. The resonance frequency of the vibrating rod decreases as the fluid density increases. For the viscosity measurement with the D-V sensor, a physical model was developed which describes the elastic properties of the resonator and utilizes the Navier-Stokes equation to describe the flow around the resonator. The viscosity measurement is inferred from monitoring the decay of the resonance[21] and the sensor is characterized with standard reference fluids that cover a wide range of viscosity values. Typical viscosities of borehole fluids are 0.3 cp for water, 2-3 cp for diesel, 3-10 cp for oil and 0.015 cp for gas.

3.5 Optical Theory

DFA is a concept used to determine several fluid properties based on bulk optical spectroscopy over the visible and near infrared (Vis-NIR) range (300 nm to 2400 nm).[23-28] DFA utilizes downhole spectroscopy by measuring the transmittance (T_λ), of light, at a particular wavelength, through a fluid. Since transmittance can vary over a wide range, it is more convenient to use optical density (OD) which is determined from the equation below.

$$OD = \log (1/T_\lambda)$$

The OD is inversely proportional to the transmittance, so relatively high OD corresponds to relatively less light being transmitted through the fluid. The ODs over the Vis-NIR for several fluids are presented as absorption spectra and are shown in Figure 3.8. The absorption spectra is the OD sum of three components; scattering, molecular vibrational absorption, and electronic absorption.

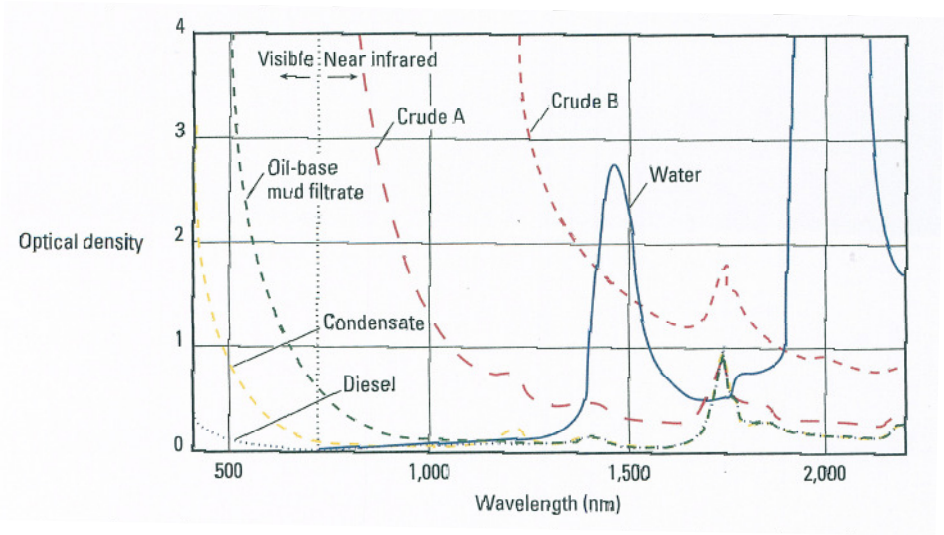

Figure 3.8: Absorption spectra for various fluids across the Vis-NIR. [19]

The contribution to the overall OD from the scattering of light occurs due to the solid particles, bubbles, or emulsions in the fluid that is pumped past the OFA. Scattering redirects light and tends to increase the OD but does not contribute to the absorption. Depending on the type of scattering, it may be accounted for and corrected. The molecular vibrational absorption is due to chemical bond resonance in which photons are absorbed at specific wavelengths. This absorption component provides a method to differentiate between oil and water since water has distinctive double absorption peaks at approximately 1450 nm and 2000 nm, while crude oils tend to have an absorption peak at approximately 1700 nm. The electronic absorption, or color, is a selective absorption process whereby the shorter wavelengths are absorbed first. Electrons from chemical compounds in the fluid absorb photon energy and change their energy state and light is converted to heat. Color, used in the context of this report is not necessarily red, blue, yellow, orange,

etc.; instead it is best described as a measure of the "lightness" or 'darkness' of the fluid. Research by Mullins[8] showed that petroleum fluids exhibit the exponential Urbach absorption tail (or absorption edge) and that asphaltenes were responsible for the electronic absorption edge shown in Figure 3.9. With increasing asphaltene concentration, more of the shorter wavelengths are absorbed causing the oil to be darker.

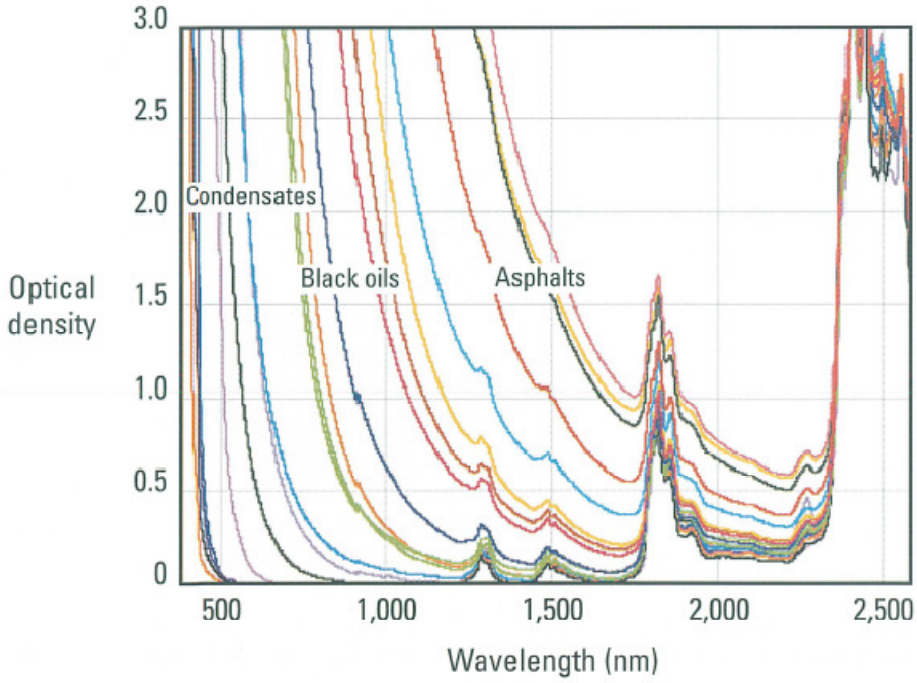

Figure 3.9: Urbach tails for several petroleum fluids.[19]

The absorption coefficient (α_λ) is a wavelength dependent property intrinsic to a particular material and is exponentially related to the ratio of the photon energy (h_w) to the Urbach decay width (E_o). The absorption coefficient is defined by the equation below and was determined for a wide range of petroleum fluid compositions.

$$\alpha = \alpha_0 \exp\left(\frac{\hbar\omega}{E_0}\right)$$

The transmittance (T_λ) can be determined by measuring the ratio of the intensity of light exiting the fluid to the intensity of light entering the fluid shown below.

$$T_\lambda = I_\lambda / I_{\lambda o}$$

Utilizing a known optical path length (L), the absorption coefficient can be determined from the measured transmittance acquired through real-time DFA operations using Lambert's Law shown in the equation below.

$$T_\lambda = 10^{-\alpha\lambda L}$$

Composition of the fluid can be inferred by comparing the calculated absorption coefficient to the range of absorption coefficients with known compositions.[29-31]

3.6 Optical Properties of Downhole Fluids

Downhole spectroscopy started off primarily as a method to monitor OBM contamination to ensure sample quality.[32,33] Later, improved wavelength resolution around the hydrocarbon peak shown in Figure 3.10 provided the ability to distinguish between the methane peak and the heavier oil peak. From the ratio of the oil peak to the methane peak, GOR can be inferred.

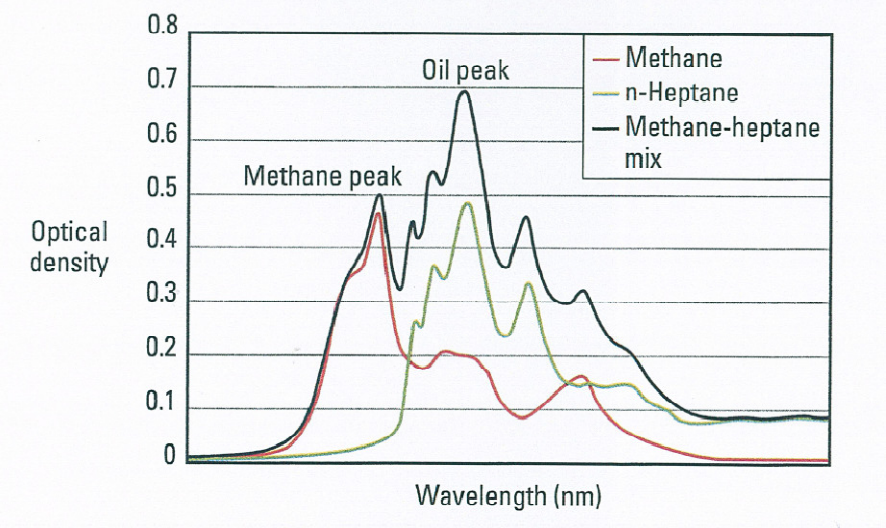

Figure 3.10: Absorption spectra showing the methane peak and oil peak.[19]

Since shorter wavelengths are absorbed first, only methane contributes to the methane absorbed at the oil peak. This same selective absorption process is related to the proportion of asphaltenes in the fluid and from this basic premise, the ratio of the oil peak to the methane peak can be used to predict the time required for 'clean up' which can be estimated by monitoring certain channels. The correction for OBM contamination is assessed by analyzing the color absorption and the methane molecular vibrational absorption. This approach is possible because it can be assumed that OBM contains no methane while reservoir hydrocarbon contains significant amounts of methane. When fluid initially is drawn into the sampling probe and pumped through the flowline past the OFA, the fluid contains a mixture of OBM and reservoir fluid. Over time the fluid from further away from the wellbore enters the flowline and the fraction of OBM in the flowline decreases and the methane content increases. The estimated time required is determined from the equation below.

$$ODm = ODm\_\inf - \frac{D}{t\text{^}(\frac{5}{12})}$$

OD_m is the difference between the OD of the methane channel and the OD of the oil reference channel. OD_{m_inf} is the OD of the methane channel if the fluid in the flowline was pure reservoir fluid and D is a constant. OD_{m_inf} and D are calculated by fitting the OD vs. time curve to this equation. Knowing the estimated time for the fluid in the flowline to 'clean up' aid the sampling operations and the estimation of the OBM contamination level allows for an OD correction for OBM. An example of this calculation is provided in Chapter IV Methodology.

For the laboratory samples, the time frame for correcting for OBM is obviously different than the real time OD correction. Since even minor mud filtrate contamination can have a significant impact on the thermodynamic properties of the reservoir fluid and introduces uncertainty into the EOS modeling that follows, an effort needs to be made to decontaminate the samples. OBM is miscible with the reservoir fluid; therefore a procedure of subtracting the mass of the mud oil from the reservoir oil can be used under certain conditions and with certain assumptions to determine a decontaminated composition of the sampled fluid. For this project, it is assumed that there is full miscibility between the OBM and the reservoir fluid and that the composition of the OBM is known. The basic premise behind decontamination of reservoir samples in the laboratory is that a decreasing exponential relationship exists for the C8+ portion of real petroleum fluids versus molecular weight. A semi-log plot of the C8+ compositional portion of a clean reservoir fluid sample versus molecular weight will yield a straight line. For a contaminated sample, there will be a deviation from this straight line over the range of components that are in common with the drilling mud composition.

There are two approaches to decontamination. The first is to "skim" the concentration of the contaminants that deviate from the semi-log straight line. The assumption is that the fitted line can be used to determine the composition of the uncontaminated fluid. For the skimming method, the specific composition of the drilling mud is not required but it should only be used with drilling muds that are known to have a narrow range composition. The second approach is the subtraction method. For this method, a certain amount of drilling mud with a known composition is subtracted from the contaminated sample. The C8+ portion of the resulting composition is then used to fit an exponential distribution function. The procedure is

repeated for different levels of drilling mud contamination and the composition which provides the best fit to the exponential distribution function is determined to be the uncontaminated reservoir fluid. Decontamination procedures were performed for the laboratory samples in Chapter IV Methodology.

3.7 Asphaltenes

Asphaltenes are the solid component of crude oil and until recently little was known about their size and structure. The Yen-Mullins model provided a breakthrough in describing the size and structure of asphaltenes and the corresponding chemistry and physics governing asphaltene behavior. Asphaltenes are not large molecules; instead asphaltenes are monomers which, depending on asphaltene concentration, will group with other asphaltene molecules to form nano-aggregates and at even greater concentrations, nano-aggregates will group to form clusters. Asphaltene size and structure according to the Yen-Mullins model is shown in Figure 3.11.

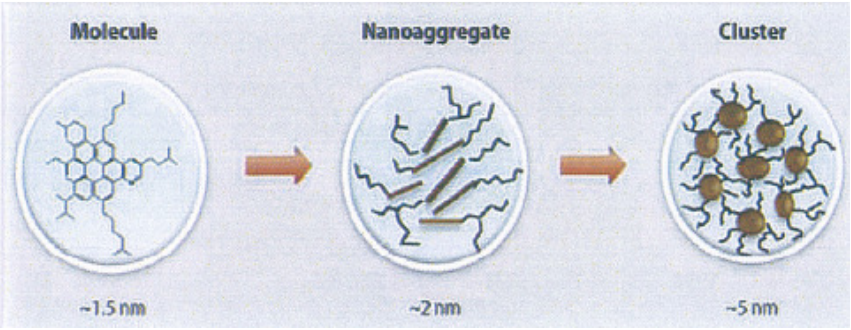

Figure 3.11: Asphaltene size and structure based on the Yen-Mullins model.[5]

The type of asphaltene found in the reservoir fluid is closely tied to the type of petroleum fluid found in the reservoir. Asphaltenes found as molecules are indicative of condensate reservoirs, asphaltenes found as nano-aggregates are indicative of black oil reservoirs, and asphaltenes found as clusters are indicative of heavy oil reservoirs.

When hydrocarbon is generated in the source rock, the heavy components such as asphaltenes are the first to evolve and start the migration from the source rock

to the reservoir. Although asphaltenes are the first components to migrate to the reservoir they have by far the lowest diffusivity constant among all hydrocarbon components. From knowing the size and structure of asphaltenes and their subsequent mixing behavior, an analysis of the asphaltene gradient can provide information about reservoir connectivity.

3.8 Asphaltene Gradients

Since this study analyzes asphaltenes in an oil column it is useful to discuss asphaltenes in terms of a gradient. It has been observed that asphaltene gradients grade continuously in an oil column which is in fluid equilibrium [5]. Density is the driving force in the oil and gas column so asphaltenes as the heaviest component in crude will tend to settle respectively lower in the column. Therefore, with increasing depth it is expected that asphaltene concentration increases and OD which is directly related to the asphaltene concentration, will increase with depth. While a continuous asphaltene gradient is not definite proof of fluid equilibrium a considerable amount of fluid flow has to occur and existence of a continuous asphaltene gradient is another clue and would lend support to the case that the reservoir fluids are in equilibrium.[5]

3.9 Flory-Huggins-Zuo Equation of State

Cubic equations of state (EOS) such as the Peng-Robinson EOS have traditionally been used to describe hydrocarbon fluid equilibrium. However, cubic EOSs are only able to address the liquid and gas equilibrium and are unable to account for the solid components in crude such as asphaltenes. The Flory-Huggins-Zuo (FHZ) EOS was developed to account for the effect that asphaltenes have on fluid equilibrium in the oil column.[34] The left hand side of the equation is the color gradient or OD gradient at a particular wavelength. The first term on the right hand side of the equation is the solubility term, the second term is the gravity term, and the third term is the Flory-Huggins entropy term.

$$\frac{OD(h_2)}{OD(h_1)} = \frac{\phi_a(h_2)}{\phi_a(h_1)} = \exp\left\{\frac{v_a}{RT}\left[(\delta_a - \delta)^2_{h_1} - (\delta_a - \delta)^2_{h_2}\right]\right\} \exp\left\{\frac{v_a g(\rho - \rho_a)(h_2 - h_1)}{kT}\right\} \exp\left\{v_a\left[\left(\frac{1}{v}\right)_{h_2} - \left(\frac{1}{v}\right)_{h_1}\right]\right\}$$

R, ϕ, v, δ, k, T, g, ρ, and h are the universal gas constant, volume fraction, molar volume, solubility parameter, Boltzmann constant, temperature, gravitational acceleration, density, and depth, respectively. The different contributing terms that make up the FHZ can play a relatively larger role at different locations in the oil column or in different fluid types. The gravity term and the entropy term tend to increase the asphaltene gradient while the solubility term tends to decrease the asphaltene gradient. Recall that asphaltenes are not soluble in lighter components which would be indicative of higher GOR. For this project, waxy low GOR fluids were encountered and therefore, the solubility term has a negligible effect on the gradient and the gravity term dominates. From the fluid properties acquired with DFA, the FHZ EOS can be used to predict the OD at different depths.

3.10 Reservoir Connectivity

An interpretation of reservoir connectivity is based on all the available information. Within this context, the asphaltene gradient determined from the ODs after correcting for baseline and OBM contamination can be compared to the predicted asphaltene gradient from the FHZ EOS. The predicted asphaltene gradients can be generated based on the type of asphaltene and corresponding asphaltene diameter (molecule = 1.5 nm, nano-aggregate = 2 nm, or cluster = 5 nm) as shown in Figure 3.12.

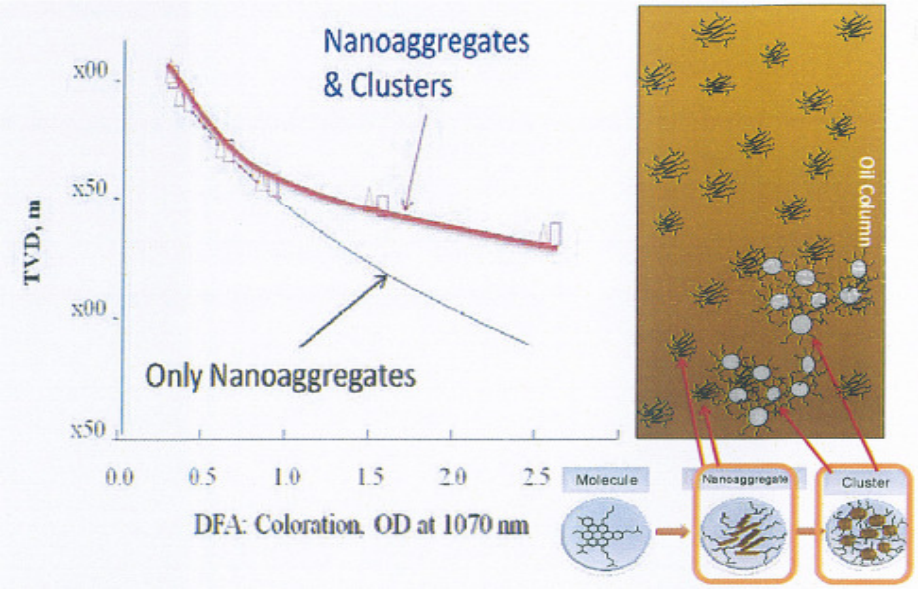

Figure 3.12: Predicted asphaltene gradients for different asphaltene sizes.[5]

If the measured ODs fit on the predicted FHZ EOS gradient, then the reservoir has a higher probability of being connected.

CHAPTER IV

METHODOLOGY

The objective of the study is to implement a workflow using pressure and fluid property data to determine connectivity in a sand common to Wells M1, M2, and M3. The latest geological interpretation is that M1 and M2 are connected but that a flow barrier of some kind separates M3 from the other wells as shown in Figure 4.1.

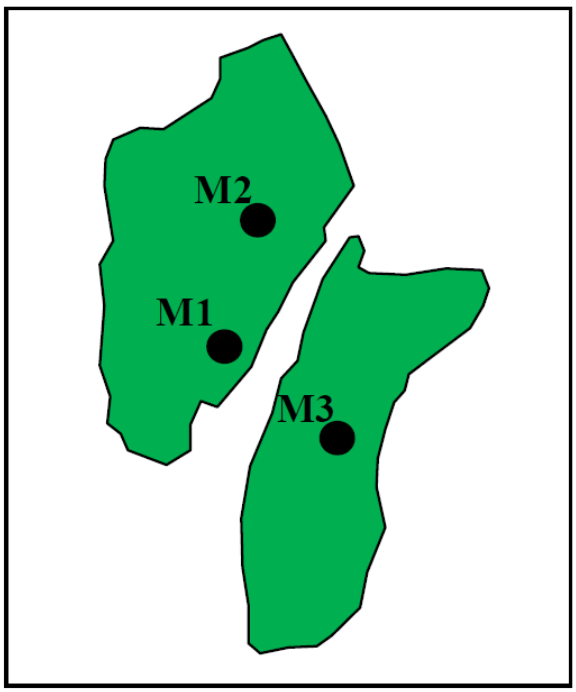

Figure 4.1: Areal map of M1, M2, and M3.

The stratigraphic map shown in Figure 4.2 depicts the connection of Sand F between M1 and M2. Outside the scope of the figure and visualizing in three dimensions, Sand F slopes downward from M1 and M2 to M3.

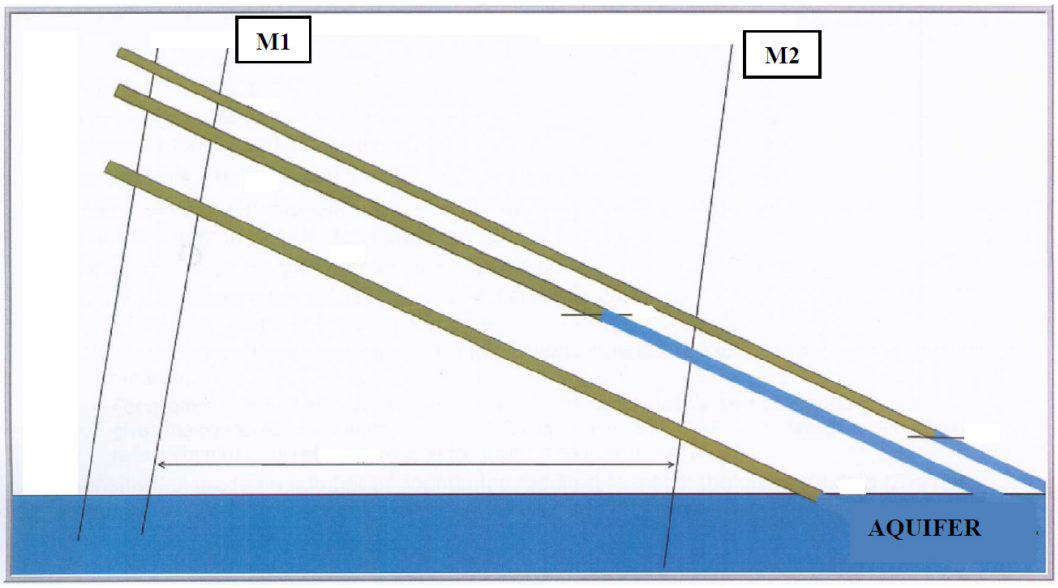

Figure 4.2: Stratigraphic map showing thin beds sands in relation to M1 and M2.

As described in Chapter III Theory and Concept, if the fluid in Sand F is in equilibrium, wells which intersect Sand F have a higher likelihood of being in fluid connection. The OD of a reservoir with fluid equilibrium should increase with depth in the oil column. Therefore, for this project, if the reservoir is connected one should observe the OD increasing with depth from M1 to M2 to M3.

The methodology used to determine connectivity is described as follows: The available pressure and fluid data was listed in an inventory which distinguished the data with respect to location and depth. In the Preparation of Data section, the pressure and fluid data was reviewed to assess sample validity and a description of the procedure for preparing the DFA and laboratory data for subsequent modeling was provided. The methodology is described in greater detail in the following sections and a summary of the steps based on the methodology is provided at the end of this chapter.

4.1 Inventory of Data

Incorporating the latest geological interpretation which shows thinly bedded sands that are steeply sloping, all the available data from DFA operations as well as PVT laboratory results were used to arrive at a final interpretation. M1 was the first

well to be drilled and was logged with an earlier generation DFA tool, the Live Fluid Analyzer (LFA). Large diameter sampling probes were utilized for sampling in all three wells due to the anticipated low permeability of the formation. M2 and M3 were logged with a new generation DFA tool, the Insitu Fluid Analyzer (IFA). The IFA runs in M2 and M3 utilized a dual packer configuration to perform an Interval Pressure Transient Test (IPTT). Samples from Sand F for all three wells were sent away for lab analysis and are available for comparison. A summary of the data available is provided in Table 4.1.

Table 4.1: Summary of data available for Sand F.

Well and Station	Relative TVDSS (ft)	DFA tool	Equipment	Pressure Operations	PVT?
M1 Station 83	291	LFA	Large diameter single probe	Pretest	YES
M2 Station 136	1004	IFA	Large diameter probe, dual packer	Pretest, IPTT	YES
M3 Station 18	1889	IFA	Large diameter probe, dual packer	Pretest, IPTT	YES

4.2 Preparation of Data

The preparation of data was performed in the same sequence as it was acquired, from M1 to M2 to M3, and was broken down into five main steps:

1. Discuss sampling conditions, equipment, and location of samples in relation to each other.
2. Assess the validity of the sample from the pretest.
3. Plot OD versus time to determine if the sample was representative of the reservoir fluid.
4. Describe the procedure to correct the OD for baseline and OBM contamination so that the OD could be compared from well to well.
5. Describe the decontamination procedure for the laboratory samples.

4.2.1 M1 Station 83

Figure 4.3 shows an interval with a typical first run 'triple combo' including a Gamma Ray measurement in Track 1, Neutron/Density measurements in Track 2, and a Resistivity measurement in Track 3. The subsequent DFA log was depth-matched with the triple combo log and they were presented together including a pressure survey in Track 1, drawdown mobility calculation in the depth track, and OD measurements in Track 4.

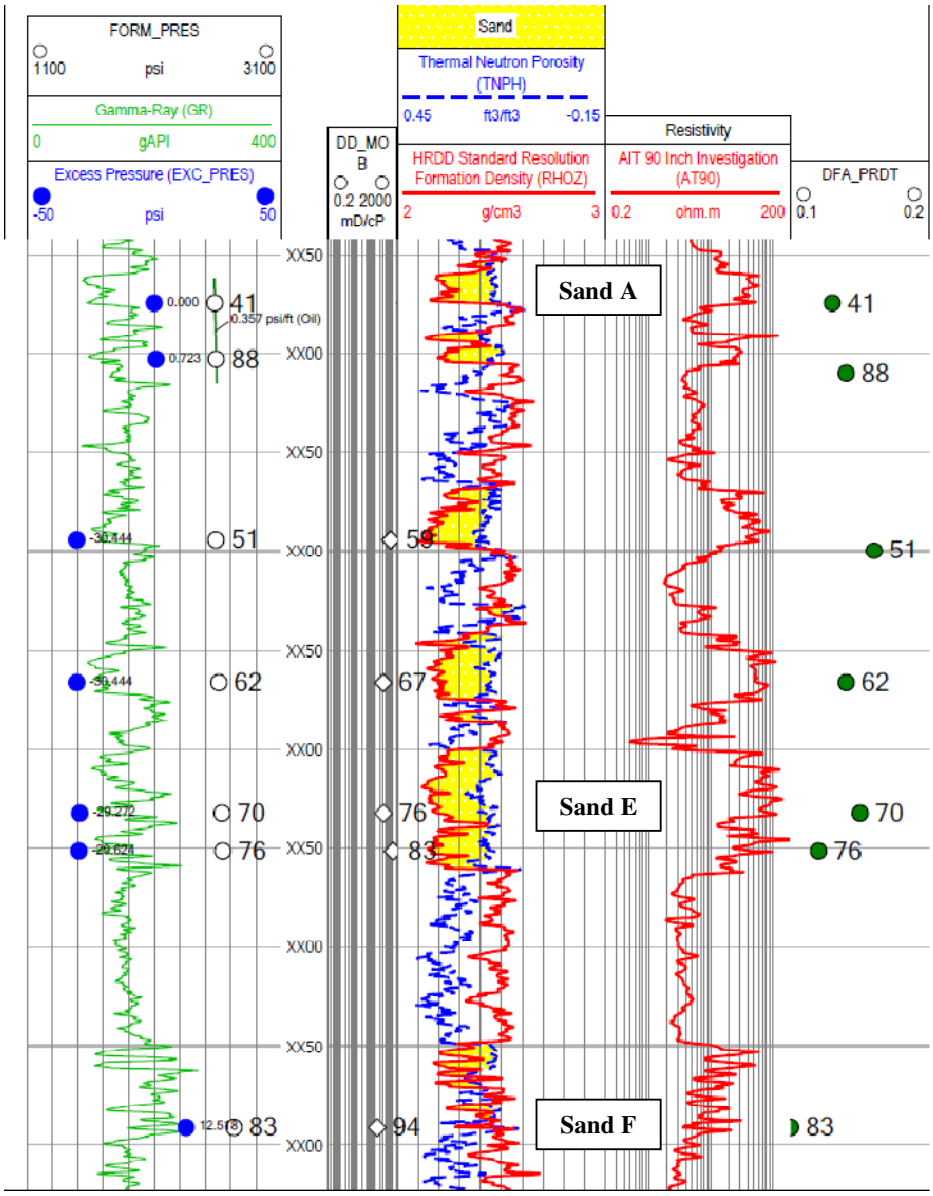

Figure 4.3: M1 Station 83 log interval.

This interval for M1 includes several thin bedded sands which are shown to provide context for the subsequent analysis of M2 and M3 which may or may not include those sands. The focus of this study is to assess the connectivity of the bottom zone, Sand F, between wells M1, M2, and M3 from the given data. For Station 83 in M1, the characteristics observed in the pretest shown in Figure 4.4 indicate that the formation is tight. However, a valid pretest was acquired as the pressure eventually stabilized. The formation pressure was determined to be 2738 psi from the stabilized pressure reading after approximately 2300 s.

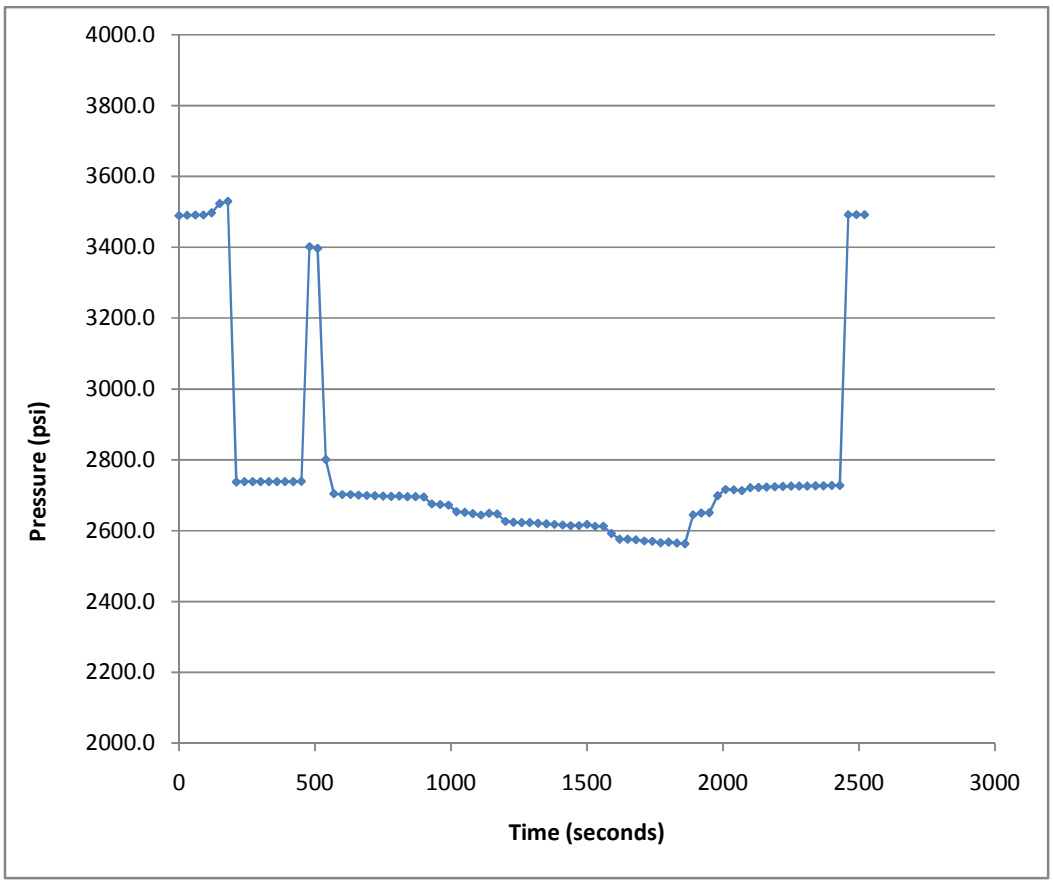

Figure 4.4: M1 Station 83 pretest.

During the pressure drawdown, fluid was pulled into the FT and oil was detected as 12 liters of fluid were pumped through the flowline past the LFA. Figure 4.5 shows the OD recorded over time during LFA sampling operations. The channels that exhibit relatively high ODs (>3) would be indicative of channels that correspond

to shorter wavelengths and these wavelengths are completely absorbed. In most cases, the fluid that is initially going past the analyzer will be highly contaminated with OBM and it is possible that all channels will exhibit 'highly absorbing' behavior. However, over time the channels which are indicative of longer wavelengths will show a reduction in OD and this can be observed after approximately 1100 s.

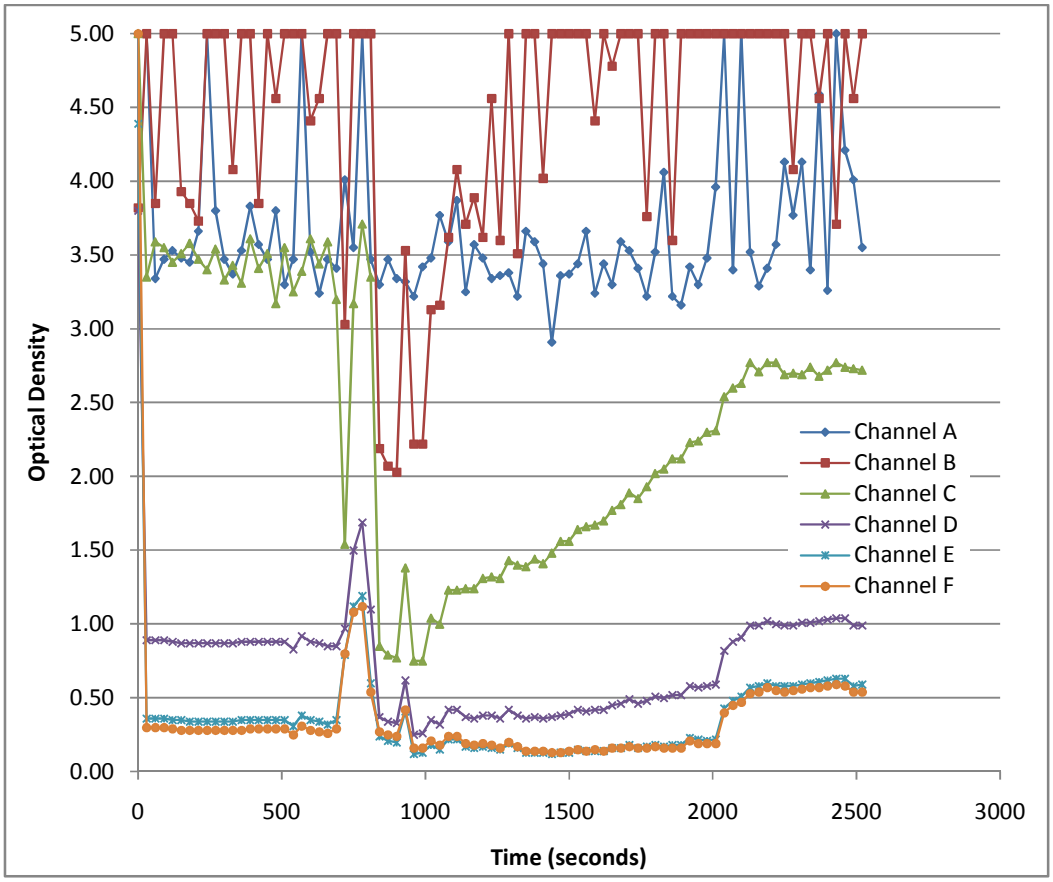

Figure 4.5: M1 Station 83 OD vs. Time

The fluid that is pumped past the analyzer 'cleans up' as mud filtrate is replaced with reservoir fluid. An increasing fraction of reservoir hydrocarbon is confirmed by the steady rise from t=1000 s to 2000 s observed in a channel which is indicative of methane content. Since OBM does not generally contain methane this would not be typical of mud filtrate. When the OD of the channels corresponding to color stabilized, a sample was taken. Several fluid properties can be inferred from the

measured optical properties and these fluid properties are summarized for all three wells in Table 4.5.

The wells analyzed in this project were logged with different generations of DFA technology (LFA and IFA) and the OD acquired in each of the wells needed to be compared to assess connectivity. Although the LFA and IFA have many similarities, a technological improvement in the IFA aimed at obtaining higher resolution over the wavelength range around the hydrocarbon peak resulted in a shifting of some of the channels. Therefore, it was necessary to process all of the ODs that were subject to comparison. The LFA ODs needed to be adjusted with an LFA baseline OD and the IFA ODs needed to be adjusted with an IFA baseline[13]. For all the wells, OD measurements based on a common wavelength were compared. For M1, DFA operations acquired an OD = 0.51. The baseline correction equation is shown below.

$$ODbaseline\ corrected = OD\lambda - ODbaseline$$

In addition to the baseline corrections, the OD had to be adjusted for the OBM contamination[13] as the level of contamination was different in each sample. Analysis of the OD vs. Time plot shown on Figure 4.5 indicated that the fluid flowing past the LFA cleaned up rather quickly, however the contamination of the sample turned out to be relatively high. Although sampling equipment and techniques are constantly evolving and have generally resulted in lower contamination levels and reduced sampling times, the downhole environment can be harsh and unpredictable and can still occasionally result in samples with elevated contamination due to a number of factors. Elevated contamination levels introduce a higher level of uncertainty into subsequent modeling so an effort should be made to obtain samples with contamination levels as low as possible and to correct the ODs for OBM contamination when comparing the ODs. The OBM correction equation is shown below.

$$OD\ obm\ corrected = \frac{ODbaseline\ corrected}{(1 - \text{OBM contamination})}$$

This OD from M1 corrected for baseline and OBM contamination was used as the starting point for the FHZ EOS modeling which was then used to predict the OD in M2 and M3.

Turning to the analysis of the M1 Station 83 sample that was sent off for PVT analysis, some of the key parameters from the laboratory results used in the PVT model are listed in Table 4.2.

Table 4.2: M1 Station 83 summary of key data from laboratory analysis.

Reservoir Conditions		
Res. Temperature	119	C
Res. Pressure	2738	psia
Saturation Conditions		
Sat. Temperature	119	C
Sat. Pressure	485	psia
Sat. Fluid Density	0.779	g/cm^3
MW	151	lb/lbmol
Single Stage Flash to Stock Tank Conditions		
ST Temperature	15.6	C
ST Pressure	14.7	psia
STO Density	0.8305	g/cm^3
Bo	1.08	
GOR	68.5	SCF/STB
MW of Plus Fractions		
C7+ =	169	lb/lbmol
C12+ =	177	lb/lbmol
C20+ =	340	lb/lbmol
C30+ =	436	lb/lbmol

For the laboratory samples, the component compositions up to C30+ were entered into the PVT model. Estimated molecular weights (MW) for the components could be entered automatically in the PVT model based on the Katz and Firoozabadi 1978 (KF) or the Whitson 1983 conventions. KF was chosen as the default for all the samples analyzed in this project; however, the MW of certain plus fractions (C7+, C12+, C20+, and C30+) were determined in the laboratory. For those cases, the laboratory MWs were used. In addition, since the KF MWs between the laboratory determined plus fractions (C8, C9, C13, C14, C21, C22, etc.) would no longer apply, those plus fractions were determined from interpolation of the laboratory determined plus fractions. For the sample at M1 Station 83, the plus fractions determined in the

laboratory as well as the interpolated compositions are provided in the initial contamination studies performed in Chapter V Results and Discussion. The plot of the composition of the downhole sample taken at Station 83 is shown in Figure 4.6. The OBM contamination in this sample is evident from the hump in composition from C11 through C15.

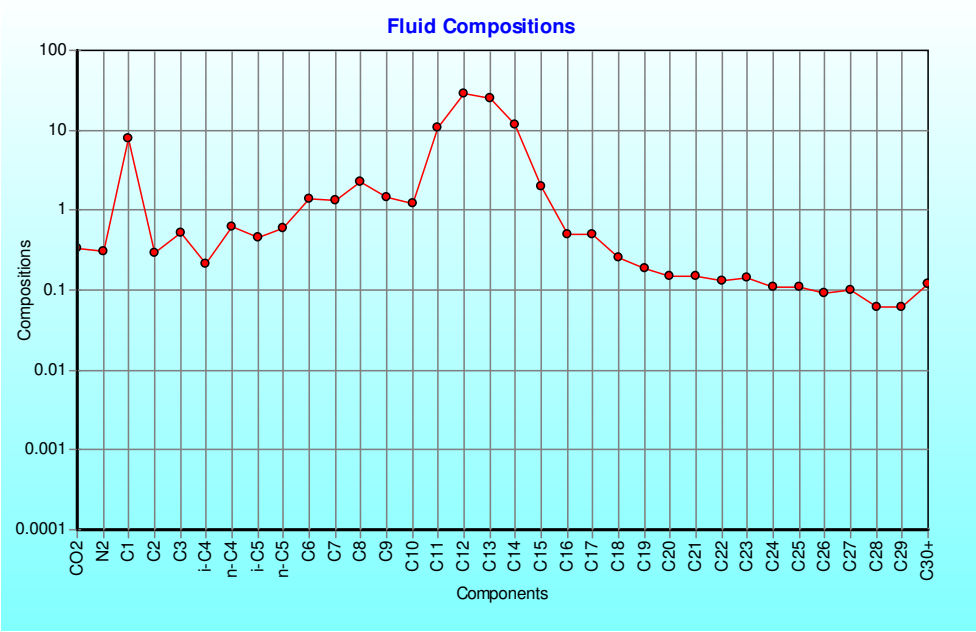

Figure 4.6: M1 fluid composition (mol%) before initial contamination study.

Based on the level of contamination, composition of the contaminated reservoir fluid, and the composition of the drilling mud, an initial contamination study can be generated in the PVT analysis which shows the calculated composition of the 'uncontaminated fluid.' Note that 'uncontaminated fluid' is just a term used in the PVT model to describe this calculated composition. If this initial contamination study still shows significant contamination for the 'uncontaminated fluid,' additional decontamination steps are required before modeling. After the initial contamination study, the additional steps required for decontamination are:

1. Group the OBM composition as a mud pseudo component and determine properties of the pseudo component such as critical temperature and critical pressure, etc.

2. Create a new sample that contains the mud pseudo component from Step 1 along with the composition of the original sample.
3. Adjust the composition of the 'uncontaminated fluid' components by the mol% of 'uncontaminated fluid' determined from the initial contamination study. Adjust the mud pseudo component from Step 2 by the mol% contamination determined from the initial contamination study. The sum (mol %) of the adjusted uncontaminated fluid components and the mud pseudo component should be 100%.
4. Characterize and tune the combined composition determined in Step 3 so that the resultant phase envelope fits the available experimental data.
5. Set the mud pseudo component mol% to zero and re-normalize the sample composition. The resulting composition models the sample as if it was free of OBM contamination and is considered 'decontaminated.' The decontaminated sample should not be re-characterized, that way the decontaminated fluid EOS is the same as the contaminated fluid EOS.
6. The decontaminated sample should be tuned again with the experimental data available. The decontaminated sample is then ready for modeling.

The PVT model used for this study provides 3 distribution functions and 6 property correlations that can be tried in a number of different combinations to characterize the contaminated sample and generate a phase envelope which best describes the fluid at different pressures and temperatures and fits the experimental data. The choices of distributions are:

1. Exponential (Pedersen, 1988)
2. Three Parameter Gamma (Whitson, 1988)
3. Modified Pedersen Exponential (DBR, 2001)

The choices of property correlations are:

1. Pedersen et al. (1988) for Tc, Pc & ω
2. Riazi and Daubert (1980) for Tc& Pc, Thomassen (1986) for ω
3. Lee-Kesler (1976) for Tc, Pc & ω
4. Cavett (1964) for Tc& Pc, Edmister (1958) for ω
5. Lee-Kesler (1976) for Tc& Pc, Edmister (1958) for ω
6. Twu (1984) for Tc& Pc, Lee-Kesler (1976) for ω

Lumping of the defined components (mud pseudo component, CO2, N2, C1-C6) and lumping of the C7+ fractions can then be specified. For this project, the defined components were not lumped and the C7+ fractions were lumped into 3 pseudo component groups (C7-C15, C16-C25, and C26-C80). A set of critical properties, interaction parameters, and compositions were then generated based on the

chosen distribution, correlation, and lumping configuration. However, these initially determined values required tuning with experimental data before they were accepted as being representative of the contaminated sample.

Model tuning is an iterative process and for this project it involved first adjusting the interaction parameters of the lumped plus fractions to fit the saturation pressure and temperature and then adjusting the volume translation to fit the oil density. The interaction parameters update after each iteration until, ideally, the calculated saturation pressure equals the experimental saturation pressure. The iterative tuning process is then repeated by adjusting the volume translation of each of the 3 lumped plus fraction pseudo components until, ideally, the calculated oil density equals the experimental oil density. The results of the characterization and tuning procedures described are provided in Chapter V Results and Discussion.

4.2.2 M2 Station 136

Further down dip in Sand F, Figure 4.7 shows the log interval for M2. DFA Station 136 was acquired in Sand F using the IFA, and an IPTT was conducted which utilized a dual packer with a large diameter probe to pump out approximately 177 liters of fluid identified as oil past the fluid analyzer. For M2 Station 136, the pressure response in the tight formation could be observed from the IPTT which is shown in Figure 4.8.

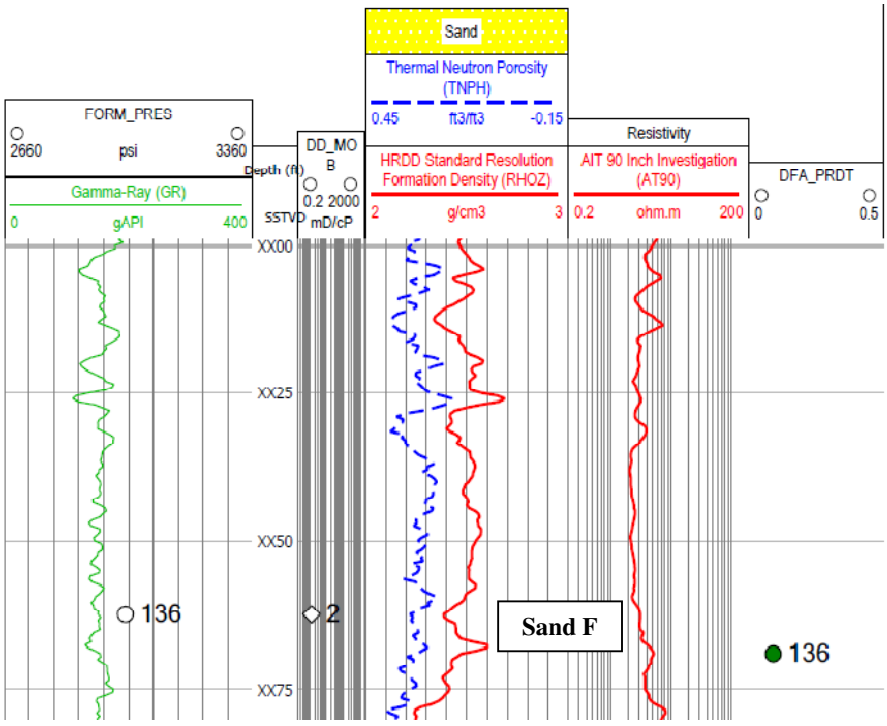

Figure 4.7: M2 Station 136 log interval.

As part of a pressure survey from an earlier run, several valid pretests were acquired and the formation pressure determined from the IPTT was 2978 psi.

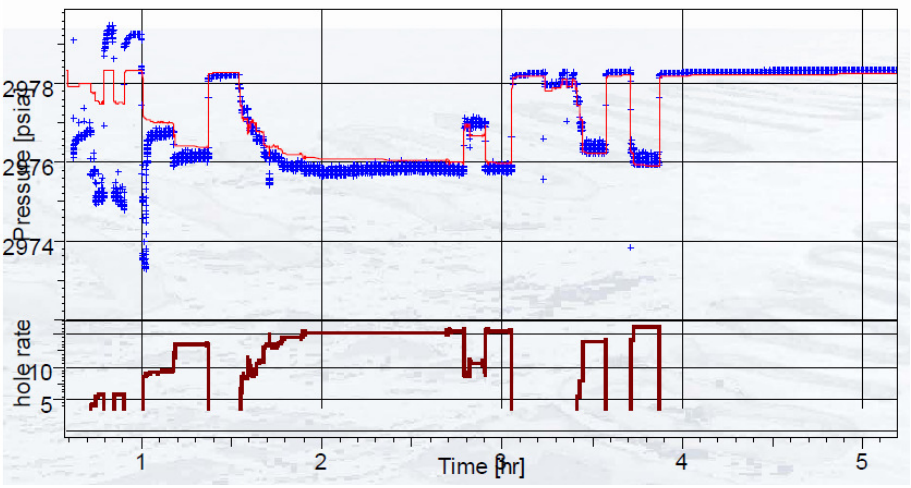

Figure 4.8: M2 Station 136 pressure response from IPTT.

Analysis of the OD vs. Time plot shown in Figure 4.9 indicated that the fluid flowing past the LFA began to clean up after t = 4000 s.

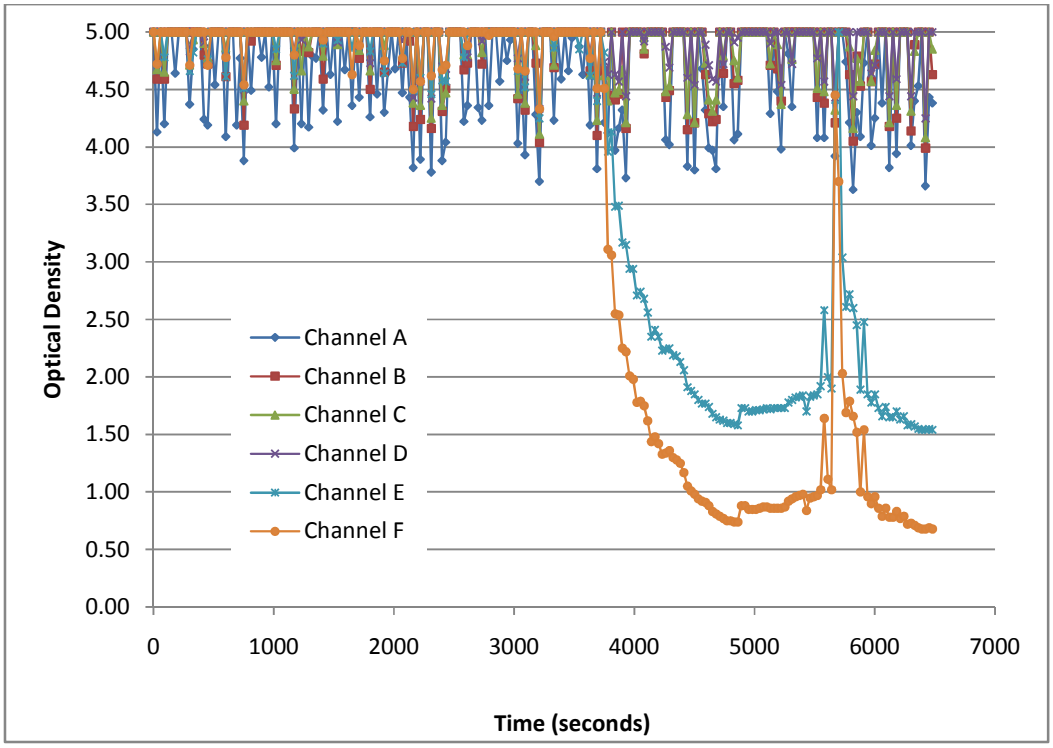

Figure 4.9: M2 Station 136 OD vs. Time.

For M2, DFA operations acquired an OD = 1.55. Corrections for baseline and OBM contamination are provided in Chapter V Results and Discussion.

Turning to the analysis of the M2 Station 136 sample that was sent off for PVT analysis, some of the key parameters from the laboratory results are listed in Table 4.3.

Table 4.3: M2 Station 136 summary of key data from laboratory analysis.

Reservoir Conditions		
Res. Temperature	128	C
Res. Pressure	2978	psia
Sample Properties		
ST Temperature	15.6	C
ST Pressure	14.7	psia
ST Fluid Density	0.8905	g/cm^3
MW	225	lb/lbmol
MW of Plus Fractions		
C7+ =	96	lb/lbmol
C12+ =	161	lb/lbmol
C20+ =	275	lb/lbmol
C30+ =	461	lb/lbmol

The same steps that were detailed in the preparation of the laboratory data for M1 Station 83 were followed for M2 Station 136. Similar to M1, the MW of certain plus fractions (C7+, C12+, C20+, and C30+) were determined in the laboratory so for those cases, the laboratory MWs were used in the model as well as the interpolated MWs (C8, C9,...C13, C14,…C21, C22,…etc.) calculated from the laboratory determined plus fractions. For the sample at M2 Station 136, the plus fractions determined in the laboratory as well as the interpolated compositions are provided in the initial contamination study shown in Chapter V Results and Discussion. The plot of the composition of the downhole sample taken at Station 136 is shown in Figure 4.10. Although the contamination is much lower than observed in the plot of the sample composition for M1 Station 83, the OBM contamination for the sample at M2 Station 136 was still evident from the slight hump in composition from C11 through C15.

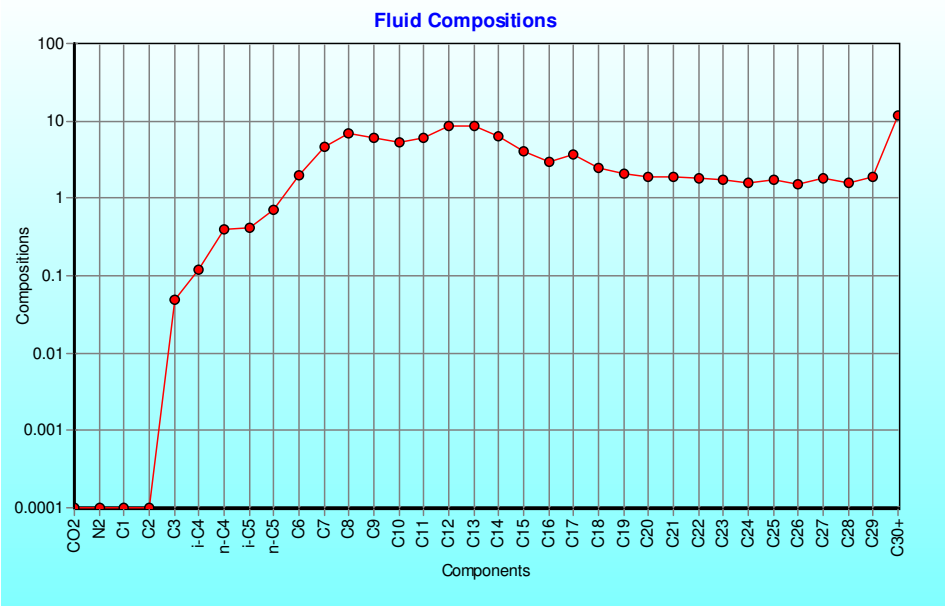

Figure 4.10: M2 fluid composition (mol%) before initial contamination study.

Based on the level of contamination, composition of the contaminated reservoir fluid, and the composition of the drilling mud, an initial contamination study was generated. The results of the initial contamination study, the decontamination procedures, and the subsequent PVT modeling are provided in Chapter V Results and Discussion. To maintain consistency, the decontamination procedure, characterization parameters, tuning parameters, and PVT modeling were performed in the same manner as for M1.

4.2.3 M3 Station 18

Further down dip in Sand F, Figure 4.11 shows the log interval for M3. DFA Station 18 was acquired in Sand F using the IFA, and an IPTT was conducted which utilized a dual packer with a large diameter probe to pump out approximately 97 liters of fluid identified as oil past the fluid analyzer.

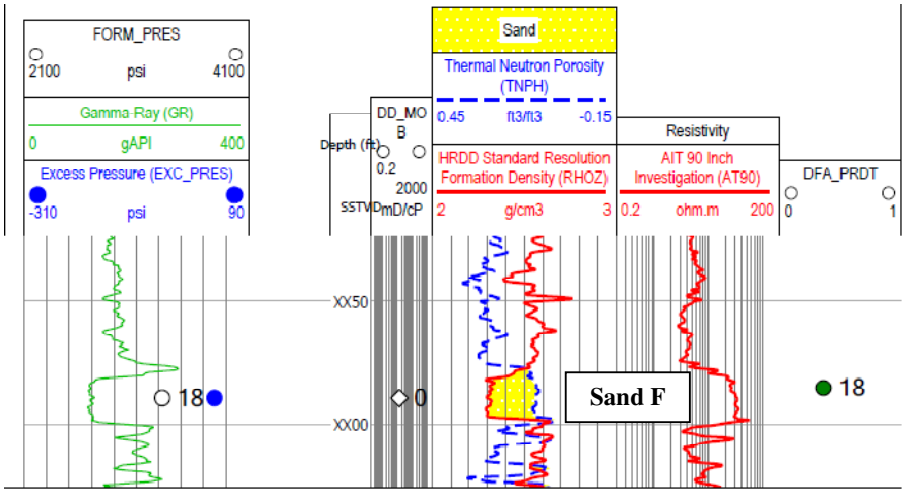

Figure 4.11: M3 Station 18 log interval.

As part of a pressure survey from an earlier run, several valid pretests were acquired and the formation pressure determined from the IPTT shown in Figure 4.12 was 3316 psi.

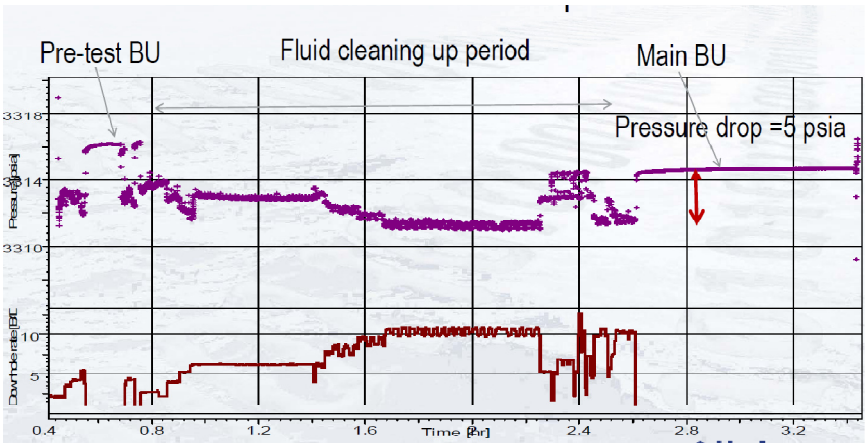

Figure 4.12: M3 Station 18 pressure response from IPTT.

Analysis of the OD vs. Time plot shown in Figure 4.13 would indicate that the fluid flowing past the IFA began to clean up after t = 4000 s as the channels associated with color stabilized.

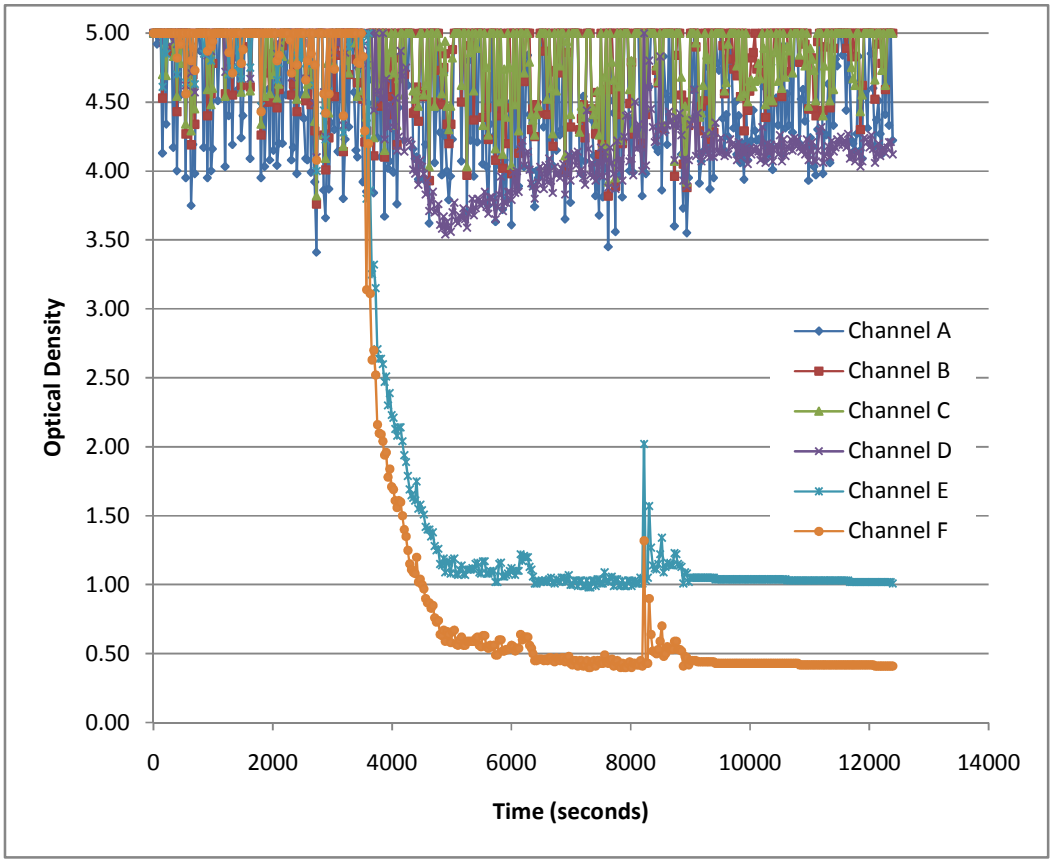

Figure 4.13: M3 Station 18 OD vs. Time.

For M3, DFA operations acquired an OD = 1.02. Corrections for baseline and OBM contamination are provided in Chapter V Results and Discussion.

Turning to the analysis of the M3 Station 18 sample that was sent off for PVT analysis, some of the key parameters from the laboratory results are listed in Table 4.4.

Table 4.4: M3 Station 18 summary of key data from laboratory analysis.

Reservoir Conditions		
Res. Temperature	135	C
Res. Pressure	3316	psia
Saturation Conditions		
Sat. Temperature	135	C
Sat. Pressure	1225	psia
Sat. Fluid Density	0.773	g/cm^3
MW	175	lb/lbmol
Single Stage Flash to Stock Tank Conditions		
ST Temperature	15.6	C
ST Pressure	14.7	psia
STO Density	0.8695	g/cm^3
Bo	1.17	
GOR	166	SCF/STB
MW of Plus Fractions		
C7+ =	231	lb/lbmol
C12+ =	263	lb/lbmol
C20+ =	384	lb/lbmol
C30+ =	461	lb/lbmol

The same steps that were detailed in the preparation of the laboratory data for M1 and M2 were followed for M3 Station 18. The MW of certain plus fractions (C7+, C12+, C20+, and C30+) were determined in the laboratory so for those cases, the laboratory MWs were used in the model as well as the interpolated MWs (C8, C9,...C13, C14,…C21, C22,…etc.) calculated from the laboratory determined plus fractions. For the sample at M3 Station 18, the plus fractions determined in the laboratory as well as the interpolated compositions are provided in the initial contamination study shown in Chapter V Results and Discussion. The plot of the composition of the downhole sample taken at M3 Station 18 is shown in Figure 4.14. A slight hump in the composition from C11 through C15 was indicative of OBM contamination.

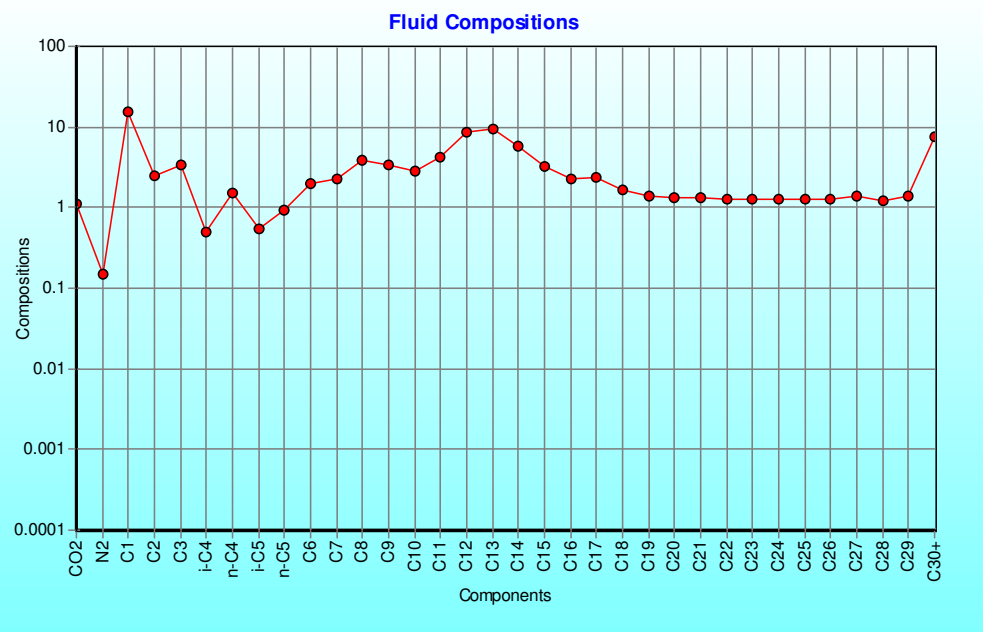

Figure 4.14: M3 fluid composition (mol%) before initial contamination study.

Based on the level of contamination, composition of the contaminated reservoir fluid, and the composition of the drilling mud, an initial contamination study was generated. The results of the initial contamination study, the decontamination procedures, and the subsequent PVT modeling are provided in Chapter V Results and Discussion. To maintain consistency, the decontamination procedure, characterization parameters, tuning parameters, and PVT modeling were used and performed in the same manner as M1 and M2.

4.2.4 Data Preparation Summary

A summary of the DFA results for all three wells is provided in Table 4.5. Relative depth increased from M1 to M2 to M3, and as was expected, the formation pressure and temperature also increased with depth. For low GOR measurements (<600 scf/stb), the DFA GOR measurement should be qualitatively assessed. In other words, it can be said that the fluids encountered in this study have low GOR but the difference in GOR from well to well should not be assessed quantitatively. Note that M1 was logged with the LFA which is not enabled for composition, density, or viscosity determination. M2 and M3 were logged with the IFA which provides

composition as well as density and viscosity measurements. From M2 to M3, the density and viscosity measurements exhibited a slight decrease with increasing depth and temperatures. The initial observation for the OD measurements before corrections for baseline and OBM contamination was that an inversion in OD occurs at M3.

Table 4.5: Summary of DFA results for M1, M2, and M3.

Measurement	M-1 Station 83	M-2 Station 136	M-3 Station 18
Depth (relative TVDss, ft)	291	1004	1889
Pressure (psia)	2738	2978	3316
Temperature (degF)	246	260	275
GOR (scf/stb)	NA	130	73
C1 (wt %)	NA	0.77	0.32
C2 (wt %)	NA	0.54	0.47
C3-C5 (wt %)	NA	4.19	1.74
C6+ (wt %)	NA	94.5	97.17
CO2 (wt %)	NA	0	0
Density (g/cm3)	NA	0.793	0.783
Viscosity (cp)	NA	3.6	3.1
Contamination (wt %)	38	8	20
$OD_{uncorrected}$	0.510	1.550	1.020

4.3 Modeling

The modeling for this study was separated into two parts. The first part was the modeling of the real-time OD data from DFA utilizing the FHZ EOS for DFA prediction. The second part of the modeling section focused on PVT modeling where the decontaminated laboratory samples were modeled for different conditions which would correspond to different locations in the oil column.

Recall from Chapter III Theory and Concept that the FHZ EOS is comprised of a gravity term, an entropy term, and a solubility term. The GOR determined for the fluids in this project were all less than 200 scf/stb. It has been well established in previous studies that when GOR < 600, the gravity term dominates and the solubility

and entropy terms are negligible. The simplified version of the FHZ EOS for low GOR fluids, showing the relationship of the gravity term to the OD gradient is shown below.

$$\frac{OD\ (h_2)}{OD\ (h_1)} = \exp\left\{\frac{v_a\, g\, (\rho - \rho_a)(h_2 - h_1)}{kT}\right\}$$

With this equation, provided an initial OD measurement from DFA operations at a location in the oil column, OD(h_1), the various components that make up the exponential term can then be determined in order to generate a predicted OD, OD(h_2), at a different depth in the oil column. Those components are explained in more detail here. For $v_a g$, the asphaltene volume based on the type of asphaltene (molecule, nano-aggregate, or cluster) found in the reservoir is multiplied by the acceleration of gravity. (ρ - ρ_a) is the difference between the asphaltene density and the average reservoir fluid density, ($h_2 - h_1$) is the difference in height in the oil column for the calculation interval, and kT is the Boltzmann constant multiplied by reservoir temperature. With these inputs, the predicted OD at the new depth can be determined. Reservoir connectivity from well to well was then assessed by comparing the measured OD from DFA operations to the predicted OD.

The second part of the modeling section provided an alternative to the DFA prediction interpretation for connectivity. A PVT model was provided using the decontaminated samples for M1 and M3 modeled at different reservoir conditions for comparison, or were compared to the DFA composition at M2. The approach for comparing the model composition to the actual data, whether the model was compared to the decontaminated laboratory samples or compared to the composition determined from DFA operations, was dependent on the data available. If the fluid compositions were determined to be essentially the same, then the reservoir was likely in fluid equilibrium and was therefore expected to have a higher probability of being connected.

Another approach that was used to assess connectivity utilized the PVT model and the FHZ EOS to create a 'synthetic' OD. The PVT model cannot directly model the FHZ EOS. Instead, it determines parameters that are inputs for the FHZ EOS. In

the gravity term of the FHZ EOS, assuming there is a starting OD at one location in the oil column, the only unknown parameter is the difference in fluid density between the asphaltene density and the average density of the reservoir fluid. Once this difference in fluid density is determined, the OD at the other location in the oil column can be calculated and compared to the OD from the DFA prediction process described earlier.

4.3.1 Modeling Workflow Summary

The steps for the workflow used in the project have been summarized in this section. The workflow progression was developed with DFA prediction in mind, to match the actual sequence of evaluation for this field where M1 was logged first, then M2, and finally M3. For the PVT modeling section, each well presented a unique set of circumstances that had to be considered. Due to these unique circumstances, different approaches were used to utilize the laboratory data for M1, M2, and M3. M1 Station 83 was a bottomhole sample with relatively high contamination but was thought to be in fluid communication with M2 which had a much lower and acceptable level of contamination. Therefore, it was assumed that if the sample at M1 Station 83 could be decontaminated and modeled at the reservoir conditions of M2 Station 136, the M1 composition determined from the model could be compared to the M2 composition from DFA operations. Based on a comparison of the compositions, fluid equilibrium could be assessed between M1 and M2. This approach was also attempted in the other direction; the decontaminated sample of M3 Station 18 was modeled at the reservoir conditions of M2 Station 136 and the compositions of the PVT models from M1 and M3 and the DFA composition from M2 were compared. Based on the results of this comparison, connectivity was assessed and discussed.

4.3.2 DFA Prediction

M1 Station 83

1. Process OD (Starting point for prediction).
2. Determine the gravity component for the FHZ EOS.
3. Create the OD prediction curve based on the starting point OD in Step 1 and the gravity component from the FHZ EOS in Step 2.

M2 Station 136

4. Process the OD (Compare to the FHZ EOS prediction in Step 3).

M3 Station 18

5. Process the OD (Compare to the FHZ EOS prediction in Step 3).

4.3.3 PVT Modeling

M1 Station 83

6. Enter lab analysis compositions for sample and OBM into the PVT model.
7. Perform the decontamination procedure with the subtraction method.
8. Simulate the decontaminated sample at reservoir conditions which correspond to conditions at M2.

M2 Station 136

9. Enter lab analysis compositions for sample and OBM into the PVT model.
10. Perform the decontamination procedure with the subtraction method.

M3 Station 18

11. Enter the lab analysis compositions for sample and OBM into the PVT model.
12. Perform the decontamination procedure with the subtraction method.
13. Simulate the decontaminated sample at reservoir conditions which correspond to conditions at M2.
14. Compare the compositional simulations for M1 and M3, at M2 Station 136 reservoir conditions, to the composition acquired for M2 Station 136 as part of DFA operations.

CHAPTER V

RESULTS AND DISCUSSIONS

This chapter describes the results and analysis based on the methodology described in the previous chapter. The results and analysis are broken down into two main sections, DFA Prediction which is based on the OD data acquired downhole in real-time as part of advanced FT operations, and PVT modeling which is based on the analysis of the samples retrieved and brought to the surface and sent off to the laboratory. The results of these two approaches are then compared and discussed.

5.1 DFA Prediction

In Chapter IV Methodology, the uncorrected ODs were determined from channels which correspond to a common wavelength across different generations of DFA technology (LFA vs. IFA). The uncorrected ODs acquired from DFA operations are summarized in Table 5.1.

Table 5.1: Summary of OD processing.

Well and Station	Depth Relative TVDss (ft)	OBM %	OD @ 1070 nm Uncorrected
M1 Station 83	291	38	0.51
M2 Station 136	1004	8	1.55
M3 Station 18	1889	20	1.02

In order to compare ODs from well to well, the uncorrected OD must first be corrected for baseline and OBM contamination. With the corrected OD at M1 as a starting point, the FHZ EOS was used to predict the OD at different depths in Sand F. This predicted OD gradient was then compared to the actual DFA OD measurements, after corrections for baseline and OBM contamination, for the subsequent wells M2 and M3. The baseline and OBM contamination correction calculations as well as the modeling procedure and results are detailed in the following sections.

5.1.1 M1 Station 83

For this sample, the LFA baseline OD = 0.08 and the OD adjusted for baseline was determined from the calculation shown below.

$$ODbaseline\ corrected = 0.51 - 0.08 = 0.43$$

For M1, the DFA contamination based on the OCM algorithm was determined to be 38%. Utilizing the baseline corrected OD (0.43) and the OBM contamination (0.38), the OBM correction calculation is shown below.

$$OD\ obm\ corrected = \frac{0.43}{(1 - 0.38)} = 0.694$$

This corrected OD from M1 (0.694) was then used as a starting point for the EOS modeling used to predict the OD in M2 and M3. Using the baseline corrected and OBM corrected OD for M1 (OD = 0.694) as a starting point, the DFA prediction curve was generated based on the gravity term from the FHZ EOS shown below.

$$\frac{OD(h_2)}{OD(h_1)} = \exp\left(-\frac{V_a g(\rho_a - \rho)(h_2 - h_1)}{kT}\right)$$

For clarity, a sample procedure is provided with the DFA prediction curve calculations broken down into contributing components. The OD gradient on the left hand side of the equation is equal to an exponential term representing the FHZ EOS gravity component. In the numerator, the contributing components to the calculation include the volume of the asphaltene structure multiplied by the acceleration of gravity ($V_a g$), the difference between the asphaltene density and the measured fluid density ($\rho_a - \rho$), and the difference in height of the two locations in the oil column ($h_2 - h_1$). In the denominator, the Boltzmann constant is multiplied by the temperature (kT).

The volume of the asphaltene structure (V_a) is based on the type of asphaltene structure and the corresponding asphaltene diameter of the structure (molecule; d_a = 1.5 nm, nano-aggregate; d_a = 2 nm, or cluster; d_a = 5 nm). The low GOR, waxy crudes in this project are best described, in the context of the FHZ EOS, as black oil. Therefore, the nano-aggregate diameter was used to determine V_a.

$$V_a = \frac{1}{6} * \pi * \mathrm{d_a} * (1.00\mathrm{E} - 10)^3 \;\; = \;\; 4.187\mathrm{E} - 27\ \mathrm{m3}$$

V_ag was then directly calculated where g = 9.81 m/s2; the units in this calculation component were meaningless so they were momentarily omitted but were taken into account in the final calculation.

$$V_a\mathrm{g} = \; 4.19\mathrm{E} - 27 * 9.81 = \; 4.107\mathrm{E} - 26$$

The density of the asphaltene structure (ρ_a) for this project was assumed to be 1200 kg/m3 and the estimated reservoir fluid density was approximately 0.8 g/cm3 or 800 kg/m3. The difference in density is shown in the calculation below.

$$\rho_a - \rho \;\; = \;\; 1200\,\frac{\mathrm{kg}}{\mathrm{m3}} - 800\,\frac{\mathrm{kg}}{\mathrm{m3}} = 400\ \mathrm{kg/m3}$$

The difference in height for two points in the oil column ($h_2 - h_1$) is arbitrary when constructing the FHZ EOS prediction curve and for this project, most of the intervals were chosen to be 80 ft. The component in the denominator of the gravity term is the Boltzmann constant (k) multiplied by the reservoir temperature in Kelvin (T) and this product is shown below. Boltzmann's constant is 1.380654E-23 $m^2 \cdot kg \cdot s^{-2} \cdot K^{-1}$ and the reservoir temperature at M1 Station 83 was 392K (246 degF); the units in this calculation component were meaningless so they were momentarily omitted but were taken into account in the final calculation.

$$k\mathrm{T} = \; 1.380654\mathrm{E} - 23 \; * 392\mathrm{K} = 5.412\mathrm{E} - 21$$

The gravity term of the FHZ EOS was then manipulated to solve for OD(h_2) at any particular depth in the oil column from the starting point, OD(h_1).

$$OD(h2) = \exp\left(-\frac{V_a g(\rho_a - \rho)(h_2 - h_1)}{kT}\right) * OD(h_1)$$

Where:

$V_a g$ = 4.107E-26

$(\rho_a - \rho)$ = 400 kg/m3

$(h_2 - h_1)$ = 29ft or 8.834m (most intervals were 80 ft)

kT =5.412E-21

OD(h_1) = 0.694

Plugging these components into the equation above, the OD calculated at relative TVDss =320 ft (in this case 29 ft deeper than M1 Station 83) was determined to be 0.713. This calculation was repeated to generate the predicted OD at 80 ft intervals as well as for the depths of interest corresponding to M2 and M3. The results are shown in Table 5.2.

Table 5.2: OD from the FHZ EOS based on M1 starting point.

Relative TVDSS (ft)	OD From FHZ EOS (2 nm)
0	0.530
80	0.571
160	0.615
240	0.662
291	0.694
320	0.713
400	0.768
480	0.827
560	0.890
640	0.958
720	1.032
800	1.111
880	1.197
960	1.289
1004	1.342
1040	1.388
1120	1.495
1200	1.610
1280	1.733
1360	1.866
1440	2.010
1520	2.164
1600	2.331
1680	2.510
1760	2.703
1840	2.911
1889	3.046
1920	3.134
2000	3.375
2080	3.635
2160	3.914

The FHZ EOS from Table 5.2 was plotted and shown with the M1 starting point in Figure 5.1. At this point, only the FHZ EOS prediction curve assuming the nano-aggregate asphaltene size was shown. As the subsequent wells M2 and M3

were added, the appropriate prediction curve (molecule, nano-aggregate, or cluster can be reevaluated based on which prediction curve would best fit the data.

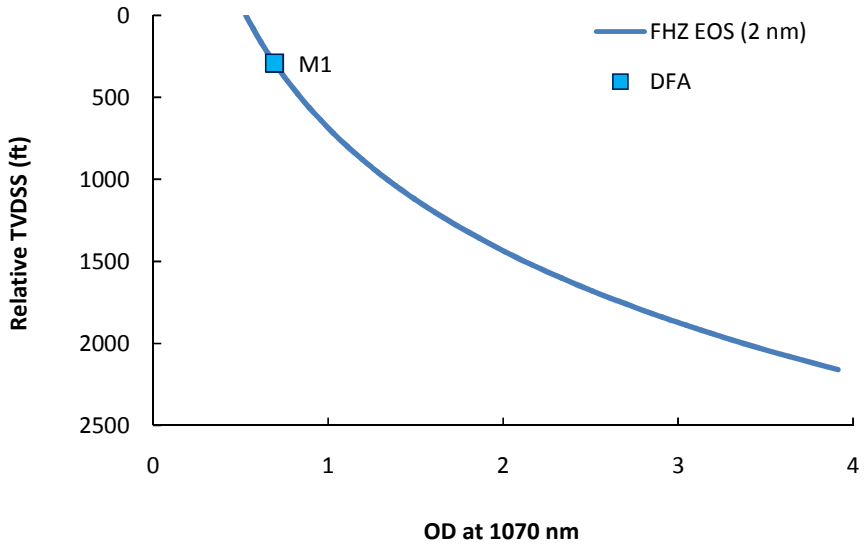

Figure 5.1: DFA prediction curve with M1 as starting point.

Assuming that M1 Station 83 was the first fluid sample evaluated in Sand F, Figure 5.1 shows what the reservoir engineer monitoring the fluid sampling operations could be observing and the value of the OD that the reservoir engineer could be anticipating for DFA stations at deeper locations in the reservoir.

5.1.2 M2 Station 136

Similar to the procedure and calculations described for M1, the OD acquired for M2 needed to be adjusted with an IFA baseline OD and also needed to be corrected for OBM contamination. For this sample, the IFA baseline OD = 0.31 and the OD adjusted for baseline was determined from the OD baseline correction calculation.

$$ODbaseline\ corrected = OD\lambda - ODbaseline = 1.55 - 0.31 = 1.24$$

For M2, DFA operations achieved an 8% OBM contamination level. Using the baseline corrected OD and the 8% OBM contamination as inputs, the OBM corrected OD was calculated below.

$$OD\ obm\ corrected = \frac{ODbaseline\ corrected}{(1 - \text{OBM contamination})} = \frac{1.24}{(1 - 0.08)} = 1.348$$

The final OD corrected for baseline and OBM contamination and ready to be plotted on the DFA prediction curve was determined to be 1.348. The DFA prediction curve with OD corrected values for M1 and M2 are shown in Figure 5.2.

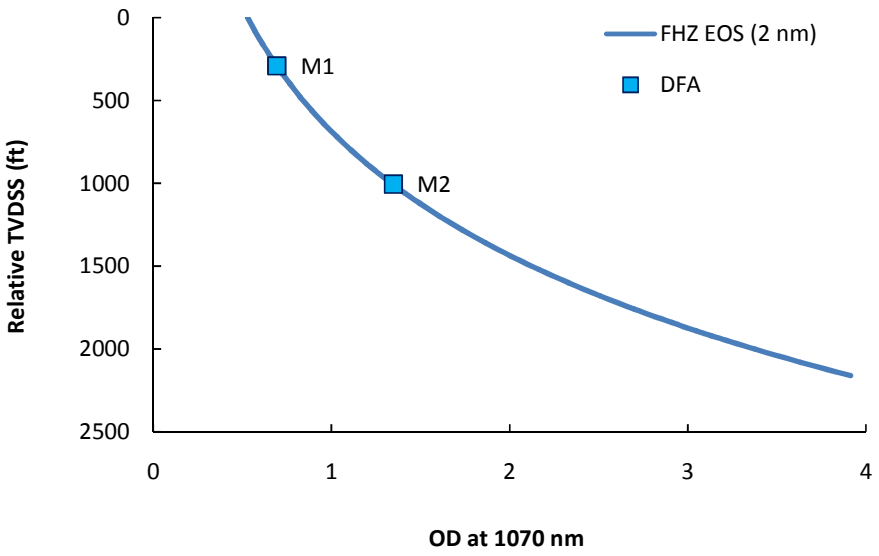

Figure 5.2: DFA prediction curve for M1 and M2.

If there was some type of barrier between M1 and M2 which prevented the reservoir fluid from achieving an equilibrium state, it would have been more likely that the OD from M2 would not have matched the FHZ EOS prediction curve. However, the corrected OD measurement fit the DFA prediction curve very well. Therefore, the initial real-time interpretation based on DFA would have been that M1 and M2 are likely connected.

5.1.3 M3 Station 18

Similar to the procedure and calculations described for M1 and M2, the OD acquired for M3 needed to be adjusted with an IFA baseline OD and also needed to be corrected for OBM contamination. For this sample, the IFA baseline OD = 0.16 and the OD adjusted for baseline was determined from the calculation shown below.

$$ODbaseline\ corrected = OD\lambda - ODbaseline = 1.02 - 0.16 = 0.86$$

For M3, DFA operations achieved a 20% OBM contamination level. Using the baseline corrected OD and the 20% OBM contamination as inputs, the OBM corrected OD was calculated below.

$$OD\ obm\ corrected = \frac{ODbaseline\ corrected}{(1 - \text{OBM contamination})} = \frac{0.86}{(1 - 0.20)} = 1.075$$

The final OD corrected for baseline and OBM contamination and ready for comparison to the other wells was determined to be 1.075. For M3 Station 18 in Sand F, the OD corrected for baseline and OBM contamination (OD = 1.075) was then added to the DFA prediction curve and is shown in Figure 5.3.

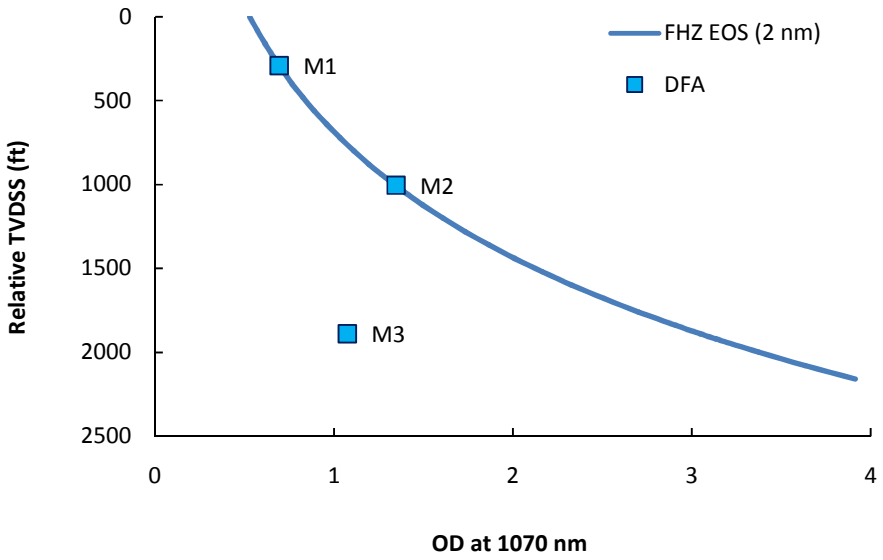

Figure 5.3: DFA prediction curve for M1, M2, and M3.

If the reservoir fluid between M3 and the other wells (M1 and M2) was in equilibrium and therefore likely connected, the OD from M3 would have likely matched the DFA prediction curve. However, the OD from M3 significantly deviates from the DFA prediction curve. Therefore, the initial real time interpretation based on DFA would have been that M3 was likely not connected to M1 or M2.

5.1.4 DFA Prediction Discussion

The nano-aggregate FHZ EOS prediction curve, appropriate for black oil reservoirs, was appropriate for the low GOR, waxy crude in Sand F. An inversion in the asphaltene gradient was observed between M3 and the other wells (M1 and M2); furthermore, the OD from M3 Station 18 deviated significantly from the DFA prediction curve. Therefore, the interpretation based on the analysis of the OD data was that M1 and M2 are likely connected, but M3 is likely not connected to M1 and M2.

5.2 PVT Modeling

The compositions of the contaminated samples shown in Figures 4.6, 4.10, and 4.14 are summarized here in Table 5.3. Recall that M1 Station 83 and M3 Station 18 were bottomhole samples, while M2 Station 136 was a sample taken at stock tank conditions. Initial contamination studies were performed as described in Chapter IV Methodology and the calculated results for the mol% of the drilling mud, mol% of the 'uncontaminated fluid,' and the composition of the 'uncontaminated fluid' were used for the decontamination procedure that followed.

Table 5.3: Summary of contaminated fluid composition for M1, M2, and M3.

Component	M1 Station 83	M2 Station 136	M3 Station 18
	mole %	mole %	mole %
CO2	0.33	0.00	1.12
N2	0.30	0.00	0.15
C1	8.05	0.00	15.54
C2	0.29	0.00	2.45
C3	0.53	0.05	3.36
i-C4	0.21	0.12	0.50
n-C4	0.62	0.39	1.52
i-C5	0.46	0.41	0.54
n-C5	0.59	0.72	0.92
C6	1.38	1.96	1.94
C7	1.33	4.55	2.23
C8	2.24	6.78	3.86
C9	1.46	6.07	3.32
C10	1.23	5.33	2.86
C11	10.87	5.96	4.19
C12	28.47	8.46	8.78
C13	25.14	8.46	9.52
C14	11.90	6.20	5.73
C15	1.95	4.13	3.19
C16	0.50	2.97	2.22
C17	0.49	3.62	2.35
C18	0.25	2.49	1.69
C19	0.19	2.06	1.41
C20	0.15	1.93	1.33
C21	0.15	1.92	1.32
C22	0.13	1.79	1.27
C23	0.14	1.76	1.27
C24	0.11	1.61	1.25
C25	0.11	1.76	1.28
C26	0.09	1.54	1.26
C27	0.10	1.81	1.37
C28	0.06	1.57	1.22
C29	0.06	1.88	1.36
C30+	0.12	11.70	7.68
	100.00	100.00	100.00

The decontaminated samples were then modeled with the aim of changing the conditions of one sample (e.g., M1) to match the conditions of another sample (e.g., M2 or M3) and analyzing the compositions of the different samples under similar reservoir temperature and pressure conditions. For consistency, all samples were set up and modeled assuming the following criteria:

1. Subtraction method for decontamination.
2. Katz and Firoozabadi (1978) MW and SG.
3. Peng-Robinson (1978) EOS with constant volume translation.
4. Van der Waals mixing rules with temperature independent Kij.
5. Lohrenz-Bray-Clark viscosity correlation.

The justification for using the subtraction method was that detailed compositional breakdown of the drilling mud (up through C30+) was available from the laboratory analysis. It is well accepted that when drilling mud composition is available the recommended course of action is to implement the subtraction method of decontamination instead of the skimming method. The theory behind the subtraction method was covered in more detail in Chapter III Theory and Concept. The other parameters (Parameters 2-5) that were chosen to set up each model were either not particularly significant (Parameters 2, 4, and 5) when changes to the various parameters were used in different combinations or were observed to be a worse fit to the experimental data (Parameter 3). An example of a parameter that had little effect on the analysis was the assumption of the Katz and Firoozabadi (1978) convention over the Whitson (1983) convention for the determination of MW and SG. It was not significant since the MW of the plus fractions used in the models were determined in the laboratory analysis. Only the defined components (CO2, N2, C1-C6) were taken from the default values provided by Katz and Firoozabadi and they were the same as the MWs provided in the Whitson convention. An example of the latter situation, in which a worse fit to the experimental data was observed, was when the Peng-Robinson (1978) EOS was replaced with the Soave-Redlich-Kwong EOS. Therefore, the parameters that were chosen and listed above were used for the sample at M1

Station 83 and then kept the same for the samples at M2 Station 136 and M3 Station 18 for consistency.

5.2.1 M1 Station 83

The initial contamination study was used as an input for the decontamination calculations that followed. The plot of the initial contamination study is shown in Figure 5.4 and the tabulated results of the initial contamination study are provided in Table 5.4. As discussed in Chapter IV Methodology, the reservoir fluid for a contaminant free sample would roughly exhibit a semi-log straight line behavior for carbon numbers greater than C8. The plot shows a hump in composition from C11 to C15 and this deviation from the straight line behavior corresponds with the composition of the drilling mud contaminant.

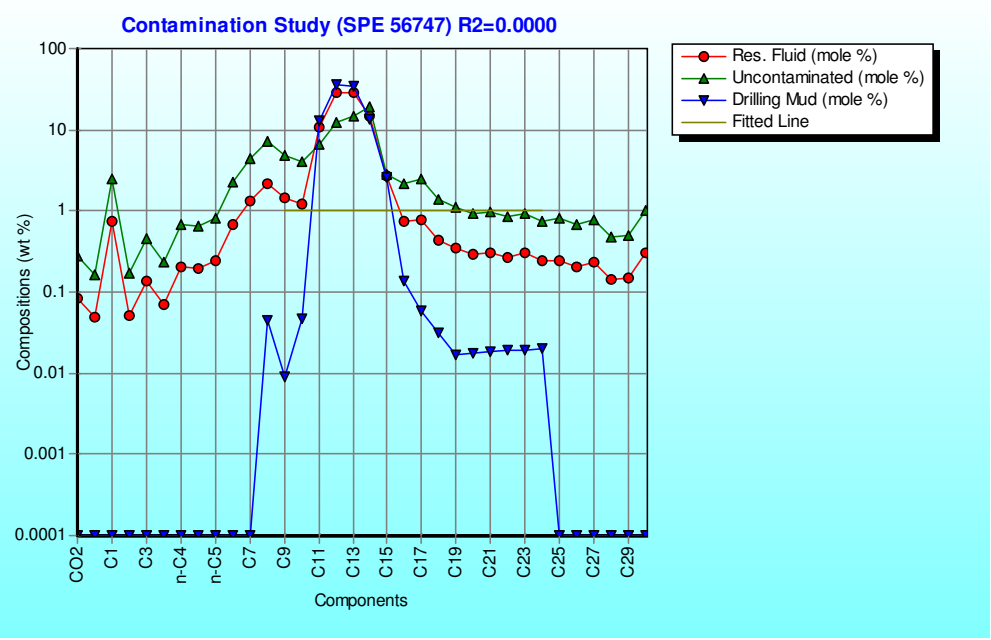

Figure 5.4: M1 Station 83 initial contamination study.

In Table 5.4, the laboratory analysis of the drilling mud shows the OBM composition used in M1 ranges from C8 to C24. Although the composition largely

consists of components from C10 to C16, for the decontamination procedure a mud pseudo component is created which groups together all the individual components of the drilling mud composition.

Table 5.4: M1 Station 83 initial contamination study.

Component	MW	Res. Fluid	Uncontaminated Fluid	Drilling Mud
	lb/lbmol	wt %	mole %	mole %
CO2	44.01	0.08	0.91	0.00
N2	28.01	0.05	0.83	0.00
C1	16.04	0.75	22.32	0.00
C2	30.07	0.05	0.80	0.00
C3	44.10	0.14	1.47	0.00
i-C4	58.12	0.07	0.58	0.00
n-C4	58.12	0.21	1.72	0.00
i-C5	72.15	0.19	1.28	0.00
n-C5	72.15	0.25	1.64	0.00
C6	84.00	0.67	3.83	0.00
C7	169.00	1.30	3.69	0.00
C8	171.00	2.21	6.12	0.05
C9	172.00	1.45	4.03	0.01
C10	174.00	1.24	3.32	0.05
C11	175.00	10.99	5.52	13.89
C12	177.00	29.10	10.00	38.89
C13	197.00	28.60	10.64	33.32
C14	218.00	14.98	12.61	11.50
C15	238.00	2.68	1.74	2.07
C16	259.00	0.75	1.21	0.10
C17	279.00	0.79	1.29	0.04
C18	299.00	0.43	0.66	0.02
C19	320.00	0.35	0.51	0.01
C20	340.00	0.29	0.40	0.01
C21	350.00	0.30	0.40	0.01
C22	359.00	0.27	0.34	0.01
C23	369.00	0.30	0.37	0.01
C24	378.00	0.24	0.29	0.01
C25	388.00	0.25	0.31	0.00
C26	398.00	0.21	0.25	0.00
C27	407.00	0.24	0.28	0.00
C28	417.00	0.14	0.17	0.00
C29	426.00	0.15	0.17	0.00
C30+	436.00	0.30	0.33	0.00
		100.00	100.00	100.00

The relative level of contamination for M1 Station 83 was determined in the laboratory to be 70% which when used in conjunction with the computed MW of the drilling mud yields a 63.93 mol% as shown in Table 5.5.

Table 5.5: M1 Station 83 contamination level.

Stream	MW	Mole %	Weight %
Uncontaminated Fluid	144.02	36.0713	30
Drilling Mud	189.61	63.9287	70

The uncontaminated fluid mol% and the drilling mud mol% values in Table 5.5 were used in the calculations that followed to determine the contributions of the uncontaminated fluid and the drilling mud to the 'pseudo reservoir fluid' composition shown in Figure 5.7. The calculated properties for the mud pseudo component for the drilling mud used in M1 are shown in Table 5.6.

Table 5.6: M1 Station 83 mud pseudo component properties.

			MW	Critical P.	Critical T.	Acentric	Volume Trans.	Liquid
Component Name	From	To	lb/lbmol	psia	F			Mole Frac.
Mudpseudo1 _83-1	C8	C24	189.61	253.1	742.5	0.6032	0.1009	1.00

Note that it is possible to break the OBM composition into several mud pseudo components if so desired. For this project, the critical properties were determined for one mud pseudo component. For M1 Station 83, the mud components from C8 to C24 are all inclusive and grouped together, therefore the liquid mole fraction of Mudpseudo1_83-1 is equal to 1. Whatever the number of pseudo components and their individual liquid mole fractions used to describe the OBM, the sum of liquid mole fractions of the mud pseudo components should be equal to one.

The next step required was the modification of Table 5.4 so that the drilling mud composition was represented by the mud pseudo component. Table 5.7 shows the composition of the calculated 'pseudo reservoir fluid' which was comprised of the 'uncontaminated fluid' adjusted by its mole fraction (0.3607) and the OBM, which was represented by the mud pseudo component, adjusted by its mole fraction (0.6393).

Table 5.7: M1 Station 83 fluid composition with mud pseudo component.

Component	MW	Res. Fluid	Uncontaminated	Drilling Mud	Pseudo Res. Fluid
	lb/lbmol	wt %	mole %	mole %	mole %
Mudpseudo1_83-1	189.61				63.93
CO2	44.01	0.08	0.91	0.00	0.33
N2	28.01	0.05	0.83	0.00	0.30
C1	16.04	0.75	22.32	0.00	8.05
C2	30.07	0.05	0.80	0.00	0.29
C3	44.10	0.14	1.47	0.00	0.53
i-C4	58.12	0.07	0.58	0.00	0.21
n-C4	58.12	0.21	1.72	0.00	0.62
i-C5	72.15	0.19	1.28	0.00	0.46
n-C5	72.15	0.25	1.64	0.00	0.59
C6	84	0.67	3.83	0.00	1.38
C7	169	1.30	3.69	0.00	1.33
C8	171	2.21	6.12	0.05	2.21
C9	172	1.45	4.03	0.01	1.45
C10	174	1.24	3.32	0.05	1.20
C11	175	10.99	5.52	13.89	1.99
C12	177	29.10	10.00	38.89	3.61
C13	197	28.60	10.64	33.32	3.84
C14	218	14.98	12.61	11.50	4.55
C15	238	2.68	1.74	2.07	0.63
C16	259	0.75	1.21	0.10	0.44
C17	279	0.79	1.29	0.04	0.46
C18	299	0.43	0.66	0.02	0.24
C19	320	0.35	0.51	0.01	0.18
C20	340	0.29	0.40	0.01	0.14
C21	350	0.30	0.40	0.01	0.14
C22	359	0.27	0.34	0.01	0.12
C23	369	0.30	0.37	0.01	0.13
C24	378	0.24	0.29	0.01	0.10
C25	388	0.25	0.31	0.00	0.11
C26	398	0.21	0.25	0.00	0.09
C27	407	0.24	0.28	0.00	0.10
C28	417	0.14	0.17	0.00	0.06
C29	426	0.15	0.17	0.00	0.06
C30+	436	0.30	0.33	0.00	0.12
		100.00	100.00	100.00	100.00

The composition shown in Table 5.7 which included contamination represented by the mud pseudo component was then characterized and tuned to fit the available experimental data. For the sample at M1 Station 83, the saturation temperature and pressure of the reservoir fluid and the oil density determined at stock tank conditions from Table 4.2 were used to tune the model. The summary of the tuning results using the Modified Exponential Pedersen distribution and the Pedersen property correlation is shown in Table 5.8.

Table 5.8: M1 Station 83 model tuning results before decontamination.

Test	Item	Unit	Exp. Data	Cal. Result Bef. Tuning	Cal. Result Aft. Tuning
Bubble/Dew	Bubble Point	psia	485	485.01	485.01
PT Flash	Liq. Density	g/cm^3	0.8305	0.8305	0.8305

Note that Table 5.8 shows the result of the final iteration where the calculated result after tuning equals the experimental data. This table is generated after each iteration so earlier iterations would show deviations from the experimental data which would necessitate another iteration or a different tuning approach. The different approach may require tuning for oil density first, then tuning for saturation pressure, or choosing an entirely different distribution and correlation and a restart of the tuning procedure. The phase envelope for the contaminated sample fit to the experimental data is shown in Figure 5.5.

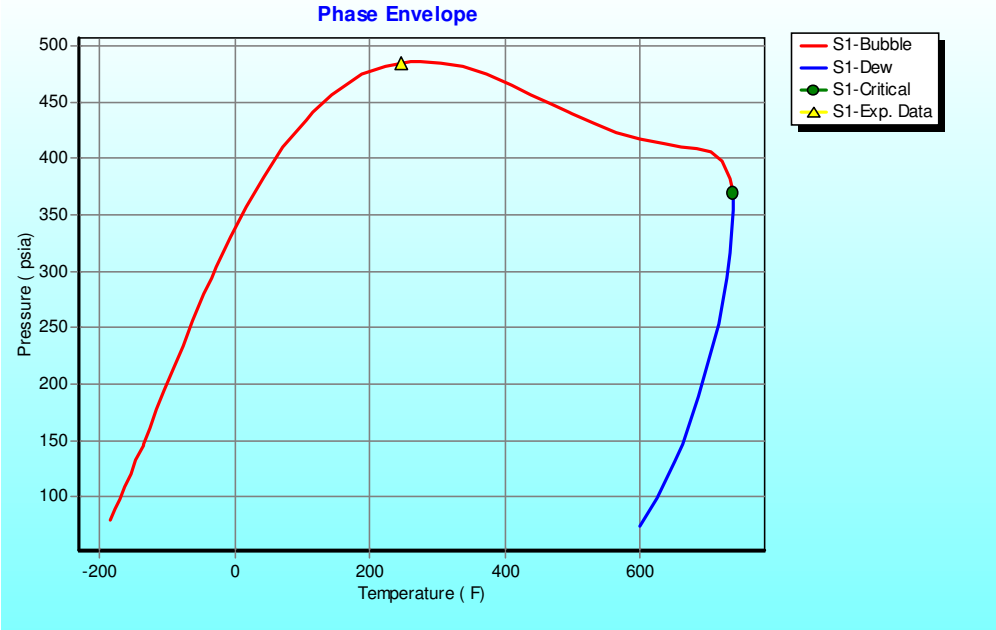

Figure 5.5: M1 Station 83 phase envelope before decontamination.

The phase envelope has an unusual shape due to the relatively high level of OBM contamination. After the contaminated sample with the mud pseudo component shown in Table 5.7 was characterized and tuned to the experimental data, the decontamination procedure proceeded. The mud pseudo component was set to zero and the overall fluid composition was re-normalized. The resultant composition shown in Table 5.9 was representative of the reservoir fluid with 0% OBM contamination. At this point in the procedure, the sample was considered 'decontaminated.' For M1 Station 83, the full summary of characterization and tuning results for the contaminated sample which includes interaction parameters, critical properties, and compositions is provided in Appendix A.

Table 5.9: M1 Station 83 fluid composition after decontamination.

Component	MW	Density	PseudoRes. Fluid
	lb/lbmol	g/cm^3	mole %
Mudpseudo1_83-1	189.61	0.806	0.00
CO2	44.01		0.92
N2	28.01		0.83
C1	16.04		22.32
C2	30.07		0.80
C3	44.10		1.47
i-C4	58.12		0.58
n-C4	58.12		1.72
i-C5	72.15	0.616	1.28
n-C5	72.15	0.622	1.64
C6	84	0.685	3.83
C7	169	0.722	3.69
C8	171	0.745	6.13
C9	172	0.764	4.02
C10	174	0.778	3.33
C11	175	0.789	5.52
C12	177	0.800	10.01
C13	197	0.811	10.65
C14	218	0.822	12.62
C15	238	0.832	1.75
C16	259	0.839	1.22
C17	279	0.847	1.28
C18	299	0.852	0.67
C19	320	0.857	0.50
C20	340	0.862	0.39
C21	350	0.867	0.39
C22	359	0.872	0.33
C23	369	0.877	0.36
C24	378	0.881	0.28
C25	388	0.885	0.31
C26	398	0.889	0.25
C27	407	0.893	0.28
C28	417	0.896	0.17
C29	426	0.899	0.17
C30+	436	1.010	0.33
			100.00

Since the EOS of the contaminated sample should be the same as the EOS of the decontaminated sample, the decontaminated composition was not re-

characterized. Instead, it was tuned again without re-characterization with the same tuning items used before (saturation pressure and oil density). The final result of the iterative tuning process where the calculated saturation pressure and oil density are equal to the experimental data is shown in Table 5.10.

Table 5.10: M1 Station 83 model tuning results after decontamination.

Test	Item	Unit	Exp. Data	Cal. Result Bef. Tuning	Cal. Result Aft. Tuning
Bubble/Dew	Bubble Point	psia	485	485.01	485.00
PT Flash	Liq. Density	g/cm^3	0.8305	0.8305	0.8305

The phase envelope resulting from successful tuning procedures for the decontaminated sample is shown in Figure 5.6.

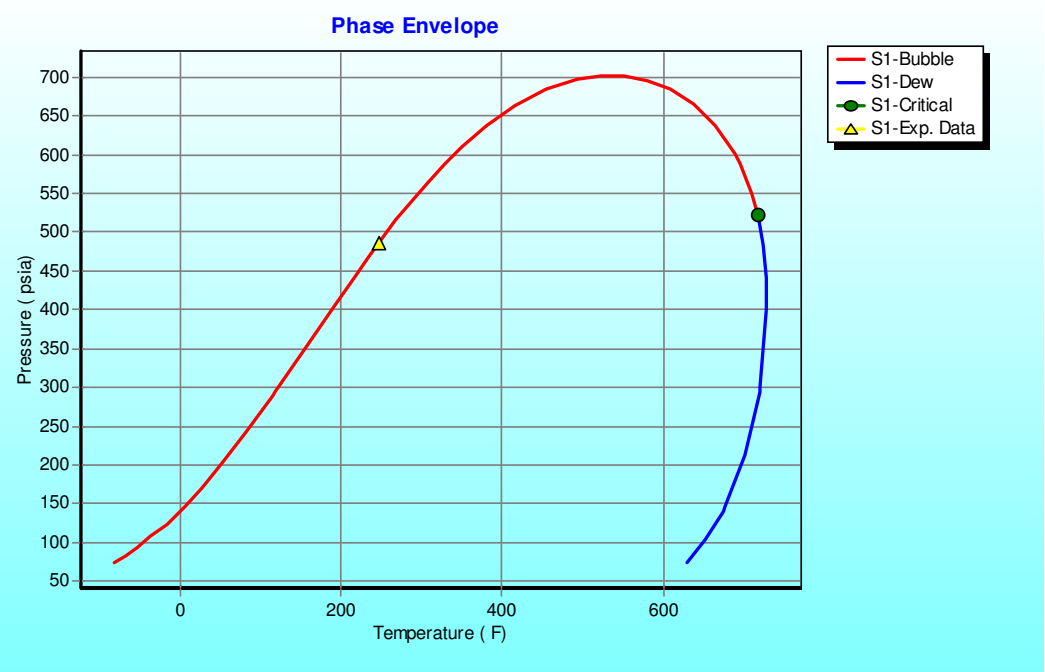

Figure 5.6: M1 Station 83 phase envelope after decontamination.

The full compilation of the critical properties, interaction parameters, compositions, and model parameters determined for the decontaminated sample are provided in Appendix A.

A plot of the decontaminated sample composition is provided in Figure 5.7. There was a noticeable improvement when comparing the plots of the fluid composition before decontamination in Figure 4.6 and after decontamination shown here in Figure 5.7. There was still a hump in the composition which would be indicative of a contaminated sample, but the composition after decontamination deviated less from the semi-log straight line behavior than the composition before decontamination.

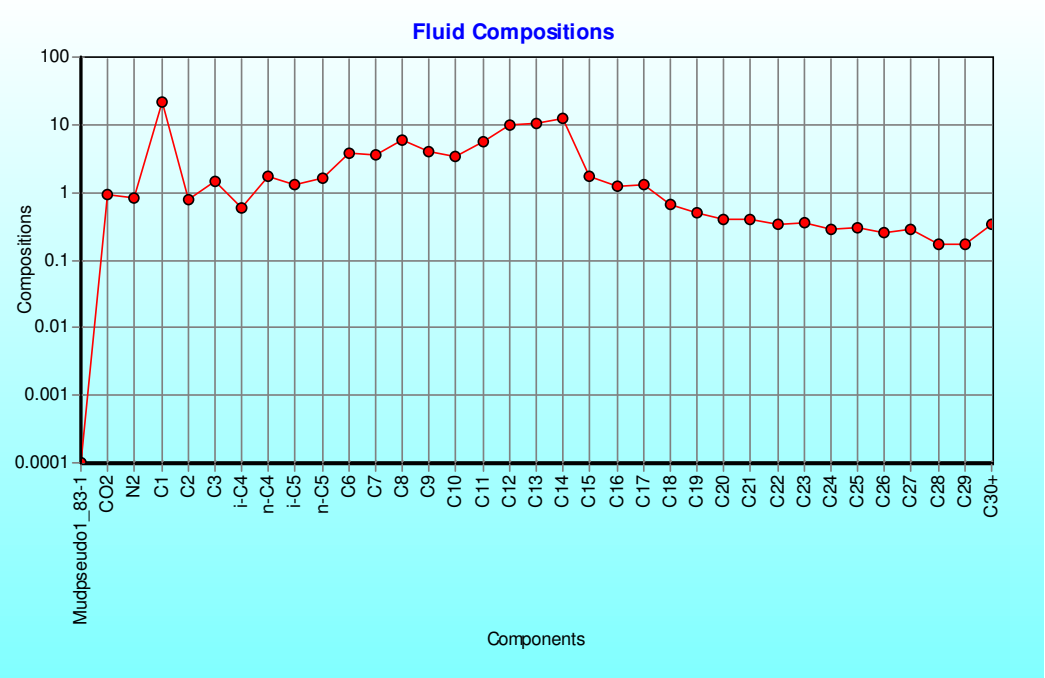

Figure 5.7: M1 Station 83 fluid composition (mol%) after decontamination.

The decontaminated sample was then ready for modeling. However, it should be noted again that similar to the considerations made for OBM contamination for DFA prediction, there really is no good substitute for a clean sample. Decontamination procedures for laboratory compositions can attempt to deal with the relatively high level of contamination that are sometimes unavoidable, but there will still be a certain level of uncertainty in the model. This should be considered when analyzing the results of the model and it is recommended that the results be checked against other sources of data if available.

The reservoir conditions for M1 Station 83 were used as a reference point for a compositional simulation for the decontaminated M1 Station 83 sample. The temperature gradient was adjusted to fit the reservoir temperatures of M2 Station 136 and M3 Station 18. The reference point data used in the compositional simulation for M1 Station 83 is shown in Table 5.11.

Table 5.11: M1 Station 83 compositional simulation reference point data.

Reference Data	
Measurement	M1 Station 83
Relative TVDss (ft)	291
Pressure (psia)	2738
Temperature (degF)	246
Temp Gradient (degF/ft)	0.018

The composition of the fluid at M1 Station 83 was then determined by the compositional simulation for several different depths at fixed steps from the reference depth. Those fixed steps are shown in Table 5.12. Since the reference point for this compositional simulation was set at the depth, temperature, and pressure for M1 Station 83, a fixed step that matches M1 Station 83 is provided at relative TVDss = 291 ft, temperature = 246 degF, and pressure = 2738 psia.

Table 5.12: M1 Station 83 compositional simulation depths analyzed.

Relative TVDss	Temperature	Pressure	Sat. Pressure
ft	degF	psia	psia
191	244.4	2705.4	488.1
291	246.2	2738.0	485.0
391	248.0	2770.0	482.0
491	249.8	2802.0	479.0
591	251.6	2834.1	476.0
691	253.4	2866.3	473.0
791	255.2	2898.5	470.1
891	257.0	2930.7	467.2
991	258.8	2963.1	464.3
1091	260.6	2995.4	461.4
1191	262.4	3027.9	458.6
1291	264.2	3060.4	455.7
1391	266.0	3093.0	452.9
1491	267.8	3125.6	450.2
1591	269.6	3158.3	447.4
1691	271.4	3191.0	444.7
1791	273.2	3223.8	442.0
1891	275.0	3256.6	439.3
1691	271.4	3191.0	444.7
1791	273.2	3223.8	442.0
1891	275.0	3256.6	439.3

For the simulation, the reservoir conditions at M2 Station 136 and M3 Station 18 did not match exactly with the fixed step depths that were generated in the model. Therefore, compositional simulation results were interpolated from the compositions determined at the fixed steps above and below the sample depths for M2 Station 136 and M3 Station 18. Additional results from the compositional simulation are provided in Appendix A. Results from the compositional simulation of M1 Station 83 for the depths of interest (M2 Station 136 and M3 Station 18) are provided in Table 5.13.

Table 5.13: M1 Station 83 compositional simulation results at selected depths.

Component	Compositional simulation for reservoir fluid from M1 Station 83					
	@ Depth = 291 ft		@ Depth = 1004 ft		@ Depth = 1889 ft	
	mole %	wt %	mol%	wt%	mol%	wt%
Mudpseudo1_83-1	0.00	0.00	0.00	0.00	0.00	0.00
CO2	0.92	0.28	0.88	0.26	0.83	0.23
N2	0.83	0.16	0.80	0.15	0.76	0.13
C1	22.32	2.49	20.32	2.17	18.10	1.84
C2	0.80	0.17	0.76	0.15	0.70	0.13
C3	1.47	0.45	1.40	0.41	1.31	0.37
i-C4	0.58	0.24	0.56	0.22	0.53	0.20
n-C4	1.72	0.69	1.65	0.64	1.56	0.57
i-C5	1.28	0.64	1.24	0.60	1.20	0.55
n-C5	1.64	0.82	1.59	0.76	1.53	0.70
C6	3.83	2.23	3.79	2.12	3.72	1.98
C7-15	57.71	76.04	58.52	73.87	59.06	70.90
C16-25	5.71	12.33	6.95	14.37	8.65	17.00
C26-C80	1.19	3.46	1.54	4.28	2.05	5.40
	100.00	100.00	100.00	100.00	100.00	100.00

Constant Composition Expansion (CCE) tests were performed on the decontaminated reservoir fluid from M1 Station 83 with the aim of determining the bulk fluid density at reservoir conditions corresponding to M2 Station 136 and M3 Station 18. The results of the test for those specific conditions were summarized in Table 5.14.

Table 5.14: M1 Station 83 CCE test results.

	CCE Test Summary for M1 Station 83 Fluid Composition		
Res. Conditions (T and P)	M1 Station 83	M2 Station 136	M3 Station 18
Temp (degF)	246	260	275
Pressure (psia)	2738	2978	3316
Bulk Density (g/cm3)	0.745	0.742	0.741
Mudpseudo1_83-1 (mol%)	0.00	0.00	0.00
CO2 (mol%)	0.92	0.92	0.92
N2 (mol%)	0.83	0.83	0.83
C1 (mol%)	22.32	22.32	22.32
C2 (mol%)	0.80	0.80	0.80
C3 (mol%)	1.47	1.47	1.47
i-C4 (mol%)	0.58	0.58	0.58
n-C4 (mol%)	1.72	1.72	1.72
i-C5 (mol%)	1.28	1.28	1.28
n-C5 (mol%)	1.64	1.64	1.64
C6 (mol%)	3.83	3.83	3.83
C7-C15(mol%)	57.71	57.71	57.71
C16-C25(mol%)	5.71	5.71	5.71
C26-C80 (mol%)	1.19	1.19	1.19

The fluid density from the CCE test result was then used in conjunction with the FHZ EOS to generate a synthetic OD at locations in the oil column which corresponded to the actual OD measurement from DFA operations. Those calculations are provided in sections 5.2.2 and 5.2.3.

5.2.2 M2 Station 136

The plot of the initial contamination study shown in Figure 5.8 exhibits a hump in composition from C11 to C15 and this deviation from the straight line behavior corresponds with the composition of the drilling mud contaminant.

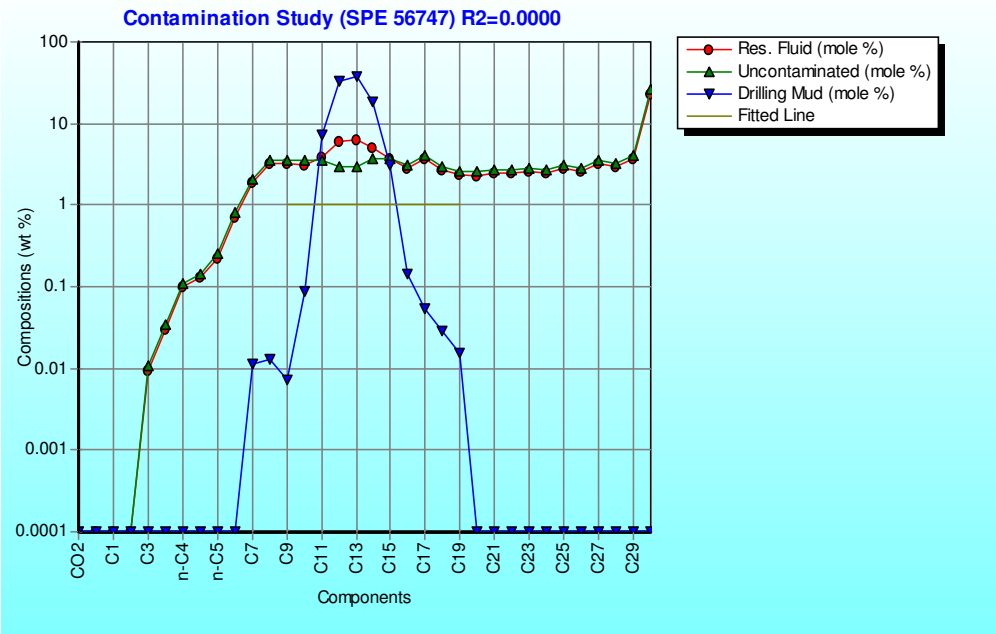

Figure 5.8: M2 Station 136 initial contamination study.

The tabulated results of the initial contamination study which include the original contaminated reservoir fluid, 'uncontaminated fluid,' and drilling mud composition is provided in Table 5.15.

Table 5.15: M2 Station 136 initial contamination study.

Component	MW	Res. Fluid	Uncontaminated Fluid	Drilling Mud
	lb/lbmol	wt %	mole %	mole %
CO2	44.01	0.00	0.00	0.00
N2	28.01	0.00	0.00	0.00
C1	16.04	0.00	0.00	0.00
C2	30.07	0.00	0.00	0.00
C3	44.10	0.01	0.06	0.00
i-C4	58.12	0.03	0.14	0.00
n-C4	58.12	0.10	0.45	0.00
i-C5	72.15	0.13	0.47	0.00
n-C5	72.15	0.23	0.83	0.00
C6	84	0.72	2.26	0.00
C7	96	1.90	5.25	0.02
C8	109	3.22	7.83	0.02
C9	122	3.22	7.01	0.01
C10	135	3.13	6.14	0.11
C11	148	3.84	5.59	8.34
C12	161	5.93	4.33	35.07
C13	175	6.45	4.03	37.01
C14	190	5.13	4.58	16.68
C15	204	3.67	4.37	2.56
C16	218	2.82	3.41	0.11
C17	232	3.66	4.18	0.04
C18	247	2.68	2.87	0.02
C19	261	2.34	2.38	0.01
C20	275	2.31	2.23	0.00
C21	294	2.46	2.22	0.00
C22	312	2.43	2.07	0.00
C23	331	2.54	2.03	0.00
C24	349	2.45	1.86	0.00
C25	368	2.82	2.03	0.00
C26	387	2.60	1.78	0.00
C27	405	3.19	2.09	0.00
C28	424	2.90	1.81	0.00
C29	442	3.62	2.17	0.00
C30+	461	23.49	13.51	0.00
		100.00	100.00	100.00

Similar to the procedure for M1, additional steps were required for decontamination after the initial contamination study. The relative level of

contamination for M2 Station 136 was determined in the laboratory to be 10% which when used in conjunction with the computed MW of the drilling mud yields a 13.42 mol% as shown in Table 5.16.

Table 5.16: M2 Station 136 contamination level.

Stream	MW	Mole %	Weight %
Uncontaminated Fluid	238.72	86.5783	90
Drilling Mud	171.10	13.4217	10

The uncontaminated fluid mol% and the drilling mud mol% values in Table 5.16 were used in the calculations that follow to determine the contributions of the uncontaminated fluid and the drilling mud to the overall fluid composition. The calculated properties for the mud pseudo component used to represent the drilling mud for M2 are shown in Table 5.17.

Table 5.17: M2 Station 136 mud pseudo component properties.

			MW	Critical P.	Critical T.	Acentric	Volume Trans.	Liquid
Component Name	From	To	lb/lbmol	psia	F			Mole Frac.
Mudpseudo2_136-1	C7	C19	171.10	248.4	749.1	0.6127	0.1043	1.00

For M2 Station 136, the critical properties were determined for one mud pseudo component, Mudpseudo2_136-1 grouped from C7 to C19 with a liquid mole fraction equal to 1.

The next step required was the modification of Table 5.15 so that the drilling mud composition was represented by the mud pseudo component. Table 5.18 shows the composition of the calculated 'pseudo reservoir fluid' which was comprised of the 'uncontaminated fluid' adjusted by its mole fraction (0.8658) and the OBM, which was represented by the mud pseudo component, adjusted by its mole fraction (0.1342).

Table 5.18: M2 Station 136 fluid composition with mud pseudo component.

Component	MW	Res. Fluid	Uncontaminated Fluid	Drilling Mud	Pseudo Res. Fluid
	lb/lbmol	wt %	mole %	mole %	mole %
Mudpseudo2_136-1	171.10				13.42
CO2	44.01	0.00	0.00	0.00	0.00
N2	28.01	0.00	0.00	0.00	0.00
C1	16.04	0.00	0.00	0.00	0.00
C2	30.07	0.00	0.00	0.00	0.00
C3	44.1	0.01	0.06	0.00	0.05
i-C4	58.12	0.03	0.14	0.00	0.12
n-C4	58.12	0.10	0.45	0.00	0.39
i-C5	72.15	0.13	0.47	0.00	0.41
n-C5	72.15	0.23	0.83	0.00	0.72
C6	84	0.72	2.26	0.00	1.96
C7	96	1.90	5.25	0.02	4.55
C8	109	3.22	7.83	0.02	6.78
C9	122	3.22	7.01	0.01	6.07
C10	135	3.13	6.14	0.11	5.32
C11	148	3.84	5.59	8.34	4.84
C12	161	5.93	4.33	35.07	3.75
C13	175	6.45	4.03	37.01	3.49
C14	190	5.13	4.58	16.68	3.96
C15	204	3.67	4.37	2.56	3.79
C16	218	2.82	3.41	0.11	2.96
C17	232	3.66	4.18	0.04	3.61
C18	247	2.68	2.87	0.02	2.49
C19	261	2.34	2.38	0.01	2.06
C20	275	2.31	2.23	0.00	1.93
C21	294	2.46	2.22	0.00	1.92
C22	312	2.43	2.07	0.00	1.79
C23	331	2.54	2.03	0.00	1.76
C24	349	2.45	1.86	0.00	1.61
C25	368	2.82	2.03	0.00	1.76
C26	387	2.60	1.78	0.00	1.54
C27	405	3.19	2.09	0.00	1.81
C28	424	2.90	1.81	0.00	1.57
C29	442	3.62	2.17	0.00	1.88
C30+	461	23.49	13.51	0.00	11.70
		100.00	100.00	100.00	100.00

The composition shown in Table 5.18 which includes contamination represented by the mud pseudo component was then characterized and tuned to fit the experimental data. The critical properties of the defined components (mud pseudo component, CO2, N2,C1-C6) and the C7+ fractions were then determined. The full compilation of the critical properties, interaction parameters, compositions, and model parameters generated for the contaminated sample resulting from the characterization procedures for M2 Station 136 are provided in Appendix B.

For consistency with M1 Station 83, the sample from M2 Station 136 was characterized based on the Modified Exponential Pedersen distribution with the Pedersen property correlation and then was tuned with the available laboratory data. Results of the tuning process for M2 Station 136 are shown in Table 5.19.

Table 5.19: M2 Station 136 model tuning results before decontamination.

Test	Item	Unit	Exp. Data	Cal. Result Bef. Tuning	Cal. Result Aft. Tuning
PT Flash	Liq. Density	g/cm^3	0.8905	0.8905	0.8905

The phase envelope showing a match with the experimental data is shown in Figure 5.9.

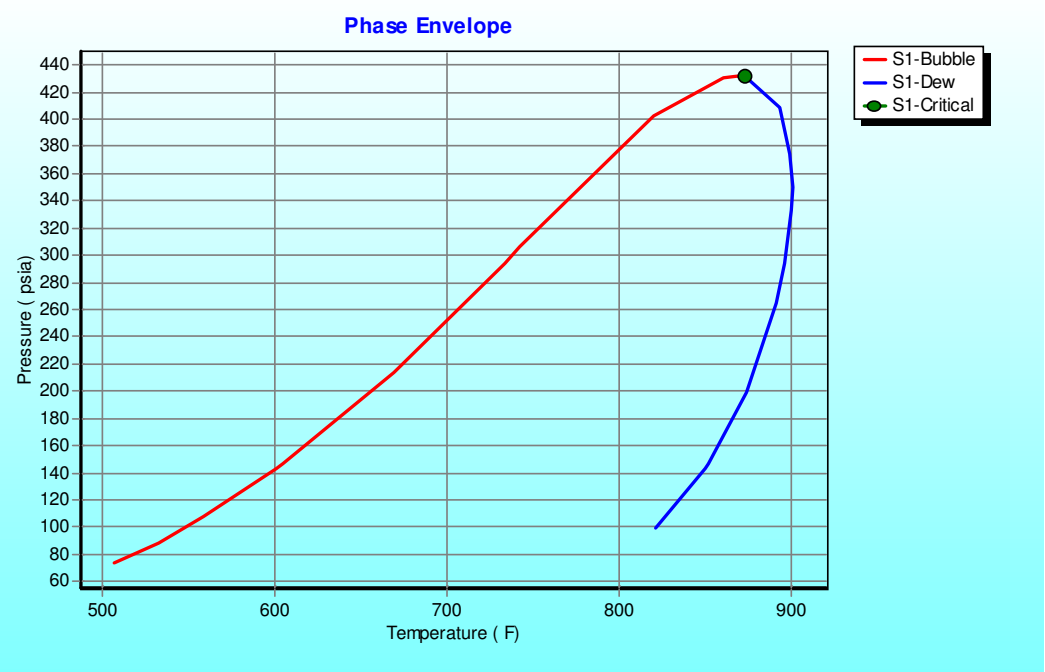

Figure 5.9: M2 Station 136 phase envelope before decontamination.

This composition was tuned with experimental data from the laboratory analysis and then the mud pseudo component was set to zero.

Table 5.20: M2 Station 136 fluid composition after decontamination.

Component	MW	Density	Pseudo Res. Fluid
	lb/lbmol	g/cm^3	mole %
Mudpseudo2_136-1	171.10	0.808	0.00
CO2	44.01		0.00
N2	28.01		0.00
C1	16.04		0.00
C2	30.07		0.00
C3	44.10		0.06
i-C4	58.12		0.14
n-C4	58.12		0.45
i-C5	72.15	0.616	0.47
n-C5	72.15	0.622	0.83
C6	84	0.685	2.26
C7	96	0.722	5.25
C8	109	0.745	7.83
C9	122	0.764	7.01
C10	135	0.778	6.14
C11	148	0.789	5.59
C12	161	0.800	4.33
C13	175	0.811	4.03
C14	190	0.822	4.57
C15	204	0.832	4.38
C16	218	0.839	3.42
C17	232	0.847	4.17
C18	247	0.852	2.88
C19	261	0.857	2.38
C20	275	0.862	2.23
C21	294	0.867	2.22
C22	312	0.872	2.07
C23	331	0.877	2.03
C24	349	0.881	1.86
C25	368	0.885	2.03
C26	387	0.889	1.78
C27	405	0.893	2.09
C28	424	0.896	1.81
C29	442	0.899	2.17
C30+	461	1.010	13.51
			100.00

The overall fluid composition was then re-normalized and the resulting composition is shown in Table 5.20. This composition was representative of the

reservoir fluid with 0% OBM contamination and the sample was considered 'decontaminated.' Since the EOS of the contaminated sample should be the same as the EOS of the decontaminated sample, the decontaminated composition was not re-characterized. Instead, it was tuned again with the experimental data without re-characterization. The final result of the iterative tuning process shows the calculated oil density equal to the experimental data in Table 5.21.

Table 5.21: M2 Station 136 model tuning results after decontamination.

Test	Item	Unit	Exp. Data	Cal. Result Bef. Tuning	Cal. Result Aft. Tuning
PT Flash	Liq. Density	g/cm^3	0.8905	0.8905	0.8905

The phase envelope resulting from successful tuning procedures for the decontaminated composition is shown in Figure 5.10.

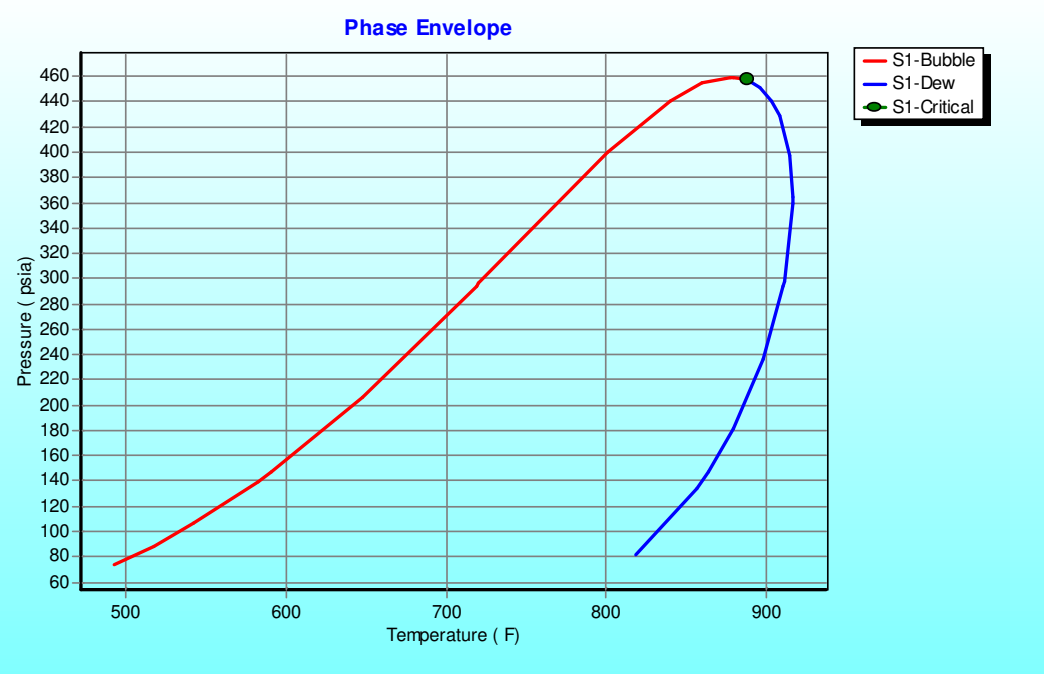

Figure 5.10: M2 Station 136 phase envelope after decontamination.

For M2 Station 136, the sample was relatively clean to begin with and while the hump indicative of contamination was not as severe as it was in the M1 Station 83

sample, it was still clear that there was a deviation from a semi-log straight line behavior.

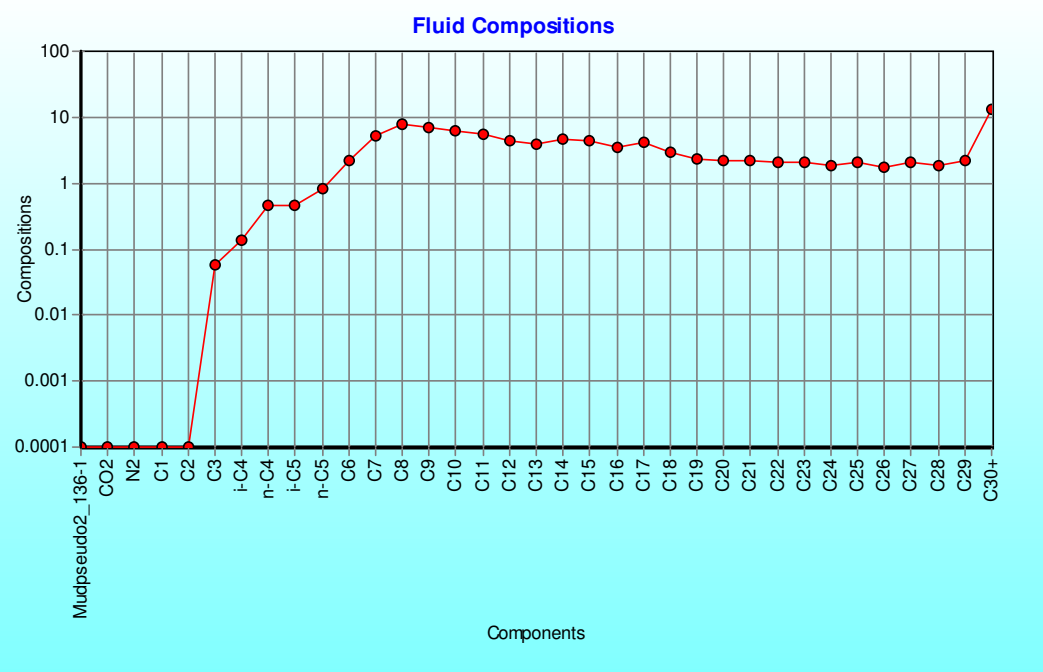

Figure 5.11: M2 Station 136 fluid composition (mol%) after decontamination.

After decontamination, the hump that was evident in the contaminated sample was hard to distinguish as the decontaminated composition shown in Figure 5.11 deviates even less from a semi-log straight line behavior. At this point, the decontaminated sample was ready for modeling. The exercise of decontamination for the sample at M2 Station 136 highlights the advantages of being able to start the modeling process with a relatively clean sample.

For M2 Station 136, one challenge introduced to the modeling process was that a bottomhole sample was not acquired for PVT analysis. Instead, the sample was taken at stock tank conditions and gas composition was not available. Due to these limitations, a different approach was used to assess the connectivity of M2 Station 136 with M1 Station 83. The DFA composition acquired from real time operations was summarized and compared to the composition of the decontaminated sample from M1Station 83, modeled at the reservoir conditions of M2 Station 136. The IFA

version of DFA technology lumps C3-C5 and C6+ as weight percentages; those separate components from the compositional simulation were grouped in order to compare the results in Table 5.22.

Table 5.22: Comparison of M1 and M2 composition at M2 Station 136 conditions.

	Comparison at M2 Station 136 reservoir conditions	
	Simulation Results	DFA
Component	Fluid from M1 Station 83	M2 Station 136
N2 (wt%)	0.15	NA*
C1 (wt %)	2.17	0.77
C2 (wt %)	0.15	0.54
C3-C5 (wt %)	2.63	4.19
C6+ (wt %)	94.64	94.50
CO2 (wt %)	0.26	0.00
	100.00	100.00

* DFA is unable to detect N2.

Since there was no bottomhole sample from M2 Station 136, the following approach was based on the assumption that if Sand F was connected between M1 and M2, the fluid compositions of M1 Station 83 and M2 Station 136 would likely be the same when modeled under the same reservoir conditions.

Fluid density determined from the CCE test based on the M1 Station 83 fluid composition was used to determine a synthetic OD using the FHZ EOS at M2 Station 136 reservoir conditions. Following the same procedure detailed in Section 5.1.1, the only variable that changed in the calculations from that example based on the equation below was the fluid density (from 0.8 to 0.742) taken from Table 5.14.

$$OD(h2) = \exp\left(-\frac{V_a g(\rho_a - \rho)(h_2 - h_1)}{kT}\right) * OD(h_1)$$

The synthetic OD based on the decontaminated sample from M1 Station 83 modeled at M2 Station 136 conditions was determined to be 1.478. Recall that the actual OD measurement from DFA operations for M2 Station 136 was 1.348. A

comparison of the actual DFA OD measurement to the synthetic OD in relation to the DFA prediction curve is shown in Figure 5.12.

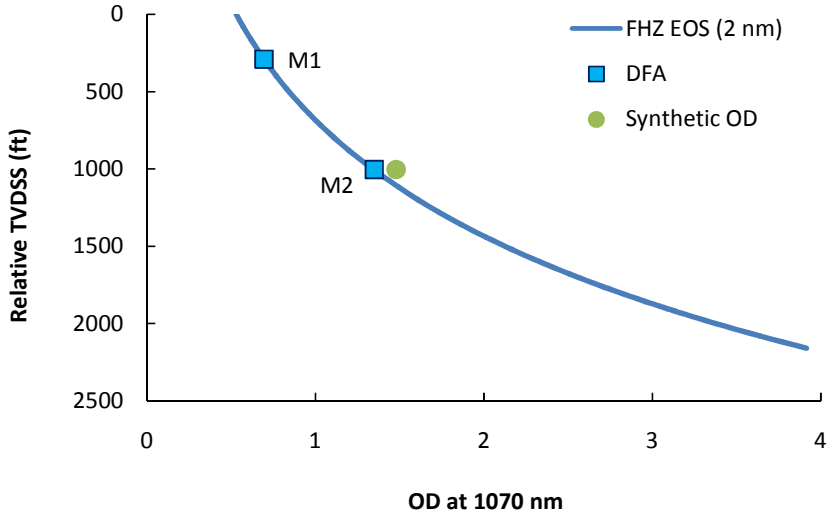

Figure 5.12: Comparison of actual DFA OD measurement and synthetic OD.

For low GOR fluids this approach is completely dependent on the fluid density. Therefore, a sensitivity analysis of the synthetic OD calculation to the modeled fluid density was analyzed for the M1 Station 83 fluid composition at M2 Station 136 reservoir conditions. The fluid densities were varied over a range from 0.650 g/cm3 to 0.950 g/cm3 and are shown in Figure 5.13.

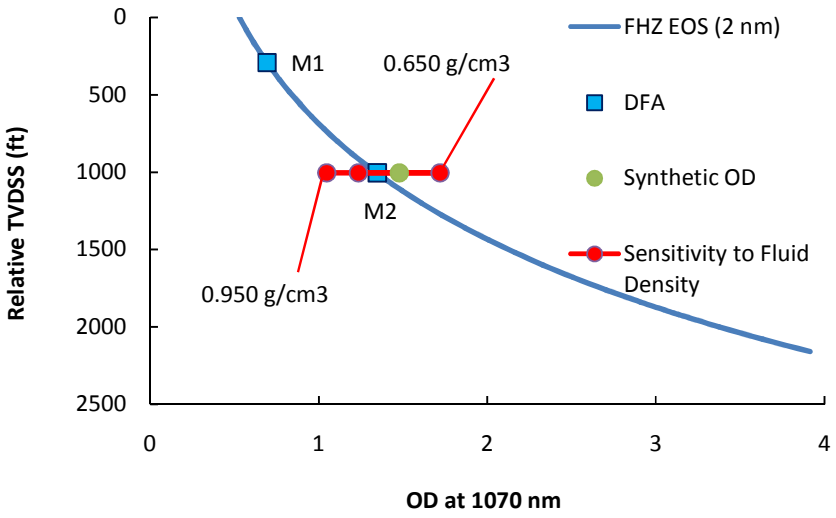

Figure 5.13: Sensitivity analysis of the synthetic OD.

The procedure seemed to confirm the interpretation for connectivity between M1 and M2. Therefore, the procedure was repeated at reservoir conditions for M3 Station 18 in the Section 5.2.3 to determine whether it was valid for a case to confirm whether two wells were not connected.

5.2.3 M3 Station 18

The plot of the initial contamination study shown in Figure 5.14 exhibits a hump in composition from C11 to C15 and this deviation from the straight line behavior corresponds with the composition of the drilling mud contaminant.

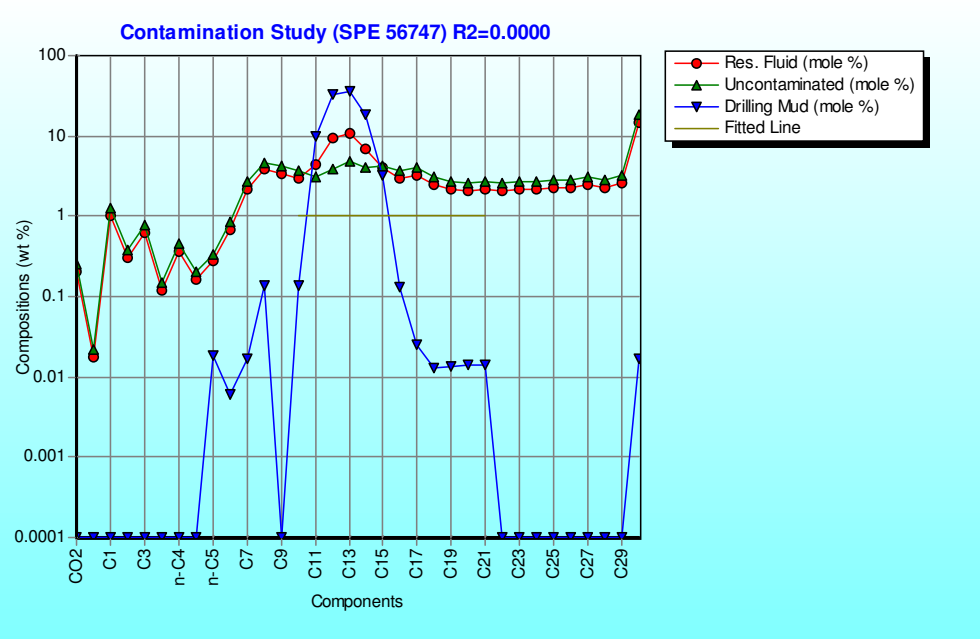

Figure 5.14: M3 Station 18 initial contamination study.

The tabulated results of the initial contamination study which include the compositions of the original contaminated reservoir fluid, 'uncontaminated fluid,' and drilling mud are provided in Table 5.23.

Table 5.23: M3 Station 18 initial contamination study.

Component	MW	Res. Fluid	Uncontaminated Fluid	Drilling Mud
	lb/lbmol	wt %	mole %	mole %
CO2	44.01	0.20	1.36	0.00
N2	28.01	0.02	0.18	0.00
C1	16.04	1.03	18.87	0.00
C2	30.07	0.31	2.97	0.00
C3	44.10	0.61	4.08	0.00
i-C4	58.12	0.12	0.61	0.00
n-C4	58.12	0.37	1.85	0.00
i-C5	72.15	0.16	0.66	0.00
n-C5	72.15	0.27	1.10	0.07
C6	84	0.67	2.35	0.02
C7	231	2.13	2.70	0.02
C8	237	3.79	4.65	0.16
C9	244	3.35	4.03	0.00
C10	250	2.96	3.44	0.15
C11	257	4.46	2.81	10.65
C12	263	9.56	3.42	33.84
C13	278	10.96	4.14	34.64
C14	293	6.95	3.23	17.40
C15	308	4.07	3.26	2.87
C16	324	2.98	2.67	0.11
C17	339	3.30	2.85	0.02
C18	354	2.48	2.05	0.01
C19	369	2.15	1.71	0.01
C20	384	2.11	1.61	0.01
C21	392	2.14	1.60	0.01
C22	399	2.10	1.54	0.00
C23	407	2.14	1.54	0.00
C24	415	2.15	1.52	0.00
C25	423	2.24	1.55	0.00
C26	430	2.24	1.53	0.00
C27	438	2.48	1.66	0.00
C28	446	2.25	1.48	0.00
C29	453	2.55	1.65	0.00
C30+	461	14.66	9.32	0.01
		100.00	100.00	100.00

Similar to the procedure for M1 and M2, additional steps were required for decontamination after the initial contamination study. The relative level of contamination for M3 Station 18 was determined in the laboratory to be 20% which

when used in conjunction with the computed MW of the drilling mud yields a 17.63 mol% as shown in Table 5.24.

Table 5.24: M3 Station 18 contamination level.

Stream	MW	Mole %	Weight %
Uncontaminated Fluid	234.53	82.3721	80
Drilling Mud	273.98	17.6279	20

The uncontaminated fluid mol% and the drilling mud mol% values in Table 5.24 were used in the calculations that followed to determine the contributions of the uncontaminated fluid and the drilling mud to the overall fluid composition. The calculated properties for the mud pseudo component for the drilling mud used in M3 are shown in Table 5.25.

Table 5.25: M3 Station 18 mud pseudo component properties.

Component			MW	Critical P.	Critical T.	Acentric	Volume Trans.	Feed
	From	To	lb/lbmol	psia	F			Mole Frac.
Mudpseudo3_18-1	n-C5	C30+	273.98	249.5	747.1	0.6105	0.1029	1.00

For M3 Station 18, the critical properties were determined for one mud pseudo component, Mudpseudo3_18-1 grouped from n-C5 to C30+ with a liquid mole fraction equal to 1. Note that the MW determined for Mudpseudo3_18-1 represents a weighted average of the mud components and the MW was not affected greatly by the inclusion of the small portion of the mud composition contributed by C30+. Nevertheless, the entire composition of the mud must be accounted for and that was the reason that the mud pseudo component had a much larger range than the mud pseudo components determined for M1 and M2.

The next step required was the modification of Table 5.23 so that the drilling mud composition was represented by the mud pseudo component. Table 5.26 shows the composition of the calculated 'pseudo reservoir fluid' which was comprised of the 'uncontaminated fluid' adjusted by its mole fraction (0.8237) and the OBM, which was represented by the mud pseudo component, adjusted by its mole fraction (0.1763).

Table 5.26: M3 Station 18 fluid composition with mud pseudo component.

Component	MW	Res. Fluid	Uncontaminated	Drilling Mud	Pseudo Res. Fluid
	lb/lbmol	wt %	mole %	mole %	mole %
Mudpseudo3_18-1	273.98				17.63
CO2	44.01	0.20	1.36	0.00	1.12
N2	28.01	0.02	0.18	0.00	0.15
C1	16.04	1.03	18.87	0.00	15.54
C2	30.07	0.31	2.97	0.00	2.45
C3	44.10	0.61	4.08	0.00	3.36
i-C4	58.12	0.12	0.61	0.00	0.50
n-C4	58.12	0.37	1.85	0.00	1.52
i-C5	72.15	0.16	0.66	0.00	0.54
n-C5	72.15	0.27	1.10	0.07	0.91
C6	84	0.67	2.35	0.02	1.94
C7	231	2.13	2.70	0.02	2.23
C8	237	3.79	4.65	0.16	3.83
C9	244	3.35	4.03	0.00	3.32
C10	250	2.96	3.44	0.15	2.83
C11	257	4.46	2.81	10.65	2.31
C12	263	9.56	3.42	33.84	2.81
C13	278	10.96	4.14	34.64	3.41
C14	293	6.95	3.23	17.40	2.66
C15	308	4.07	3.26	2.87	2.68
C16	324	2.98	2.67	0.11	2.20
C17	339	3.30	2.85	0.02	2.35
C18	354	2.48	2.05	0.01	1.69
C19	369	2.15	1.71	0.01	1.41
C20	384	2.11	1.61	0.01	1.33
C21	392	2.14	1.60	0.01	1.32
C22	399	2.10	1.54	0.00	1.27
C23	407	2.14	1.54	0.00	1.27
C24	415	2.15	1.52	0.00	1.25
C25	423	2.24	1.55	0.00	1.28
C26	430	2.24	1.53	0.00	1.26
C27	438	2.48	1.66	0.00	1.37
C28	446	2.25	1.48	0.00	1.22
C29	453	2.55	1.65	0.00	1.36
C30+	461	14.66	9.32	0.01	7.68
		100.00	100.00	100.00	100.00

The pseudo reservoir fluid composition shown in Table 5.26 was then characterized and tuned to fit the experimental data. For consistency with the analysis

of M1 and M2, the defined components were not lumped and the C7+ fractions were lumped into 3 pseudo component groups. Similar to the iterative tuning process described for M1, the interaction parameters of the lumped plus fractions (C7-C15, C15-C26, and C26-C80) were tuned to fit the saturation pressure and temperature determined in the laboratory. The iterative tuning process was then repeated by adjusting the volume translation of each of the 3 lumped plus fraction pseudo components until the calculated oil density matched the experimental oil density. Similar to the characterization of the samples for M1 and M2, M3 Station 18 was characterized based on the Modified Exponential Pedersen distribution and the Pedersen property correlation. The summary of the tuning results is shown in Table 5.27.

Table 5.27: M3 Station 18 model tuning results before decontamination.

Test	Item	Unit	Exp. Data	Cal. Result Bef. Tuning	Cal. Result Aft. Tuning
Bubble/Dew	Bubble Point	psia	1225	1225	1225
PT Flash	Liq. Density	g/cm^3	0.8695	0.8695	0.8695

The phase envelope for the contaminated sample from M3 Station 18 represented by the mud pseudo component is shown in Figure 5.15.

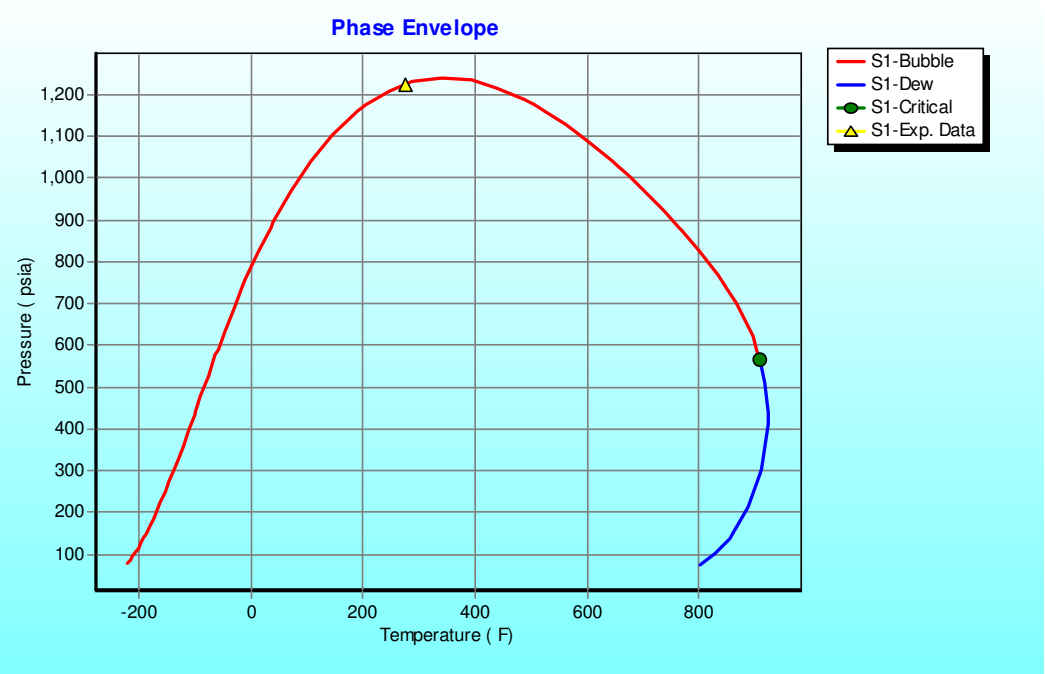

Figure 5.15: M3 Station 18 phase envelope before decontamination.

For M3 Station 18, the full summary of characterization and tuning results of the contaminated sample which includes interaction parameters, critical properties, and compositions is included in Appendix C. The decontamination procedure proceeded by setting the mud pseudo component to zero for the characterized composition. The overall fluid composition was re-normalized and the new composition shown in Table 5.28 was representative of the reservoir fluid with 0% OBM contamination. At this point, the sample was considered 'decontaminated.'

Table 5.28: M3 Station 18 fluid composition after decontamination.

Component	MW	Density	Pseudo Res. Fluid
	lb/lbmol	g/cm^3	mole %
Mudpseudo3_18-1	273.98	0.808	0.00
CO2	44.01		1.36
N2	28.01		0.18
C1	16.04		18.87
C2	30.07		2.97
C3	44.10		4.08
i-C4	58.12		0.61
n-C4	58.12		1.85
i-C5	72.15	0.616	0.66
n-C5	72.15	0.622	1.10
C6	84	0.685	2.36
C7	231	0.722	2.71
C8	237	0.745	4.65
C9	244	0.764	4.03
C10	250	0.778	3.44
C11	257	0.789	2.80
C12	263	0.800	3.41
C13	278	0.811	4.14
C14	293	0.822	3.23
C15	308	0.832	3.25
C16	324	0.839	2.67
C17	339	0.847	2.85
C18	354	0.852	2.05
C19	369	0.857	1.71
C20	384	0.862	1.61
C21	392	0.867	1.60
C22	399	0.872	1.54
C23	407	0.877	1.54
C24	415	0.881	1.52
C25	423	0.885	1.55
C26	430	0.889	1.53
C27	438	0.893	1.66
C28	446	0.896	1.48
C29	453	0.899	1.65
C30+	461	1.010	9.32
			100.00

The sample composition with the mud pseudo component set to zero (0% OBM contamination) was not re-characterized since the EOS of the contaminated sample should be the same as the EOS of the decontaminated sample. Instead, the composition with 0% OBM contamination was tuned again with the experimental data without re-characterization. The final result of the iterative tuning process showing the calculated saturation pressure and oil density equal to the experimental data is shown in Table 5.29.

Table 5.29: M3 Station 18 model tuning results after decontamination.

Test	Item	Unit	Exp. Data	Cal. Result Bef. Tuning	Cal. Result Aft. Tuning
Bubble/Dew	Bubble Point	psia	1225	1225	1225
PT Flash	Liq. Density	g/cm^3	0.8695	0.8695	0.8695

The phase envelope resulting from successful tuning procedures without re-characterization for the decontaminated composition is shown in Figure 5.16.

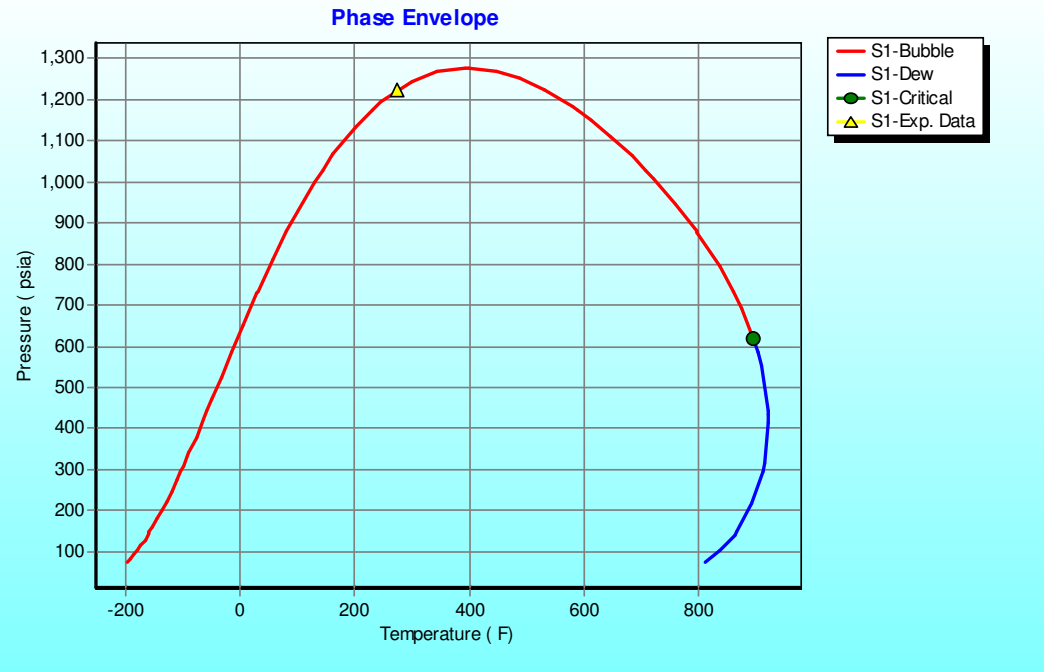

Figure 5.16: M3 Station 18 phase envelope after decontamination.

The full compilation of the critical properties, interaction parameters, compositions, and model parameters determined for the decontaminated sample is provided in Appendix C.

A plot of the decontaminated sample composition is shown in Figure 5.17. Note the relatively small deviation from a semi-log straight line behavior that one would expect from a clean sample.

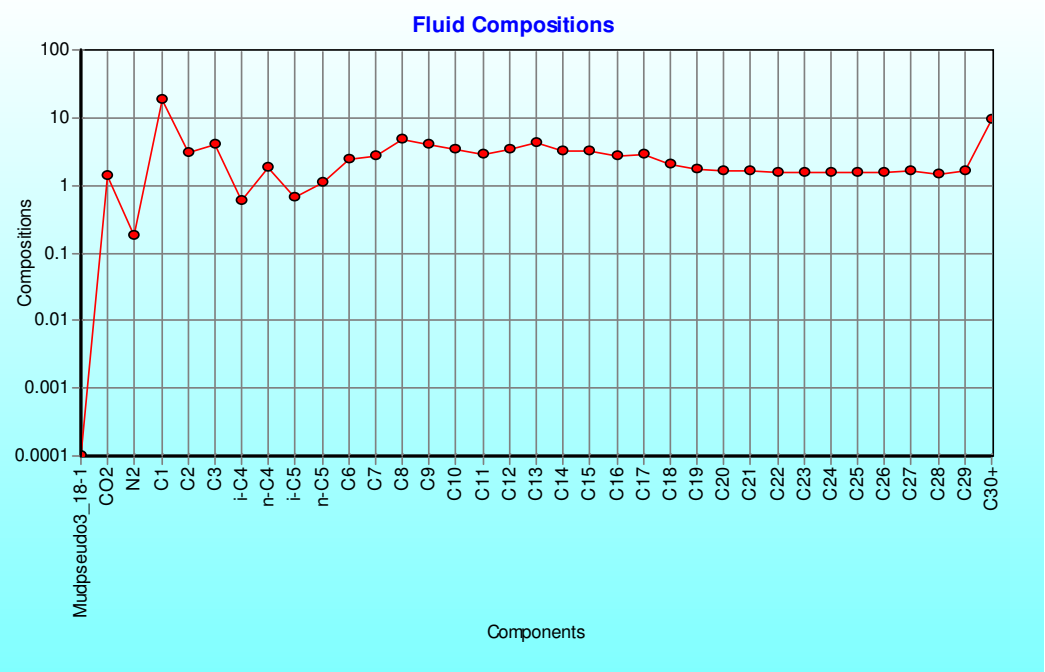

Figure 5.17: M3 Station 18 fluid composition (mol%) after decontamination.

At this point, the decontaminated sample was ready for modeling. The hump that was evident from C11 through C14 had basically been eliminated through the decontamination process. Regardless of the success in decontaminating a sample, the potential uncertainty that comes from working with a processed sample should be considered when analyzing the results of the model and it is recommended that the results be checked against other sources of data if available.

For M3 Station 18, the combination of having a relatively clean bottomhole sample with laboratory determined C30+ composition and DFA composition acquired from real time operations provided an opportunity to compare the two measurements.

This comparison was not possible for M1 Station 83 (LFA is not enabled for determining composition) or for M2 Station 136 (no bottomhole sample or gas composition available). The IFA version of DFA technology lumps C3-C5 and C6+ so those separate components from the decontaminated laboratory composition were grouped in order to compare the results which are shown in Table 5.30.

Table 5.30: M3 Station 18 DFA compared to decontaminated lab composition.

	M3 Sample 136 reservoir conditions	
	Decontaminated	DFA
Component	Fluid from M3 Station 18	M3 Station 18
N2 (wt%)	0.02	NA*
C1 (wt %)	1.29	0.32
C2 (wt %)	0.38	0.47
C3-C5 (wt %)	1.92	1.74
C6+ (wt %)	96.14	97.47
CO2 (wt %)	0.26	0.00
	100.00	100.00

* DFA is unable to detect N2.

The reservoir conditions for M3 Station 18 were used as a reference point for a compositional simulation for the decontaminated M3 Station 18 sample. The temperature gradient was adjusted to fit the reservoir temperatures of M1 Station 83 and M2 Station 136. The reference point data used in the compositional simulation for M3 Station 18 is shown in Table 5.31.

Table 5.31: M3 Station 18 compositional simulation reference point data.

Reference Data	
Measurement	M1 Station 83
Depth (ft)	1889
Pressure (psia)	3316
Temperature (degF)	275
Temp Gradient (degF/ft)	0.018

The composition of the fluid at M3 Station 18 was then determined by the compositional simulation for several different depths at fixed steps from the reference depth. Those fixed steps are shown in Table 5.32. Since the reference point for this

compositional simulation was set at the depth, temperature, and pressure for M3 Station 18, a fixed step that matches M3 Station 18 is provided at TVDss = 1889 ft, temperature = 275 degF, and pressure = 3316 psia.

Table 5.32: M3 Station 18 compositional simulation depths analyzed.

Relative TVDss	Temperature	Pressure	Sat. Pressure
ft	degF	psia	psia
289	246.2	2750.8	1449.3
389	248.0	2786.0	1433.3
489	249.8	2821.2	1417.7
589	251.6	2856.4	1402.3
689	253.4	2891.7	1387.3
789	255.2	2927.0	1372.5
889	257.0	2962.3	1357.9
989	258.8	2997.6	1343.6
1089	260.6	3032.9	1329.6
1189	262.4	3068.3	1315.8
1289	264.2	3103.6	1302.2
1389	266.0	3139.0	1288.8
1489	267.8	3174.4	1275.7
1589	269.6	3209.8	1262.7
1689	271.4	3245.2	1250.0
1789	273.2	3280.6	1237.4
1889	275.0	3316.0	1225.1
1989	276.8	3350.7	1212.9
2089	278.6	3385.4	1200.8
2189	280.4	3420.2	1189.0
2289	282.2	3454.9	1177.3

For the compositional simulation, the reservoir conditions at M1 Station 83 and M2 Station 136 did not match exactly with the fixed step depths that were generated for the model. Therefore, compositional simulation results were interpolated from the compositions determined at the fixed steps above and below the sample depths for M2 Station 136 and M3 Station 18. Additional results from the compositional simulation are provided in Appendix C. Results from the compositional simulation of M1 Station 83 for the depths of interest (M2 Station 136 and M3 Station 18) are provided in Table 5.33.

Table 5.33: M3 Station 18 compositional simulation results at selected depths.

	Compositional simulation for reservoir fluid from M3 Station 18					
Component	Depth = 291 ft		Depth = 1004 ft		Depth = 1889 ft	
	mole %	wt %	mol%	wt%	mol%	wt%
Mudpseudo3_18-1	0.00	0.00	0.00	0.00	0.00	0.00
CO2	1.56	0.32	1.47	0.29	1.36	0.26
N2	0.20	0.03	0.19	0.02	0.18	0.02
C1	21.97	1.62	20.48	1.45	18.87	1.29
C2	3.55	0.49	3.27	0.44	2.97	0.38
C3	4.85	0.98	4.48	0.87	4.08	0.77
i-C4	0.71	0.19	0.66	0.17	0.61	0.15
n-C4	2.20	0.59	2.03	0.52	1.85	0.46
i-C5	0.77	0.26	0.72	0.23	0.66	0.20
n-C5	1.31	0.43	1.21	0.39	1.10	0.34
C6	2.73	1.06	2.56	0.95	2.36	0.84
C7-C15	28.24	33.95	29.71	34.41	31.66	35.33
C16-C25	17.27	29.63	18.00	29.74	18.66	29.71
C26-C80	14.63	30.46	15.21	30.51	15.65	30.24
	100.00	100.00	100.00	100.00	100.00	100.00

With the compositional simulations for M1 Station 83 and M3 Station 18 and the DFA composition from M2 Station 136, the compositions from all three wells at reservoir conditions for M2 Station 136 were compared side by side in Table 5.34.

Table 5.34: Comparison of simulations to DFA at M2 Station 136 conditions.

	Comparison at M2 Sample 136 reservoir conditions		
	Simulation Results	DFA	Simulation Results
Component	Fluid from M-1 Station 83	M-2 Station 136	Fluid from M-3 Station 18
N2 (wt%)	0.15	NA*	0.02
C1 (wt %)	2.17	0.77	1.45
C2 (wt %)	0.15	0.54	0.44
C3-C5 (wt %)	2.63	4.19	2.18
C6+ (wt %)	94.64	94.50	95.62
CO2 (wt %)	0.26	0.00	0.29
	100.00	100.00	100.00

* DFA is unable to detect N2.

Constant Composition Expansion (CCE) tests were performed on the decontaminated reservoir fluid from M3 Station 18 with the aim of determining the bulk fluid density at reservoir conditions corresponding to M1 Station 83 and M2 Station 136. The results of the test for those specific conditions were summarized in Table 5.35.

Table 5.35: M3 Station 18 CCE test results.

	CCE Test Summary for M3 Station 18 Fluid Composition		
Res. Conditions (T and P)	M1 Station 83	M2 Station 136	M3 Station 18
Temp (degF)	246	260	275
Pressure (psia)	2738	2978	3316
Bulk Density (g/cm3)	0.812	0.810	0.808
Mudpseudo (mol%)	0.00	0.00	0.00
CO2 (mol%)	0.26	0.26	0.26
N2 (mol%)	0.02	0.02	0.02
C1 (mol%)	1.29	1.29	1.29
C2 (mol%)	0.38	0.38	0.38
C3 (mol%)	0.77	0.77	0.77
i-C4 (mol%)	0.15	0.15	0.15
n-C4 (mol%)	0.46	0.46	0.46
i-C5 (mol%)	0.20	0.20	0.20
n-C5 (mol%)	0.34	0.34	0.34
C6 (mol%)	0.84	0.84	0.84
C7-C15 (mol%)	35.33	35.33	35.33
C16-C25 (mol%)	29.71	29.71	29.71
C26-C80 (mol%)	30.24	30.24	30.24

Similar to the procedure performed on the M1 Station 83 fluid composition discussed in the previous section, the fluid density from the CCE test result for M3 Station 18 was then used in conjunction with the FHZ EOS to generate a synthetic OD at the reservoir conditions for M2 Station 136. This result was then compared to the synthetic OD determined from the M1 Station 83 fluid composition analyzed at M2 Station 136 reservoir conditions and the actual OD from the DFA measurement at M2 Station 136. Again, for low GOR fluids, the only variable that affects the OD calculations was the fluid density which was taken from Table 5.35. The synthetic OD based on the decontaminated sample from M3 Station 83 modeled at M2 Station 136 conditions was determined to be 1.321. Recall that the actual OD measurement from DFA operations for M2 Station 136 was 1.348. A comparison of the actual DFA OD measurement to the synthetic ODs determined from the modeled decontaminated fluid compositions for M1 Station 83 and M3 Station 18 in relation to the DFA prediction curve are shown in Figure 5.18.

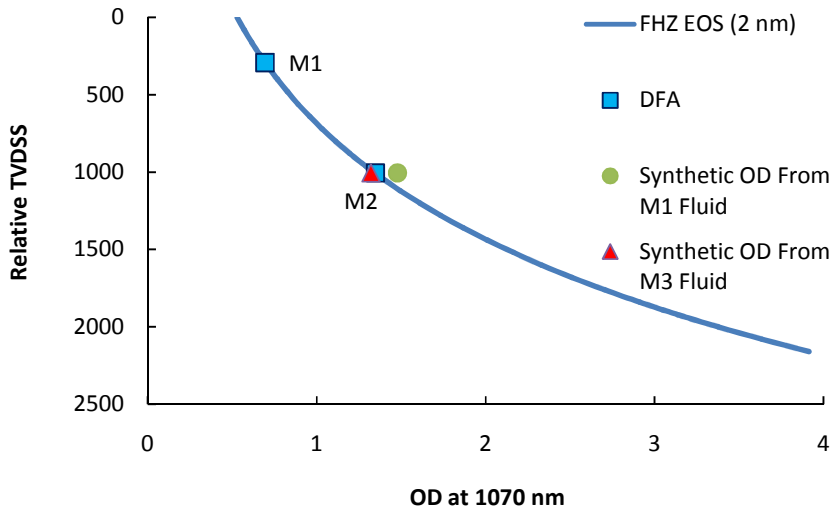

Figure 5.18: Comparison of synthetic ODs from M1 and M3.

It is assumed that the reservoir fluid in M3 is not in equilibrium with M1 and M2. Therefore, these results would indicate that for low GOR fluids, generating a

synthetic OD based on the modeled fluid density is likely not an effective approach as the synthetic OD fits the DFA prediction curve whether or not the fluid is in equilibrium.

5.2.4 PVT Modeling Discussion

The decontaminated compositions from M1, M2, and M3 are summarized and shown side by side in Table 5.36. Recall the unique characteristics of each sample. M1 Station 83 was highly contaminated and shows higher C11-C14 components compared to the cleaner samples from M2 and M3. M2 was a stock tank sample and no gas composition was provided in the laboratory reports so the lighter components such as CO2, N2, C1, and C2 are not accounted for in the composition. M3 was relatively clean but based on the latest geological interpretation, it was not thought to be in fluid communication with the other wells and therefore, the fluid composition was not expected to be the same.

Table 5.36: Summary of decontaminated fluid composition for M1, M2, and M3.

Component	Decontaminated Pseudo Reservoir Fluid		
	M1 Station 83	M2 Station 136	M3 Station 18
	mole %	mole %	mole %
Mudpseudo*	0	0	0
CO2	0.92	0	1.36
N2	0.83	0	0.18
C1	22.32	0	18.87
C2	0.8	0	2.97
C3	1.47	0.06	4.08
i-C4	0.58	0.14	0.61
n-C4	1.72	0.45	1.85
i-C5	1.28	0.47	0.66
n-C5	1.64	0.83	1.1
C6	3.83	2.26	2.36
C7	3.69	5.25	2.71
C8	6.13	7.83	4.65
C9	4.02	7.01	4.03
C10	3.33	6.14	3.44
C11	5.52	5.59	2.8
C12	10.01	4.33	3.41
C13	10.65	4.03	4.14
C14	12.62	4.57	3.23
C15	1.75	4.38	3.25
C16	1.22	3.42	2.67
C17	1.28	4.17	2.85
C18	0.67	2.88	2.05
C19	0.5	2.38	1.71
C20	0.39	2.23	1.61
C21	0.39	2.22	1.6
C22	0.33	2.07	1.54
C23	0.36	2.03	1.54
C24	0.28	1.86	1.52
C25	0.31	2.03	1.55
C26	0.25	1.78	1.53
C27	0.28	2.09	1.66
C28	0.17	1.81	1.48
C29	0.17	2.17	1.65
C30+	0.33	13.51	9.32
	100.00	100.00	100.00

The main observation from the data preparation process was that it highlighted how important it is to obtain a contaminant-free sample. The results for M2 Station 136 show that decontamination procedures for a relatively clean sample are more likely to yield a decontaminated composition that exhibits a semi-log straight line behavior which would be expected of a clean sample. This was in contrast to the M1 Station 83 sample which was highly contaminated and for which decontamination procedures proved beneficial but could only reduce the effects of contamination to a certain extent. For this reason, a great deal of time and effort is made to obtain a clean sample in both operations as well as developing new tool technology as described in Chapter III Theory and Concept. In addition, it should be noted that since decontamination procedures require a breakdown of C30+ components, (or components that entirely cover the range of the drilling mud composition) decontamination would not be initiated for at least several months after the samples were taken. DFA currently lumps C6+ and therefore the decontamination procedure used on the laboratory samples discussed in this chapter cannot be utilized on compositions determined in real-time with the DFA. In the time between when the samples are taken and the lab analysis is completed, the determination of fluid properties is dependent on DFA. The DFA measurements are corrected based on the level of contamination in the reservoir fluid flowing past the optical fluid analyzer.

5.3 Result Comparison

For fluid in a reservoir to be connected, pressure equilibrium is required. However, pressure equilibrium can be observed in reservoirs that are not in fluid communication. For this project, the interpretation of pressure gradients in line with the latest geological interpretation was that M1 and M2 were in pressure communication while M3 was not in pressure communication with the other wells. Figure 5.19 shows this interpretation of two different pressure gradients.

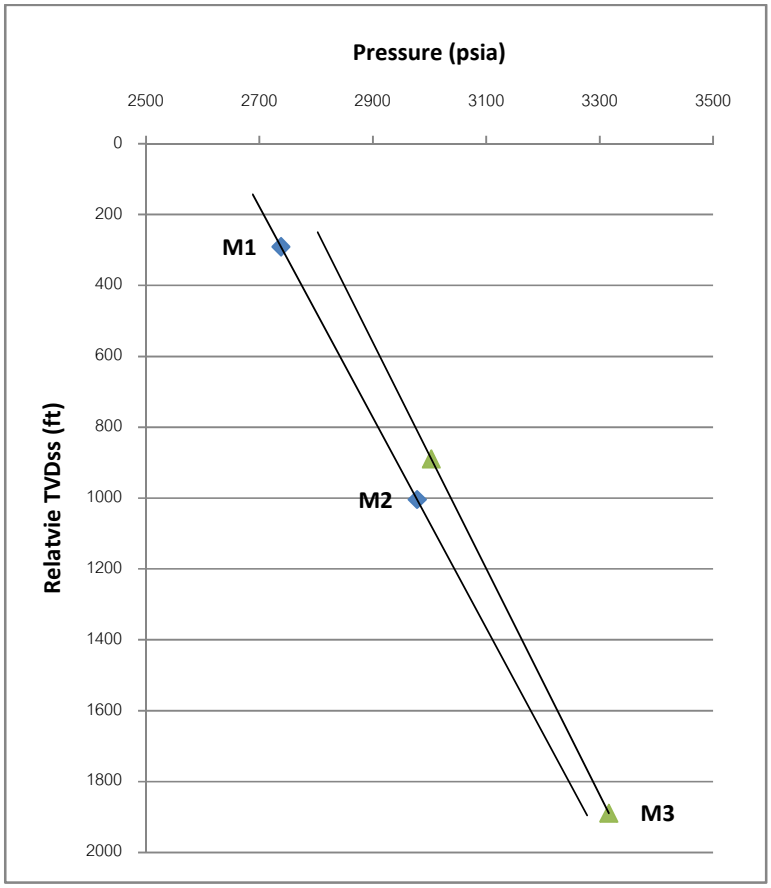

Figure 5.19: Pressure gradients for M1, M2, and M3 for Sand F.

Analyzing pressure gradients is subject to interpretation and if different fluids have similar densities a break in the pressure gradients may not be detectable. Therefore, it is beneficial to have a complementary approach such as DFA prediction. The DFA prediction curve, based on the OD from M1 as a starting point, corrected for baseline and OBM contamination, was generated based on a nano-aggregate asphaltene structure. The OD for M2 fit the prediction curve, while the OD for M3 did not. The DFA prediction results indicate that there was likely a flow barrier between M3 and the other wells (M1 and M2) which prevented the reservoir fluid in Sand F from reaching equilibrium.

The decontamination procedures performed on the laboratory samples were successful in decontaminating the samples and producing a compositional simulation. On the one hand, the compositional simulation results showed that M1 and M2 had

very similar composition, (i.e. they were the same reservoir fluid), and the reservoir was likely connected. Given the initial geological interpretation and the results of the DFA prediction analysis, this was expected. On the other hand, the compositional simulation results for M3 were inconclusive as the compositions for M3 and M2 were only slightly different and likely not great enough to justify an interpretation of a flow barrier between M2 and M3.

Low GOR, waxy reservoir fluids do not show enough of a compositional gradient to utilize composition to determine whether the reservoir fluids are the same or different from well to well. Along those same lines, the approach of generating synthetic ODs based on the densities determined from decontaminated laboratory fluid composition appeared to be flawed, at least for low GOR fluids. M3 is suspected of not being connected to the other wells and this is evident from the DFA prediction curve results and agrees with the latest geological interpretation discussed earlier. However, when the reservoir fluid from M3 was used to generate a synthetic OD, M3 appeared to be in connection to the other wells (M1 and M2). Since the synthetic OD is dependent on the difference between the density of asphaltene and the average density of the reservoir fluid, the synthetic OD derived from a low GOR fluid did not appear to be a good candidate to generate a stand-alone OD data point which could then be compared to the DFA prediction curve to assess connectivity.

CHAPTER VI

CONCLUSIONS AND RECOMMENDATIONS

This chapter presents conclusions drawn from the study of connectivity in a thin bed sand reservoir containing low GOR, waxy crude. In addition, a discussion of the limitations of the study and recommendations for future work are included.

1.1 Conclusions

For this study, fluid samples from a thin bed sand (Sand F) intersected by three wells (M1, M2, and M3) were analyzed in order to determine reservoir connectivity between the wells. There were two approaches used in the analysis. The first approach utilized the real time optical property measurements from DFA operations and the second approach utilized traditional PVT analysis. For the analysis based on DFA measurements, the OD from M1 was used as a starting point to generate a DFA prediction curve based on the FHZ EOS. The OD measurements from DFA operations in M2 and M3 were compared to this prediction curve to determine reservoir connectivity. For the analysis based on PVT modeling, the laboratory samples were decontaminated and modeled at varied reservoir conditions in order to compare the reservoir fluid sample compositions from one well to another to determine connectivity. From Chapter V Results and Discussion, it can be concluded that:

1. From the DFA prediction analysis utilizing the FHZ EOS, the reservoir fluid appeared to be in equilibrium from M1 to M2 and therefore the interpretation was that the reservoir was likely connected between M1 and M2. The reservoir fluid from M3 did not appear to be in equilibrium with

either M1 or M2, and therefore the interpretation confirmed the latest geological interpretation that a flow barrier separates M3 from M1 and M2.

2. The reservoir fluid type indicates the type of asphaltene structure and corresponding asphaltene diameter used in the FHZ EOS. The nano-aggregate asphaltene structure was appropriate for the low GOR, waxy crudes analyzed in this project. The resulting DFA prediction curve generated based on an asphaltene diameter = 2 nm fit the OD data for M1 and M2, confirming the latest geological interpretation that M1 and M2 are in fluid equilibrium.

3. There is no great substitute for a clean sample as even small amounts of OBM contamination can affect sample fluid properties and increase the uncertainty in the subsequent models and calculations that follow. However, from what is known about the typical declining exponential distribution of C8+ components for real petroleum fluids, decontamination methods can be implemented. The M1 sample was highly contaminated and decontamination procedures appeared to significantly reduce the effect of OBM contamination when comparing the plots of fluid composition and phase envelopes before and after decontamination.

4. The measured level of contamination seemed to have an effect on the final decontamination result. In other words, after decontamination samples M2 and M3 with relatively lower contamination were able to achieve a very close fit with the semi-log straight line behavior one would observe with a clean sample. For M1, which had a much higher level of contamination, decontamination procedures improved but could not achieve the same close fit to the clean sample behavior observed in the plot of fluid composition.

5. For the low GOR fluids analyzed in this study, fluid composition was not expected to change considerably with varying temperatures and pressures. This was confirmed by the results of the PVT modeling, which showed that the modeled fluid compositions were consistent with actual fluid composition measurements from DFA operations at similar reservoir conditions.

6. This study confirms that analyzing the asphaltene gradient in conjunction with the FHZ EOS is an effective method of determining connectivity for reservoirs with low GOR fluids for situations when the GOR gradient continuity is inconclusive.

1.2 Recommendations

1. Sampling operations are planned to meet specific objectives with the aim of accurately characterizing the reservoir while striking a balance with rig time and cost by minimizing the number of samples taken. That being said, increasing the number of sampling stations in each well would have provided better data coverage which may have reduced the uncertainty in the modeling and interpretation that followed. This was especially evident when analyzing M1 Station 83 which had a relatively high level of contamination both when analyzed in real time during DFA operations and from the laboratory results. Furthermore, the level of contamination varied significantly between the DFA and laboratory measurements. For the wells analyzed in this project there was only one sample taken from Sand F and consequently, there was only one data point to depend on. Attempting an additional DFA station and obtaining a cleaner sample in Sand F for M1 may have helped to reduce the uncertainty with the final decontaminated composition result. A recommended rule of thumb would

be to plan operations for a DFA station at the top and bottom of a reservoir. For thin bed reservoirs this would provide a backup in case one of the stations was contaminated and could also be helpful if vertical connectivity was in question with an adjacent thin bed.

2. It is recommended that all of the available data be utilized to determine connectivity. Increasing the level of integration of different sources of data (geological interpretation, mud logging data, geochemical fingerprinting) may shed some light on the conditions responsible for the rock and fluid complexities in this area and could help to confirm the interpretation. Ideally, this integrated approach could also provide a better understanding of the reservoir and result in the optimum number of samples and optimal sampling locations for future operations.

REFERENCES

[1] Dake, L.P. 2001. *The Practice of Reservoir Engineering*, Revised Edition. Holland: Elsevier Publishing.

[2] Mullins, O.C., 2010. *The Physics of Reservoir Fluids: Discovery Through Downhole Fluid Analysis*. USA: Schlumberger.

[3] Muggeridge, A., and Smalley, P.C., 2008. A Diagnostic Toolkit to Detect Compartmentalization Using Time Scales for Reservoir Mixing. *SPE 118323 paper presented at the Abu Dhabi International Petroleum Exhibition and Conference held in Abu Dhabi, UAE.*

[4] Vrolijk, P., James, B., Myers, R., Maynard, J., Sumpter, L., and Sweet, M., 2005. Reservoir Connectivity Analysis – Defining Reservoir Connections and Plumbing. *SPE 93577 paper presented at the SPE Middle East Oil and Gas Show and Conference held in Bahrain.*

[5] Mullins, O.C., et al., 2011. Impact of Asphaltene Nanoscience on Understanding Oilfield Reservoirs. *SPE 146649 paper presented at the SPE Annual Technical Conference and Exhibition held in Denver, USA.*

[6] Snedden, J., et al., 2007. Reservoir Connectivity: Definitions, Examples, and Strategies. *IPTC 11375 paper presented at the International Petroleum Technical Conference held in Dubai, UAE.*

[7] Pfeiffer, T., Reza, Z., Schecter, D., McCain, W., and Mullins, O.C., 2011. Determination of Fluid Composition Equilibrium Under Consideration of Asphaltenes – A Substantially Superior Way to Assess Reservoir Connectivity Than Formation Pressure Surveys. *SPE 145609 paper presented at SPE Annual Technical Conference and Exhibition held in Denver, USA.*

[8] Mullins, O.C., and Zhu, Y., 1992. First Observation of the Urbach Tail in a Multicomponent Organic System. *Applied Spectroscopy, 46, Number 2, 354-356.*

[9] Smits, A.R., Fincher, D.V., Nishida, K., Mullins, O.C., Schroeder, R.J., and Yamate, T., 1995. In-Situ Optical Fluid Analysis as an Aid to Wireline Formation Sampling. *SPE Formation Evaluation, June.*

[10] Felling, M.M., and Morris, C.W., 1998. Characterization of In-Situ Fluid Responses by Use of Optical Fluid Analysis. SPE50994. *SPE Reservoir Evaluation & Engineering, August.*

[11] O'Keefe, M., et al., 2007. In-Situ Density and Viscosity Measured by Wireline Formation Testers. *SPE 110364 paper presented at the SPE Asia Pacific Oil and Gas Conference and Exhibition held in Jakarta, Indonesia.*

[12] Dong, C., Hegeman, P., Carnegie, A., Elshahawi, H., 2006. Downhole Measurement of Methane Content and GOR in Formation Fluid Samples. *SPE Reservoir Evaluation and Engineering* Volume 9, Number 1: 7-14.

[13] Zuo, J., 2012, personal email, 27 February.

[14] Gozalpour, F., Danesh, A., Tehrani, D., Todd, A., and Tohidi, B., 1999. Predicted Reservoir Fluid Phase and Volumetric Behaviour From Samples Contaminated With Oil-Based Mud. *SPE 56747 paper presented at the SPE Annual Technical Conference and Exhibition held in Houston, USA.*

[15] Mullins, O.C. 2008. Review of the Molecular Structure and Aggregation of Asphaltenes and Petroleomics. *SPE* Journal Volume 13, Number 1: 48-57.

[16] Mullins, O.C., Elshahawi, H., and Stainforth, J., 2008. Integration of Basin Modeling Consideration With Wireline Logging. *SPWLA 2008-NN paper presented at SPWLA 49th Annual Logging Symposium held in Edinburgh, Scotland.*

[17] Zuo, J., et al., 2011. Equation of State Based Downhole Fluid Characterization. *SPE 114702 paper presented at the SPE Asia Pacific Oil an Gas Conference held in Perth, Australia.*

[18] Zuo, J., Elshahawi, H., Dong, C., Latifzai, A., Zhang, D., and Mullins, O.C., 2011. DFA Asphaltene Gradients for Assessing Connectivity in Reservoirs Under Active Gas Charging. *SPE 145438 paper presented at the SPE Annual Technical Conference and Exhibition held in Denver, USA.*

[19] Schlumberger. 2006. *Fundamentals of Formation Testing.* Texas: Schlumberger Marketing Communications.

[20] Lee, C.L., Wee, W.W., Haddad, S., and Tighe, M., 2010. Reservoir Fluid Evaluation and Flow Assurance Analysis: Offshore Field, South East Asia. *SPE 141604 paper presented at the SPE Production and Operations Symposium held in Oklahoma City, USA.*

[21] Daungkaew, S., et al., 2012. Is There a Better Way to Determine the Viscosity in Waxy Crudes. *SPE 159337 paper presented at the SPE Asia Pacific Oil & Gas Conference and Exhibition held in Perth, Australia.*

[22] Harfoushian, J. 2009. *WFT Pressures*. Powerpoint presentation from DFA School #9. Edmonton, Canada: Schlumberger. April 1.

[23] Schlumberger. 1999. *Method and apparatus for fluorescence logging*. US Patent 5912459.

[24] Schlumberger. 2000. *Methods and apparatus utilizing a derivative of a fluorescene signal for measuring the characteristics of a multiphase fluid flow in a hydrocarbon well*. US Patent 6075611.

[25] Schlumberger. 2001. *Method and apparatus for interpreting fluorescence logging data.* US Patent 6268603.

[26] Schlumberger. 2004. *Downhole fluorescence detection apparatus*. US Patent 6704109.

[27] Schlumberger. 2010. *Methods and apparatus for multi dimension fluorescence spectrum measurement and correlations downhole*. US Patent 7687769.

[28] Schlumberger. 2010. *Methods and apparatus for multi dimension fluorescence spectrum measurement downhole*. US Patent 7687770.

[29] Schlumberger. 2010. *Methods and apparatus for analysis of downhole compositional gradients and applications thereof.* US Patent 7822554.

[30] Schlumberger. 2011. *Methods and apparatus for characterization of petroleum fluid and applications thereof.* US Patent 7920970.

[31] Schlumberger. 2011. *Predicting formation fluid property through downhole fluid analysis using artificial neural network.* US Patent 7966273.

[32] Schlumberger. 2006. *Analysis of downhole OBM-contaminated formation fluid.* US Patent 6350986.

[33] Schlumberger. 2010. *Methods and apparatus to monitor contamination levels in a formation fluid*. US Patent 7711488.

[34] Schlumberger. 2011. *Methods and apparatus for analysis of downhole asphaltene gradients and applications thereof.* US Patent 7996154.

APPENDICES

APPENDIX A M1 Station 83 Additional Results

A-1: Selected critical parameters before characterization

Component	Critical P.	Critical T.	Acentric	Critical V.	Critical Z	Volume
	psia	F		ft^3/lbmol		Trans
Mudpseudo1_83-1	253.1	742.5	0.6032	12.02	0.2359	0.1009
CO2	1070.6	87.9	0.2276	1.51	0.2744	-0.0817
N2	492.3	-232.7	0.0403	1.44	0.2917	-0.1927
C1	667.0	-116.7	0.0115	1.58	0.2861	-0.1595
C2	706.6	89.9	0.0995	2.33	0.2793	-0.1134
C3	616.1	206.0	0.1523	3.20	0.2763	-0.0863
i-C4	529.1	275.0	0.1770	4.21	0.2824	-0.0844
n-C4	550.6	305.5	0.2002	4.09	0.2739	-0.0675
i-C5	490.2	369.0	0.2279	4.90	0.2702	-0.0608
n-C5	488.8	385.8	0.2515	5.01	0.2701	-0.0390
C6	436.6	453.8	0.2990	5.93	0.2641	-0.0080
C7	397.4	512.9	0.3490	6.92	0.2635	0.0033
C8	361.1	564.2	0.3980	7.88	0.2590	0.0314
C9	330.7	610.6	0.4450	8.78	0.2528	0.0408
C10	307.5	650.9	0.4890	9.66	0.2492	0.0655
C11	285.7	688.7	0.5350	10.57	0.2451	0.0701
C12	264.0	725.1	0.5750	11.42	0.2371	0.0850
C13	249.5	757.1	0.6190	12.50	0.2388	0.1213
C14	208.9	787.7	0.6810	13.30	0.2076	0.1096
C15	220.5	812.9	0.7060	14.10	0.2277	0.1481
C16	204.5	839.9	0.7420	15.51	0.2274	0.1592
C17	188.5	859.7	0.7700	16.90	0.2250	0.1678
C18	174.0	886.7	0.7900	18.53	0.2232	0.1740
C19	166.8	901.1	0.8270	19.27	0.2201	0.1854
C20	161.0	920.9	0.9070	19.62	0.2132	0.2100
C21	150.5	938.2	0.9310	21.06	0.2113	0.2174
C22	145.0	953.9	0.9690	21.75	0.2079	0.2291
C23	139.8	969.3	1.0070	22.47	0.2049	0.2408
C24	134.7	983.9	1.0440	23.19	0.2016	0.2521
C25	129.8	997.8	1.0820	23.92	0.1985	0.2638
C26	125.2	1010.8	1.1190	24.62	0.1953	0.2752
C27	120.7	1023.0	1.1560	25.34	0.1922	0.2875
C28	116.5	1034.7	1.1930	26.03	0.1891	0.2980
C29	112.3	1045.7	1.2300	26.75	0.1860	0.3094
C30+	108.2	1056.1	1.2670			0.0000

A-2: Selected critical parameters after characterization

Component	Critical P. psia	Critical T. F	Acentric	Critical V. ft^3/lbmol	Critical Z	Volume Trans
Mudpseudo1_83-1	253.2	742.6	0.6032	12.02	0.2359	0.1009
CO2	1070.7	87.9	0.2276	1.51	0.2744	-0.0817
N2	492.4	-232.7	0.0403	1.44	0.2917	-0.1927
C1	667.1	-116.6	0.0115	1.58	0.2861	-0.1595
C2	706.7	89.9	0.0995	2.33	0.2793	-0.1134
C3	616.2	206.0	0.1523	3.20	0.2764	-0.0863
i-C4	529.1	274.9	0.1770	4.21	0.2825	-0.0844
n-C4	550.6	305.5	0.2002	4.09	0.2739	-0.0675
i-C5	490.3	369.0	0.2279	4.90	0.2702	-0.0608
n-C5	488.8	385.8	0.2515	5.01	0.2701	-0.0390
C6	436.6	453.8	0.2990	5.93	0.2641	-0.0080
Pseudo1 (C7-C15)	201.2	716.3	0.7258	11.69	0.1864	0.3205
Pseudo2 (C16-C25)	206.4	913.2	1.0076	15.02	0.2104	0.2065
Pseudo3 (C25-C80)	167.4	1064.9	1.1976	15.26	0.1562	0.0497

A-3a: Relevant binary interaction coefficients before characterization (CO2 to n-C4)

	Mudpseudo1_83-1	CO2	N2	C1	C2	C3	i-C4	n-C4
Mudpseudo1_83-1	0	0	0	0	0	0	0	0
CO2		0	-0.020	0.100	0.130	0.135	0.130	0.130
N2			0	0.036	0.050	0.080	0.095	0.090
C1				0	0.003	0.014	0.026	0.013
C2					0	0.001	-0.007	0.010
C3						0	-0.008	0.003
i-C4							0	0
n-C4								0

A-3b: Relevant binary interaction coefficients before characterization (i-C5 to C12)

	i-C5	n-C5	C6	C7	C8	C9	C10	C11	C12
Mudpseudo1_83-1	0	0	0	0	0	0	0	0	0
CO2	0.125	0.125	0.125	0.125	0.125	0.125	0.125	0.125	0.125
N2	0.095	0.100	0.100	0.100	0.100	0.100	0.100	0.100	0.100
C1	-0.006	0.024	0.042	0.035	0.047	0.047	0.047	0.047	0.047
C2	0.008	0.008	0.014	0.150	0.016	0.019	0.020	0.020	0.020
C3	0.011	0.012	0.027	0.056	0.059	0.007	0.020	0.020	0.020
i-C4	-0.004	0.002	0.024	0.025	0.026	0.006	0.010	0.010	0.010
n-C4	0.017	0.017	0.017	0.019	0.012	0.010	0.010	0.010	0.010

A-3c: Relevant binary interaction coefficients before characterization (C13 to C21)

	C13	C14	C15	C16	C17	C18	C19	C20	C21
Mudpseudo1_83-1	0	0	0	0	0	0	0	0	0
CO2	0.125	0.125	0.125	0.125	0.125	0.125	0.125	0.125	0.125
N2	0.100	0.100	0.100	0.100	0.100	0.100	0.100	0.100	0.100
C1	0.047	0.047	0.047	0.047	0.047	0.047	0.047	0.047	0.047
C2	0.020	0.020	0.020	0.020	0.020	0.020	0.020	0.020	0.020
C3	0.020	0.020	0.020	0.020	0.020	0.020	0.020	0.015	0.015
i-C4	0.010	0.010	0.010	0.010	0.010	0.010	0.010	0.010	0.010
n-C4	0.010	0.010	0.010	0.010	0.010	0.010	0.010	0.010	0.010

A-3d: Relevant binary interaction coefficients before characterization (C22 to C30+)

	C22	C23	C24	C25	C26	C27	C28	C29	C30+
Mudpseudo1_83-1	0	0	0	0	0	0	0	0	0
CO2	0.125	0.125	0.125	0.125	0.125	0.125	0.125	0.125	0.125
N2	0.100	0.100	0.100	0.100	0.100	0.100	0.100	0.100	0.100
C1	0.047	0.047	0.047	0.470	0.047	0.047	0.047	0.047	0
C2	0.020	0.020	0.020	0.020	0.020	0.020	0.020	0.020	0
C3	0.015	0.015	0.015	0.015	0.015	0.015	0.015	0.015	0
i-C4	0.010	0.010	0.010	0.010	0.010	0.010	0.010	0.010	0
n-C4	0.010	0.010	0.010	0.010	0.010	0.010	0.010	0.010	0

A-4a: Relevant binary interaction coefficients after characterization (CO2 to n-C4)

	Mudpseudo1 _83-1	CO2	N2	C1	C2	C3	i-C4	n-C4
Mudpseudo1 _83-1	0	0	0	0	0	0	0	0
CO2		0	-0.020	0.100	0.130	0.135	0.130	0.130
N2			0	0.036	0.050	0.080	0.095	0.090
C1				0	0.003	0.014	0.026	0.013
C2					0	0.001	-0.007	0.010
C3						0	-0.008	0.003
i-C4							0	0
n-C4								0

A-4b: Relevant binary interaction coefficients after characterization (i-C5 to Pseudo3)

	i-C5	n-C5	C6	Pseudo1	Pseudo2	Pseudo3
Mudpseudo1 _83-1	0	0	0	0	0	0
CO2	0.125	0.125	0.125	0.125	0.125	0.125
N2	0.095	0.100	0.100	0.120	0.120	0.120
C1	-0.006	0.024	0.042	-0.486	-0.200	-0.200
C2	0.008	0.008	0.014	0	0	0
C3	0.011	0.012	0.027	0	0	0
i-C4	-0.004	0.002	0.024	0	0	0
n-C4	0.017	0.017	0.017	0	0	0

APPENDIX B M2 Station 136 Additional Results

B-1: Selected critical parameters before characterization

Component	Critical P.	Critical T.	Acentric	Critical V.	Critical Z	Volume
	psia	F		ft^3/lbmol		Trans
Mudpseudo2_136-1	248.4	749.1	0.6127	12.21	0.2338	0.1043
CO2	1070.6	87.9	0.2276	1.51	0.2744	-0.0817
N2	492.3	-232.7	0.0403	1.44	0.2917	-0.1927
C1	667.0	-116.7	0.0115	1.58	0.2861	-0.1595
C2	706.6	89.9	0.0995	2.33	0.2793	-0.1134
C3	616.1	206.0	0.1523	3.20	0.2763	-0.0863
i-C4	529.1	275.0	0.1770	4.21	0.2824	-0.0844
n-C4	550.6	305.5	0.2002	4.09	0.2739	-0.0675
i-C5	490.2	369.0	0.2279	4.90	0.2702	-0.0608
n-C5	488.8	385.8	0.2515	5.01	0.2701	-0.0390
C6	436.6	453.8	0.2990	5.93	0.2641	-0.0080
C7	397.4	512.9	0.3490	6.92	0.2635	0.0033
C8	361.1	564.2	0.3980	7.88	0.2590	0.0314
C9	330.7	610.6	0.4450	8.78	0.2528	0.0408
C10	307.5	650.9	0.4890	9.66	0.2492	0.0655
C11	285.7	688.7	0.5350	10.57	0.2451	0.0701
C12	264.0	725.1	0.5750	11.42	0.2371	0.0850
C13	249.5	757.1	0.6190	12.50	0.2388	0.1213
C14	208.9	787.7	0.6810	13.30	0.2076	0.1096
C15	220.5	812.9	0.7060	14.10	0.2277	0.1481
C16	204.5	839.9	0.7420	15.51	0.2274	0.1592
C17	188.5	859.7	0.7700	16.90	0.2250	0.1678
C18	174.0	886.7	0.7900	18.53	0.2232	0.1740
C19	166.8	901.1	0.8270	19.27	0.2201	0.1854
C20	161.0	920.9	0.9070	19.62	0.2132	0.2100
C21	150.5	938.2	0.9310	21.06	0.2113	0.2174
C22	145.0	953.9	0.9690	21.75	0.2079	0.2291
C23	139.8	969.3	1.0070	22.47	0.2049	0.2408
C24	134.7	983.9	1.0440	23.19	0.2016	0.2521
C25	129.8	997.8	1.0820	23.92	0.1985	0.2638
C26	125.2	1010.8	1.1190	24.62	0.1953	0.2752
C27	120.7	1023.0	1.1560	25.34	0.1922	0.2875
C28	116.5	1034.7	1.1930	26.03	0.1891	0.2980
C29	112.3	1045.7	1.2300	26.75	0.1860	0.3094
C30+	108.2	1056.1	1.2670			0.0000

B-2: Selected critical parameters after characterization

Component	Critical P. psia	Critical T. F	Acentric	Critical V. ft^3/lbmol	Critical Z	Volume Trans
Mudpseudo2	248.5	749.0	0.6127	12.21	0.2338	0.1043
CO2	1070.6	87.9	0.2276	1.51	0.2744	-0.0817
N2	492.3	-232.7	0.0403	1.44	0.2917	-0.1927
C1	667.0	-116.6	0.0115	1.58	0.2861	-0.1595
C2	706.6	89.9	0.0995	2.33	0.2793	-0.1134
C3	616.1	206.0	0.1523	3.20	0.2764	-0.0863
i-C4	529.1	274.9	0.1770	4.21	0.2825	-0.0844
n-C4	550.6	305.5	0.2002	4.09	0.2739	-0.0675
i-C5	490.2	369.0	0.2279	4.90	0.2702	-0.0608
n-C5	488.8	385.8	0.2515	5.01	0.2701	-0.0390
C6	436.6	453.8	0.2990	5.93	0.2641	-0.0080
Pseudo1 (C7-C15)	324.3	628.4	0.6017	8.75	0.2429	0.1218
Pseudo2 (C16-C25)	223.8	870.5	0.9378	13.77	0.2160	0.0172
Pseudo3 (C25-C80)	226.4	1108.7	1.2359	14.29	0.1921	-0.2367

B-3a: Relevant binary interaction coefficients before characterization (CO2 to n-C4)

	Mudpseudo2_136-1	CO2	N2	C1	C2	C3	i-C4	n-C4
Mudpseudo2_136-1	0	0	0	0	0	0	0	0
CO2		0	-0.020	0.100	0.130	0.135	0.130	0.130
N2			0	0.036	0.050	0.080	0.095	0.090
C1				0	0.003	0.014	0.026	0.013
C2					0	0.001	-0.007	0.010
C3						0	-0.008	0.003
i-C4							0	0
n-C4								0

B-3b: Relevant binary interaction coefficients before characterization (i-C5 to C12)

	i-C5	n-C5	C6	C7	C8	C9	C10	C11	C12
Mudpseudo2_136-1	0	0	0	0	0	0	0	0	0
CO2	0.125	0.125	0.125	0.125	0.125	0.125	0.125	0.125	0.125
N2	0.095	0.100	0.100	0.100	0.100	0.100	0.100	0.100	0.100
C1	-0.006	0.024	0.042	0.035	0.047	0.047	0.047	0.047	0.047
C2	0.008	0.008	0.014	0.150	0.016	0.019	0.020	0.020	0.020
C3	0.011	0.012	0.027	0.056	0.059	0.007	0.020	0.020	0.020
i-C4	-0.004	0.002	0.024	0.025	0.026	0.006	0.010	0.010	0.010
n-C4	0.017	0.017	0.017	0.019	0.012	0.010	0.010	0.010	0.010

B-3c: Relevant binary interaction coefficients before characterization (C13 to C21)

	C13	C14	C15	C16	C17	C18	C19	C20	C21
Mudpseudo2_136-1	0	0	0	0	0	0	0	0	0
CO2	0.125	0.125	0.125	0.125	0.125	0.125	0.125	0.125	0.125
N2	0.100	0.100	0.100	0.100	0.100	0.100	0.100	0.100	0.100
C1	0.047	0.047	0.047	0.047	0.047	0.047	0.047	0.047	0.047
C2	0.020	0.020	0.020	0.020	0.020	0.020	0.020	0.020	0.020
C3	0.020	0.020	0.020	0.020	0.020	0.020	0.020	0.015	0.015
i-C4	0.010	0.010	0.010	0.010	0.010	0.010	0.010	0.010	0.010
n-C4	0.010	0.010	0.010	0.010	0.010	0.010	0.010	0.010	0.010

B-3d: Relevant binary interaction coefficients before characterization (C22 to C30+)

	C22	C23	C24	C25	C26	C27	C28	C29	C30+
Mudpseudo2_136-1	0	0	0	0	0	0	0	0	0
CO2	0.125	0.125	0.125	0.125	0.125	0.125	0.125	0.125	0.125
N2	0.100	0.100	0.100	0.100	0.100	0.100	0.100	0.100	0.100
C1	0.047	0.047	0.047	0.470	0.047	0.047	0.047	0.047	0
C2	0.020	0.020	0.020	0.020	0.020	0.020	0.020	0.020	0
C3	0.015	0.015	0.015	0.015	0.015	0.015	0.015	0.015	0
i-C4	0.010	0.010	0.010	0.010	0.010	0.010	0.010	0.010	0
n-C4	0.010	0.010	0.010	0.010	0.010	0.010	0.010	0.010	0

B-4a: Relevant binary interaction coefficients after characterization (CO2 to n-C4)

	Mudpseudo2_136-1	CO2	N2	C1	C2	C3	i-C4	n-C4
Mudpseudo2_136-1	0	0	0	0	0	0	0	0
CO2		0	0	0	0	0	0	0
N2			0	0	0	0	0	0
C1				0	0	0	0	0
C2					0	0	0	0
C3						0	-0.008	0.003
i-C4							0	0
n-C4								0

B-4b: Relevant binary interaction coefficients after characterization (i-C5 to Pseudo3)

	i-C5	n-C5	C6	Pseudo1	Pseudo2	Pseudo3
Mudpseudo2_136-1	0	0	0	0	0	0
CO2	0	0	0	0.125	0.125	0.125
N2	0	0	0	0.120	0.120	0.120
C1	0	0	0	0	0	0
C2	0	0	0	0	0	0
C3	0.011	0.012	0.027	0	0	0
i-C4	-0.004	0.002	0.024	0	0	0
n-C4	0.017	0.017	0.017	0	0	0

APPENDIX C M3 Station 18 Additional Results

C-1: Selected critical parameters before characterization

Component	Critical P.	Critical T.	Acentric	Critical V.	Critical Z	Volume
	psia	F		ft^3/lbmol		Trans
Mudpseudo3_18-1	249.5	747.1	0.6105	12.16	0.2342	0.1029
CO2	1070.6	87.9	0.2276	1.51	0.2744	-0.0817
N2	492.3	-232.7	0.0403	1.44	0.2917	-0.1927
C1	667.0	-116.7	0.0115	1.58	0.2861	-0.1595
C2	706.6	89.9	0.0995	2.33	0.2793	-0.1134
C3	616.1	206.0	0.1523	3.20	0.2763	-0.0863
i-C4	529.1	275.0	0.1770	4.21	0.2824	-0.0844
n-C4	550.6	305.5	0.2002	4.09	0.2739	-0.0675
i-C5	490.2	369.0	0.2279	4.90	0.2702	-0.0608
n-C5	488.8	385.8	0.2515	5.01	0.2701	-0.0390
C6	436.6	453.8	0.2990	5.93	0.2641	-0.0080
C7	397.4	512.9	0.3490	6.92	0.2635	0.0033
C8	361.1	564.2	0.3980	7.88	0.2590	0.0314
C9	330.7	610.6	0.4450	8.78	0.2528	0.0408
C10	307.5	650.9	0.4890	9.66	0.2492	0.0655
C11	285.7	688.7	0.5350	10.57	0.2451	0.0701
C12	264.0	725.1	0.5750	11.42	0.2371	0.0850
C13	249.5	757.1	0.6190	12.50	0.2388	0.1213
C14	208.9	787.7	0.6810	13.30	0.2076	0.1096
C15	220.5	812.9	0.7060	14.10	0.2277	0.1481
C16	204.5	839.9	0.7420	15.51	0.2274	0.1592
C17	188.5	859.7	0.7700	16.90	0.2250	0.1678
C18	174.0	886.7	0.7900	18.53	0.2232	0.1740
C19	166.8	901.1	0.8270	19.27	0.2201	0.1854
C20	161.0	920.9	0.9070	19.62	0.2132	0.2100
C21	150.5	938.2	0.9310	21.06	0.2113	0.2174
C22	145.0	953.9	0.9690	21.75	0.2079	0.2291
C23	139.8	969.3	1.0070	22.47	0.2049	0.2408
C24	134.7	983.9	1.0440	23.19	0.2016	0.2521
C25	129.8	997.8	1.0820	23.92	0.1985	0.2638
C26	125.2	1010.8	1.1190	24.62	0.1953	0.2752
C27	120.7	1023.0	1.1560	25.34	0.1922	0.2875
C28	116.5	1034.7	1.1930	26.03	0.1891	0.2980
C29	112.3	1045.7	1.2300	26.75	0.1860	0.3094
C30+	108.2	1056.1	1.2670			0.0000

C-2: Selected critical parameters after characterization

Component	Critical P. psia	Critical T. F	Acentric	Critical V. ft^3/lbmol	Critical Z	Volume Trans
Mudpseudo3_18-1	249.5	747.1	0.6105	12.16	0.2342	0.1029
CO2	1070.7	87.9	0.2276	1.51	0.2744	-0.0817
N2	492.3	-232.7	0.0403	1.44	0.2917	-0.1927
C1	667.1	-116.6	0.0115	1.58	0.2861	-0.1595
C2	706.7	89.9	0.0995	2.33	0.2793	-0.1134
C3	616.2	206.0	0.1523	3.20	0.2764	-0.0863
i-C4	529.1	274.9	0.1770	4.21	0.2825	-0.0844
n-C4	550.6	305.5	0.2002	4.09	0.2739	-0.0675
i-C5	490.3	369.0	0.2279	4.90	0.2702	-0.0608
n-C5	488.8	385.8	0.2515	5.01	0.2701	-0.0390
C6	436.6	453.8	0.2990	5.93	0.2641	-0.0080
Pseudo1 (C7-C15)	153.6	734.1	0.9011	15.72	0.1885	0.3070
Pseudo2 (C16-C25)	188.6	992.6	1.1267	16.62	0.2011	-0.0795
Pseudo3 (C25-C80)	221.1	1117.1	1.2475	14.64	0.1912	-0.2337

C-3a: Relevant binary interaction coefficients before characterization (CO2 to n-C4)

	Mudpseudo3_18-1	CO2	N2	C1	C2	C3	i-C4	n-C4
Mudpseudo3_18-1	0	0	0	0	0	0	0	0
CO2		0	-0.020	0.100	0.130	0.135	0.130	0.130
N2			0	0.036	0.050	0.080	0.095	0.090
C1				0	0.003	0.014	0.026	0.013
C2					0	0.001	-0.007	0.010
C3						0	-0.008	0.003
i-C4							0	0
n-C4								0

C-3b: Relevant binary interaction coefficients before characterization (i-C5 to C12)

	i-C5	n-C5	C6	C7	C8	C9	C10	C11	C12
Mudpseudo3_18-1	0	0	0	0	0	0	0	0	0
CO2	0.125	0.125	0.125	0.125	0.125	0.125	0.125	0.125	0.125
N2	0.095	0.100	0.100	0.100	0.100	0.100	0.100	0.100	0.100
C1	-0.006	0.024	0.042	0.035	0.047	0.047	0.047	0.047	0.047
C2	0.008	0.008	0.014	0.150	0.016	0.019	0.020	0.020	0.020
C3	0.011	0.012	0.027	0.056	0.059	0.007	0.020	0.020	0.020
i-C4	-0.004	0.002	0.024	0.025	0.026	0.006	0.010	0.010	0.010
n-C4	0.017	0.017	0.017	0.019	0.012	0.010	0.010	0.010	0.010

C-3c: Relevant binary interaction coefficients before characterization (C13 to C21)

	C13	C14	C15	C16	C17	C18	C19	C20	C21
Mudpseudo3_18-1	0	0	0	0	0	0	0	0	0
CO2	0.125	0.125	0.125	0.125	0.125	0.125	0.125	0.125	0.125
N2	0.100	0.100	0.100	0.100	0.100	0.100	0.100	0.100	0.100
C1	0.047	0.047	0.047	0.047	0.047	0.047	0.047	0.047	0.047
C2	0.020	0.020	0.020	0.020	0.020	0.020	0.020	0.020	0.020
C3	0.020	0.020	0.020	0.020	0.020	0.020	0.020	0.015	0.015
i-C4	0.010	0.010	0.010	0.010	0.010	0.010	0.010	0.010	0.010
n-C4	0.010	0.010	0.010	0.010	0.010	0.010	0.010	0.010	0.010

C-3d: Relevant binary interaction coefficients before characterization (C22 to C30+)

	C22	C23	C24	C25	C26	C27	C28	C29	C30+
Mudpseudo3_18-1	0	0	0	0	0	0	0	0	0
CO2	0.125	0.125	0.125	0.125	0.125	0.125	0.125	0.125	0.125
N2	0.100	0.100	0.100	0.100	0.100	0.100	0.100	0.100	0.100
C1	0.047	0.047	0.047	0.470	0.047	0.047	0.047	0.047	0
C2	0.020	0.020	0.020	0.020	0.020	0.020	0.020	0.020	0
C3	0.015	0.015	0.015	0.015	0.015	0.015	0.015	0.015	0
i-C4	0.010	0.010	0.010	0.010	0.010	0.010	0.010	0.010	0
n-C4	0.010	0.010	0.010	0.010	0.010	0.010	0.010	0.010	0

C-4a: Relevant binary interaction coefficients after characterization (CO2 to n-C4)

	Mudpseudo3_18-1	CO2	N2	C1	C2	C3	i-C4	n-C4
Mudpseudo3_18-1	0	0	0	0	0	0	0	0
CO2		0	-0.020	0.100	0.130	0.135	0.130	0.130
N2			0	0.036	0.050	0.080	0.095	0.090
C1				0	0.003	0.014	0.026	0.013
C2					0	0.001	-0.007	0.010
C3						0	-0.008	0.003
i-C4							0	0
n-C4								0

Vitae

John T. Ludwig was born on August 10th, 1971. He received his Bachelor of Science degree in Geological Engineering from the University of Minesota in 1997. Then, he continued his study in Master Degree of Petroleum Engineering at graduate school of the Department of Mining and Petroleum Engineering, Chulalongkorn University since 2010.